An Epigenetic Role for Pramel7 in Pluripotent Stem Cells

Dissertation

zur

Erlangung der naturwissenschaftlichen Doktorwürde
(Dr. sc. nat.)

vorgelegt der

Mathematisch-naturwissenschaftlichen Fakultät

der

Universität Zürich

von

Urs Graf

von

Rebstein SG

Promotionskomitee

Prof. Dr. Thomas Lutz (Vorsitz)

Prof. Dr. Kurt Bürki

Prof. Dr. Christian Lehner

PD. Dr. Raffaella Santoro

PD. Dr. Paolo Cinelli (Leitung der Dissertation)

Zürich, 2014

Acknowledgements

URS has finally accomplished his work on UHRF! To achieve that, various people have given him a lot of support in one or the other way.

My utmost gratitude goes to my supervisor, PD Dr. Paolo Cinelli and the former institute director, Prof. Kurt Bürki for offering me this project in the interesting field of stem cell research. I am very grateful to Prof. Thomas Lutz for taking over the position of Prof. Kurt Bürki and agreeing to become my doctoral father. Paolo, thanks for making me become a molecular biologist and for always motivating me, even in scientifically rough times ;-).

Furthermore, my thanks go to my committee member PD Dr. Raffaella Santoro and her group, including Dr. Claudio Guetg, Eva Vollenweider, Sandra Frommel, Natasa Savic, Sergio Leone and Dominik Bär, for a great scientific but also social collaboration and for allowing me to use their facility whenever needed. I also want to thank my collaborators Dr. Olga Shakova and Akshay Ahuja for the scientific support and Rudolf Korrodi for IT advice.

I am very grateful to my committee members Prof. Thomas Lutz, Prof. Christian Lehner, Prof. Kurt Bürki, PD Dr. Raffaella Santoro and PD Dr. Paolo Cinelli for their constructive and uncomplicated support at the committee meetings.

Now comes the LTK-Gang. Fabienne Weber and Sameera Patel, you managed to spend the last four years with me. Thanks for all the jokes, lunch conversations, dinner evenings. With your positive attitude you both often relieved me from scientific depression. Of course, also in former members of the institute, Elisa Zimmermann, Aline Widmer, Igor Asner, Dagmar Schäfer and Stefan Widmer I have found good friends. Last but not least, Zsuzsi Pataki has always had an open ear for problems of all kinds and Kirsten Rappold with her effort made our daily work easier.

My girlfriend, Bianca Burkhardt, has always stood by my side throughout every moment. She deserves my highest gratefulness and hopefully, we will accompany each other's lives for a long time. Finally, I would like to deeply thank my parents who have always given me all possible support throughout my whole education.

Abstract

PRAME-like genes *(Preferentially expressed antigen in melanoma-like, Pramel)* share structural similarities with the human cancer-testis antigen (CTA) PRAME. CTAs are usually expressed in a variety of cancers and in germ cells. In the mouse, 18 members of the *PRAME-like* gene family have been suggested until now, but their molecular function is largely elusive. Expression of one member, *Pramel7*, was found in the pluripotent compartment of the mouse preimplantation embryo, the morula and the inner cell mass (ICM) of a blastocyst. During these early stages of development, a replication-coupled passive demethylation of the maternal genome is documented. When *Pramel7* is overexpressed in mouse embryonic stem cells (mESCs), the pluripotent state of these cells can be maintained even in the absence of the cytokine LIF (leukemia inhibitory factor). Moreover, when mESCs overexpressing *Pramel7* are exposed to differentiation cues, these cells show diminished differentiation capacity *in vitro* and *in vivo*. In mESCs, the expression of *Pramel7* can be induced by the activation of the LIF/STAT3 signalling and Pramel7 was shown to be a direct downstream target of STAT3. However, the molecular function of Pramel7 is unknown.

Here, we identify UHRF1 as a potent interaction partner of Pramel7 in HEK293T cells and mESCs.

The epigenetic regulator UHRF1 (Ubiquitin-like containing PHD and RING finger domains, 1) mediates the faithful transmission of DNA methylation marks from mother to daughter cells during DNA replication. To achieve this, UHRF1 is able to recognize hemimethylated DNA and guide DNMT1 (DNA methyltransferase 1) to these sites. UHRF1 is also interacting with other epigenetic regulators such as HDAC1, G9a and PARP1 or the N-terminal tail of H3. Thus, this protein is considered to link DNA modification and the establishment of chromatin patterns.

We show that a region containing LRRs (Leucine-rich repeats) in the C-terminal area of Pramel7 is critical for the interaction with UHRF1. Furthermore, the C-terminal part of UHRF1 containing SRA and RING domains significantly contributes to an efficient binding of the two proteins (Pramel7-UHRF1). In immunoprecipitation and mass spectrometry assays, we discover factors such as ElonginC, HP1γ, CHD4, SPT16, PARP1, different types of histones, Polyubiquitin and other epigenetic regulators as interaction partners of the Pramel7-UHRF1 complex, indicating a role for Pramel7 at chromatin sites. Of note, we find that overexpression of mouse *Pramel7* leads to a rapid, dose-dependent and reversible decrease of endogenous UHRF1 protein levels in HEK293T (human UHRF1) and mESCs (mouse UHRF1). Furthermore, Pramel7 mutants with deletions in the LRR region are not able to provoke the degradation of *wt (wild type)* UHRF1. Recombinant forms of UHRF1 lacking the C-terminal part of the protein cannot be degraded by *wt* Pramel7. To summarize, UHRF1 protein degradation can be specifically mediated by its direct interaction with Pramel7 and occurs via the 26S proteasome. We demonstrate that ectopic expression of *Pramel7* accompanied by a reduction of UHRF1 protein leads to drastically reduced levels of 5mC (5-methylcytosine) in mESCs. This has a significant influence on the behaviour of cells. In self-renewing conditions, mESCs overexpressing *Pramel7* exhibit a more active epigenetic profile on a global scale shown by an enrichment of activating histone marks. This is corroborated by the aberrant upregulation of the trophectodermal marker *Elf5* in *Pramel7*-overexpressing mESCs, a phenomenon also observed in mESCs with abrogated expression of the three main DNMTs.

Differentiation of mESCs requires activation of differentiation factors and silencing of pluripotency-associated genes. DNA methylation is recognized as the ultimate epigenetic silencing mark. As a consequence of absent DNA methylation, we observe that *Pramel7*-overexpressing mESCs exhibit major limitations in terminal differentiation. After 14 days of differentiation and subsequent re-exposure to culture conditions maintaining pluripotency, *Pramel7*-overexpressing mESCs are able to reconvert to a complete pluripotent state and reactivate the expression of the classical pluripotency markers alkaline phosphatase, *Oct4*, *Nanog* and *Rex1*. This indicates that upon differentiation, the presence of *Pramel7* impairs the capacity of mESCs to silence the pluripotency-associated genes.

Under consideration of our mass spectrometry data, we establish a functional model where Pramel7 acts as a substrate recognition component of an E3 Cullin-RING ligase (CRL) complex. Binding of Pramel7 and UHRF1 is thought to induce the attachment of Ubiquitin to UHRF1 and finally to lead to proteasomal degradation of UHRF1. Taken together, for the first time, we demonstrate a biologically significant role for a member of the PRAME-like protein family. This model might support the understanding of the replication-coupled, passive DNA demethylation mechanism occurring during the preimplantation development of the mouse embryo.

Zusammenfassung

Gene der *PRAME-like (Preferentially expressed antigen in melanoma-like, Pramel)* Familie teilen strukturelle Ähnlichkeiten mit dem humanen Tumor-Hoden-Antigen *PRAME*. Tumor-Hoden-Antigene sind üblicherweise in einer Vielzahl von Krebsarten und in Keimzellen exprimiert. Bis anhin sind in der Maus 18 PRAME-like-Gene identifiziert worden, ihre molekularen Funktionen sind allerdings immer noch unbekannt. *Pramel7*, ein Mitglied der *PRAME-like* Familie, ist in den pluripotenten Kompartimenten eines frühen Mausembryos exprimiert, genauer in Morula und der inneren Zellmasse des Blastozysten. Während dieser frühen Phase der Embryonalentwicklung findet eine replikationsabhängige, passive Demethylierung des mütterlichen Genoms statt. Überexpression von *Pramel7* in embryonalen Stammzellen der Maus (mESCs) erlaubt deren Propagierung auch ohne Zugabe des Cytokins LIF (leukemia inhibitory factor) zum Kulturmedium. Wenn *Pramel7*-überexprimerende mESCs zudem zur Differenzierung angeregt werden, zeigen sie eine verminderte Differenzierungskapazität *in vitro* und *in vivo*. In mESCs kann die Expression von *Pramel7* durch Aktivierung des LIF/STAT3-Signalweges induziert werden, was *Pramel7* zu einem nachgeordneten Zielgen des Transkriptionsfaktors STAT3 macht. Trotzdem ist die molekulare Funktion von Pramel7 immer noch unbekannt.
In dieser Arbeit identifizieren wir UHRF1 als einen Interaktionspartner von Pramel7 in HEK293T Zellen und mESCs.
Das epigenetische Regulatorprotein UHRF1 (Ubiquitin-like containing PHD and RING finger domains, 1) dient dazu, DNA-Methylierungsmarkierungen während der DNA-Replikation zuverlässig vom Genom der Mutterzelle auf die Genome der beiden Tochterzellen zu übertragen. Dabei erkennt UHRF1 Stellen hemimethylierter DNA und führt DNMT1 (DNA-methyltransferase 1) zu diesen Positionen. Neben DNMT1 interagiert UHRF1 auch mit anderen epigenetischen Regulatorproteinen wie HDAC1, G9a oder PARP1 und mit dem N-terminalen Ende von H3. UHRF1 ist somit in der Lage, eine Verbindung zwischen DNA-modifizierungen und dem Aufbau von Chromatinmustern herzustellen.
Wir zeigen, dass eine Region im C-terminalen Teil von Pramel7 LRRs (Leucine-rich repeats) enthält und dass diese Region kritisch für eine erfolgreiche Interaktion mit URHF1 ist. Seitens UHRF1 trägt vor allem der C-terminale Teil, genauer SRA und RING Domänen, zur effizienten Bindung zwischen den beiden Proteinen bei. In Immunopräzipitationsexperimenten und massenspektrometrischen Untersuchengen identifizieren wir weitere potenzielle Bindungspartner des Pramel7-UHRF1 Komplexes, wie ElonginC, HP1γ, CHD4, SPT16, PARP1, verschiedene Histone, Polyubiquitin und andere epigenetische Regulatoren. Im Bezug auf Pramel7 könnte dies auf eine Rolle auf Chromatinebene hindeuten. Interessanterweise können wir aufzeigen, dass forcierte Expression des Mausproteins Pramel7 in HEK293T Zellen (human) und in mESCs (Maus) zu einer raschen, dosisabhängigen und reversiblen Degradation von endogenem UHRF1-Protein führt. Dabei sind Versionen von Pramel7 mit Mutationen (Deletionen) in der LRR-Region nicht in der Lage, die Degradation von *wildtyp (wt)* UHRF1 zu induzieren. Wiederum können mutierte Formen von UHRF1 (fehlender C-terminaler Teil inklusive SRA- und RING-Domänen) nicht durch Expression von *wt* Pramel7 degradiert werden. Zusammengefasst wird die Abnahme von UHRF1-Protein durch seine spezifische Interaktion mit Pramel7 vermittelt und erfolgt über den 26S-proteasomalen Degradationsweg. Als Konsequenz daraus finden wir in mESCs mit stabiler Überexpression von *Pramel7* drastisch reduzierte 5mC-Levels (5-Methylcytosin). Dies hat weitreichende Konsequenzen auf das Verhalten dieser Zellen: Unter Kulturbedingungen, die Selbsterneuerung begünstigen, weisen *Pramel7*-überexprimierende

mESCs ein erhöhtes Vorkommen aktivierender Histonmarkierungen auf. Ferner exprimieren diese Zellen den trophectodermalen Marker *Elf5,* der in *wt* mESCs normalerweise nur schwach aktiv ist, viel zu stark. Abnormale Überexpression von *Elf5* kann auch in mESCs mit fehlender Expression aller DNMTs beobachtet werden.
Ein erfolgreicher Differenzierungsprozess einer mESC erfordert die Aktivierung von Differenzierungsgenen und die Abschaltung von Pluripotenzgenen. Dabei spielt die DNA-Methylierung eine wichtige Rolle, so gilt sie doch als ultimative epigenetische Abschaltungsmarkierung. Als Konsequenz fehlender DNA-Methylierung können wir in *Pramel7*-überexprimierenden mESCs beobachten, dass ihre Fähigkeit terminal zu differenzieren stark eingeschränkt ist: Nach 14-tägiger Differenzierung und anschliessender Kultivierung unter Pluripotenz-fördernden Kulturbedingungen sind *Pramel7*-überexprimierende mESCs in der Lage, rasch wieder in ein pluripotentes Stadium überzugehen. Dabei werden mit Pluripotenz assoziierte Marker wie *Oct4*, *Nanog* und *Rex1* wieder reaktiviert. Diese Anzeichen erhärten die Annahme, dass die Präsenz von Pramel7 während des Differenzierungsprozesses die Kapazität von mESCs, Pluripotenzgene auszuschalten, drastisch vermindert.
Unter Berücksichtigung unserer Massenspektrometriedaten stellen wir ein funktionelles Modell auf, in dem Pramel7 die Rolle eines Substraterkennungsproteins in einem E3 Cullin-RING Ligase-Komplex einnimmt. Dabei wird angenommen, dass die Interaktion zwischen Pramel7 und UHRF1 zur Übertragung von Ubiquitinresten auf das UHRF1-Protein und schlussendlich zur Degradation desselben führt. Zusammengefasst präsentieren wir in dieser Arbeit zum ersten Mal überhaupt eine biologisch signifikante Rolle für ein Protein der PRAME-like-Familie. *In vivo* könnten unsere Beobachtungen einen Beitrag zum Verständnis der passiven, replikationsabhängigen Demethylierung des mütterlichen Genoms im frühen Mausembryo leisten.

Table of contents

List of figures

List of tables

Abbreviations

5mC	5-methylcytosine
5hmC	5-hydroxymethylcytosine
ßTrcp	Beta-transducin repeat-containing protein
BMP4	Bone morphogenetic protein 4
Cdx2	Caudal-type homeobox protein 2
CK1∂	Casein kinase isoform ∂
Co-IP	Co-immunoprecipitation
CRL	Cullin-RING ligase
CTA	Cancer testis antigen
DNA	Deoxyribonucleic acid
DNMT	DNA methyltransferase
ESCs	Embryonic stem cells
EZH2	Enhancer of zeste homolog 2
gDNA	Genomic DNA
H	Histone
HAT	Histone acetyltransferase
HDAC	Histone deacetylase
HDM	Histone demethylase
HEK	Human embryonic kidney
HemCpG	Hemimethylated cytosine
HMT	Histone methyltransferase
HP1	Heterochromatin protein 1
ICM	Inner cell mass
Id	Inhibitor of differentiation
IP	Immunoprecipitation
iPSCs	Induced pluripotent stem cells
LIF	Leukemia inhibitory factor
LRR	Leucine-rich repeat
MEFs	Mouse embryonic fibroblasts
Klf4	Krueppel-like factor 4
mESCs	Mouse embryonic stem cells
MGA	Mid-preimplantation gene activation
mRNA	Messenger RNA
Oct4	Octamer-binding transcription factor 4
PARP1 (ARTD1)	Poly(ADP-ribose)-polymerase 1
pBS	pBluescript

PcG	Polycomb group
PRAME	Preferentially expressed antigen in melanoma
Pramel6	Preferentially expressed antigen in melanoma-like 6
Pramel7	Preferentially expressed antigen in melanoma-like 7
PRC	Polycomb repressive complex
PTM	Post translational modification
Rex1	Reduced expression 1 (= Zfp42)
RA	Retinoic acid
RAR	Retinoic acid receptor
Rbx1	Ring-box protein 1
RING	Really Interesting New Gene
RNA	Ribonucleic acid
RTQ-PCR	Quantitative real-time polymerase chain reaction
SDS-PAGE	Sodium dodecyl sulfate polyacrylamide gel electrophoresis
SMAD	Similar to mothers against decapentaplegic
SOX2	SRY (sex determining region Y)-box 2
STAT3	Signal transducer and activator of transcription 3
SRA	SET and Ring finger associated
TCEB1 (ElonginC)	Transcription elongation factor B (SIII) polypeptide 1
TEAD4	TEA domain family member 4
TET	Ten-eleven translocation
TrxG	Trithorax group
UBL	Ubiquitin-like
UHRF1	Ubiquitin-like, containing PHD and RING finger domains, 1
USP7	Ubiquitin carboxyl-terminal hydrolase 7
VHL	Von Hippel-Lindau
Zfp42	Zinc finger protein 42 (= Rex1)
ZGA	Zygotic gene activation

A. Introduction

PRAME-like genes *(Preferentially expressed antigen in melanoma-like, Pramel)* are structurally similar to the human cancer-testis antigen (CTA) PRAME. Expression of CTAs is mainly restricted to the testis and is also found in various types of cancer. *Pramel7*, a member of this gene family, was found expressed in the morula and the inner cell mass (ICM) of the blastocyst in the preimplantation mouse embryo. Moreover, expression of *Pramel7* was implicated to support pluripotency in mouse embryonic stem cells (mESCs), shown by increased stability of *Pramel7* overexpressing mESCs in the absence of the cytokine LIF (Leukemia inhibitory factor), an extrinsic factor required for the maintenance of pluripotency *in vitro*. However, the exact molecular role of Pramel7 in the preimplantation embryo and mESCs and of PRAME-like proteins in general is still elusive. In this work, we identify UHRF1 (Ubiquitin-like, containing PHD and RING finger domains, 1) as a specific interaction partner of Pramel7. We provide data confirming that Pramel7 mediates the degradation of UHRF1 at the protein level. Thereby, Pramel7 participates in chromatin remodelling in mESCs. Finally, we draw a possible mechanistic model explaining its role in pluripotency maintenance *in vitro* and preimplantation development *in vivo*.

1. Pluripotent stem cells and epigenetic regulation of pluripotency

1.1. Characteristics of pluripotent stem cells

Stem cells are a specialized population of cells existing in multicellular organisms. The main function of these cells is to maintain tissue homeostasis by replacing damaged, injured or old terminally differentiated cells. Differentiation is defined by a transition of a cell from a higher to a lower degree of potency, finally reaching the status of a terminally differentiated and specialized cell without the ability to self-renew further. A typical feature of stem cells can be observed in cell division. Firstly stem cells can self-renew and give rise to two identical daughter stem cells. In addition, they can divide asymmetrically. One daughter cell retains stem cell properties whereas the fate of the second daughter cell will be shifted towards differentiation (Smith, 2001).

Embryonic stem cells (ESCs) are pluripotent, meaning they can give rise to tissues of all three germ layers of an adult organism, ectoderm, mesoderm and endoderm (Evans and Kaufman, 1981), (Martin, 1981). These striking features make this cell type a promising tool in clinical research and regenerative medicine. The ability to molecularly control and steer stem cells by enforcing their differentiation into a cell type of interest would enable the indefinite generation of cell pools for the treatment of diseases as diabetes, myocardial infarction or neurodegenerative disorders. However, it is challenging to achieve this, and many hurdles have to be over-

come. One drawback is characterized by the incomplete or inefficient differentiation of stem cells previously propagated in an *in* vitro environment resulting in enhanced tendency for tumour formation. Furthermore, the *in vivo* environment, the so-called stem cell niche, markedly differs from the artificial *in vitro* one. Thus, it has to be addressed how stem cells can efficiently be transferred from a culture dish into a living organism without any negative side effects such as tumorigenesis. Finally, a main goal of regenerative medicine is to overcome the problem of immunological rejection upon transplantation of foreign tissue, e.g. donor organs or stem cells.

Murine embryonic stem cells (mESCs) are derived from the inner cell mass (ICM) of a mouse blastocyst stage embryo. mESCs can be maintained *in vitro* by cultivating them in medium supplemented with leukemia inhibitory factor (LIF) and fetal bovine serum (FBS) containing bone morphogenetic protein 4 (BMP). LIF activates the transition of the transcription factor, Signal transducer and activator of transcription 3 (STAT3) from cytoplasm into the nucleus driving the expression of its target genes and maintaining self-renewal (Niwa et al., 1998). The serum component BMP4 is thought to have an anti-differentiation effect by activating *SMAD*- (Similar to mothers against decapentaplegic) and *Id*- (Inhibitor of differentiation) genes that in turn lead to the activation of the core pluripotency factors Oct4 and SOX2 (Ying et al., 2003). mESCs are the most intensively studied and thus the most well characterized type of ESCs. They can be indefinitely propagated and genetically modified *in vitro*, and when injected into a donor blastocyst, they have the potential to contribute to the development of a new embryo. These features make mESCs a very powerful tool for genetic engineering and the well-established generation of transgenic animals. These transgenic models allow the study of various diseases and support the characterization of new genes and proteins.

In 2006, Takahashi and Yamanaka presented an approach revolutionizing stem cell research. The two Japanese scientists were asking if it was possible to change the norm and reverse the order of cellular development at which cells of high developmental potency steadily differentiate into cells of lower potency. To achieve this they first screened databases for interesting candidates and isolated 24 genes that were subsequently narrowed down to four factors. Indeed, when next the four candidate genes coding for transcription factors named *Oct4*, *SOX2*, *Klf4* and *c-myc*, nowadays also called the "Yamanaka-factors", were retrovirally introduced they were able to reprogram differentiated mouse embryonic fibroblasts (MEFs) from 14 days old embryos back to so called induced pluripotent stem cells (iPSCs), resembling embryonic stem cells to a remarkably great extent (Takahashi and Yamanaka, 2006). iPSCs express the same sets of genes as ESCs and when injected into a blastocyst, they are able to participate in the development of a new organism. Furthermore, upon injection into immuno-deficient mice, iPSCs give rise to teratomas containing tissues of all three germ layers (Wernig et al., 2007). This remarkable finding potentially allows the generation of patient-specific stem cells

However, it soon became clear that iPSCs are not absolutely similar to ESCs. They exhibit a high tendency for tumour formation most likely due to genetic and epigenetic aberrations obtained during the reprogramming process. Furthermore, *c-myc* displays strong oncogenic character. Finally, there exists a feature of iPSCs termed the "epigenetic memory". During the reprogramming process, a differentiated cell of a certain tissue carrying a unique chromatin structure has to be converted into an ESC-like cell with an open and dynamic chromatin structure. Thus epigenetic marks of differentiated cells have to be erased and chromatin patterns of a pluripotent cell have to be set up. During this conversion some loci of iPSCs retain the epigenetic marks of the original somatic cell, which is termed epigenetic memory. In addition, cells acquire other genetic and epigenetic anomalies for example alterations in gene copies, compromised function of imprinted genes, changed patterns in DNA methylation or point mutations (Kim et al., 2010), (Vaskova et al., 2013). Therefore, a lot of research still has to be undertaken in this field until these cells can be used for clinical applications in regenerative medicine.

1.2. The core pluripotency network and intrinsic markers of pluripotency

The *in vitro* maintenance of pluripotent mESCs requires defined and stringent culture conditions. Generally the pluripotent state of mESCs is metastable and even minor changes in the environment of cells can lead to the loss of pluripotency and induction of differentiation. The pluripotent state is maintained through a network of numerous transcription factors activating targets that maintain pluripotency or repress factors driving differentiation. The proteins Oct4, SOX2 and Nanog represent the three core factors of this transcriptional network. Additional key players are Rex1, Sall4, Dax1 or Tcl1. All these transcription factors act in concert and in different combinations to maintain pluripotency. Moreover, chromatin-modifying enzymes regulating the accession of promoters and thus the expression of associated genes are integrated in the complexes. Studies aiming on assessing the chromatin occupancy of Oct4, SOX2 and Nanog, in combination with analyses of various other transcription factors, have led to this extremely complex regulatory networks controlling transcription of target genes and maintaining pluripotency (Orkin and Hochedlinger, 2011).

The *in vitro* characterization of pluripotent cells can be evaluated by testing the expression of the so-called *pluripotency markers*, representing the pluripotent state. Three examples are Oct4 and Nanog, members of the core pluripotency network, and Rex1.

The octamer-binding transcription factor 4 (Oct4) is encoded by the gene *POU5F1* (Takeda et al., 1992). As a special case, *Oct4* requires a precise degree of expression to maintain developmental potency. An expression above the critical level was shown to lead to differentiation of mESCs into primitive endoderm or mesoderm and expression below a certain threshold resulted in differentiation into trophectodermal tissue. Thus, *Oct4* expression needs to be kept in

a tight balance for an adequate maintenance of the pluripotent state (Niwa et al., 2000). A recent study states that a defined level of *Oct4* is required for pluripotency entry. Once the pluripotent state is reached this expression level can be decreased up to seven-fold without loss of self-renewal. Furthermore, it was observed that mESCs expressing *Oct4* at levels representing the ESC-state efficiently differentiated to all germ layers and germ line. In contrast, cells exhibiting decreased levels of *Oct4* were not able to differentiate and maintained the expression of pluripotency-associated genes. Thus, the expression level of *Oct4* is the decision maker between the establishment of pluripotency and commitment to embryonic lineages (Radzisheuskaya et al., 2013). Early mouse embryos deficient in *Oct4* fail to form an ICM and instead differentiate into trophectodermal tissue. Thus, a certain level of *Oct4* is also crucial for the regulation of pluripotency in the *in vivo* condition preventing premature differentiation of embryos and guaranteeing a faithful development of the ICM (Nichols et al., 1998).

When the homeobox protein Nanog is overexpressed mESCs deprived of LIF are very robust but not completely refractory to spontaneous differentiation (Hatano et al., 2005). On the other hand, *Nanog*$^{-/-}$ mESCs differentiate into extraembryonic endodermal tissues. *Nanog* expression is also shown to fluctuate in mESCs and its transient downregulation predisposes cells towards differentiation but does not mark commitment. When *Nanog* is genetically deleted resulting mESCs are prone to differentiation but still able to self-renew indefinitely. Moreover, *Nanog*$^{-/-}$ cells participate in the development of embryonic germ layers and are able to differentiate in multiple lineages. *Nanog*$^{-/-}$ mESCs, although recruited to the germ line, fail to reach the genital ridge. When repairing the mutant allele the defect is rescued. Thus Nanog is more likely to be important for the construction of ICM- and germ cells rather than directly involved in the housekeeping machinery maintaining the pluripotent state (Chambers et al., 2007). *Nanog*-deficient embryos analysed at E5.5 are lacking primitive endoderm and fail to further develop (Mitsui et al., 2003).

Reduced expression 1 (*Rex1*, also *Zfp42*) was first described after its specific expression had been observed in pluripotent F9 embryonic carcinoma cells (Hosler et al., 1989). *Rex1* is expressed in pluripotent cells such as ESCs (Rogers et al., 1991), multipotent adult progenitor cells (Jiang et al., 2002), amniotic fluid cells (Karlmark et al., 2005), in germ cells of testis and in the ICM and early trophectoderm of the early mouse embryo (Rogers et al., 1991). Expression of *Rex1* is positively correlated to increased pluripotency in mESCs (Toyooka et al., 2008), human embryonic stem cells (hESCs) (Brivanlou et al., 2003) and iPSCs (Chan et al., 2009) and is thus thought to be a reliable and a stringent marker for pluripotency.

1.3. History and features of epigenetics

The field of epigenetics describes mitotically and/or meiotically heritable changes in gene function that cannot be explained by changes in DNA sequence (Russo, 1996). In 1882 Walther Flemming first mentioned the term chromatin after having developed new histological staining methods enabling the observation of a specific fibrous structure in the cell nucleus. Approximately 50 years later, by identifying two different degrees of compaction in the interphase nucleus Emil Heitz made the distinction between heterochromatin and euchromatin.

Nowadays, heterochromatin is associated with tightly compacted DNA regions and silent, non-transcribed areas of the DNA. Heterochromatin can further be divided in constitutive and facultative heterochromatin. DNA regions of a given organism that are packed identically in all cells are termed constitutive heterochromatin. This type of heterochromatin is predominantly found around centromeres (centric and pericentric heterochromatin) and at telomeres. Facultative heterochromatin, on the other hand, is not comparable between different cell types. For example, depending on the requirement of a specific cell type, lineage specific genes may be present as silenced heterochromatin or active euchromatin. In contrast to heterochromatin, euchromatic regions are less compact and are actively transcribed (Gaspar-Maia et al., 2011).

The unwrapped DNA of a eukaryotic cell has a length of two to three meters. To fit this tremendous amount of information into a nucleus of around 6-10µm diameter, the DNA is tightly packed into chromosomes composed of chromatin fibre loops. These loops consist of nucleosomes, the repeating particles responsible for the primary level of DNA compaction. Each nucleosome is formed by the association of an octamer of the four core histones H2A, H2B, H3 and H4. The stretch of double stranded DNA is wrapped almost two times around each nucleosome (Luger et al., 1997) and the DNA between nucleosomes is connected by the linker histone H1 (Ramakrishnan et al., 1993).

Particles of the nucleosome complex can undergo reversible remodelling concomitant with unwrapping and rewrapping of the DNA. Furthermore, tails of histones are covalently modified by the addition of post-translational modifications (PTMs). In general, modifications are found in both histones and DNA. Methylation is the typical epigenetic mark for DNA. It is associated with transcriptional repression and mediated by DNA methyltransferases. The *maintenance* DNA methyltransferase 1 (DNMT1) is responsible for transferring the correct DNA methylation pattern from mother to daughter cells after DNA replication (Jair et al., 2006). In contrast, *de novo* DNA methyltransferases 3a and 3b (DNMT3a/3b) are able to create new methylation marks, thus, to change the epigenetic signature (Okano et al., 1999). Compared to histone modifications, methylation of DNA is typically more stable and can be inherited for several cell generations. However, DNA methylation can be lost when specific enzymes crucial for DNMT1 function are missing during replication

(Gaspar-Maia et al., 2011). Recent findings indicate that methylations at cytosine residues can be oxidized into hydroxymethyl groups by enzymes of the Tet-dioxygenase family (Tet1-3) (Tahiliani et al., 2009). Hydroxymethylation is involved in the regulation of gene expression, embryonic development, stem cell function and cancer. It is also seen to facilitate the demethylation of DNA, but the molecular circuitries underlying these features remain poorly defined (Pastor et al., 2013).

PTMs of histones are very diverse and contain features such as methylation (me), acetylation (ac), ubiquitination (ub) and sumoylation of lysine (K) residues, methylation and citrullination of arginine (R) residues, phosphorylation of serine (S) and threonine (T) residues, and ADP-ribosylation of glutamate (K) and arginine (R) residues (Bannister and Kouzarides, 2011). The most common histone marks representing active transcription are H3K4me1/3, H3K9me1, H3K9ac, H3K14ac, H3K27me1, H3K27ac and H3K79me1/2, whereas H3K9me2/3, H3K27me2/3 and H3K79me3 represent repressive modifications (Tab. 1) (Benevolenskaya, 2007), (Barski et al., 2007), (Koch et al., 2007), (Steger et al., 2008), (Rosenfeld et al., 2009), (Creyghton et al., 2010). A schematic illustration of DNA modifications and PTMs of histones is depicted in Fig. 1. This broad range is mediated and regulated by various enzymes such as histone acetyltransferases (HATs), histone deacetylases (HDACs), histone methyltransferases (HMTs), histone demethylases (HDMs), kinases or phosphatases which are able to add or remove the histone marks and are usually involved in big protein complexes (Musselman and Kutateladze, 2011). Two prominent examples are the Trithorax (trxG) and the Polycomb group (PcG) complexes. TrxG proteins were identified as activators of *Drosophila Hox*-genes important for body patterning (Schuettengruber et al., 2007). They catalyse trimethylation of histone H3K4 (H3K4me3), a mark associated with active transcription. In mammalian cells, proteins catalysing H3K4me3 are the H3K4-methylases SET1A, SET1B, and mixed lineage leukemia (MLL) proteins 1-4. As mentioned above, these factors cannot function alone and require additional subunits for activity (Shilatifard, 2012).

Tab. 1: Selected variants of histone modifications with their effector functions.
A = activation, R = repression.

Modification	Histone							
	H3K4	H3K9	H3K14	H3K27	H3K36	H3K79	H4	H4K20
Monomethylation	A	A		A		A	A	A
Dimethylation		R		R		A		
Trimethylation	A	R		R	A	A/R		
Acetylation		A	A	A				

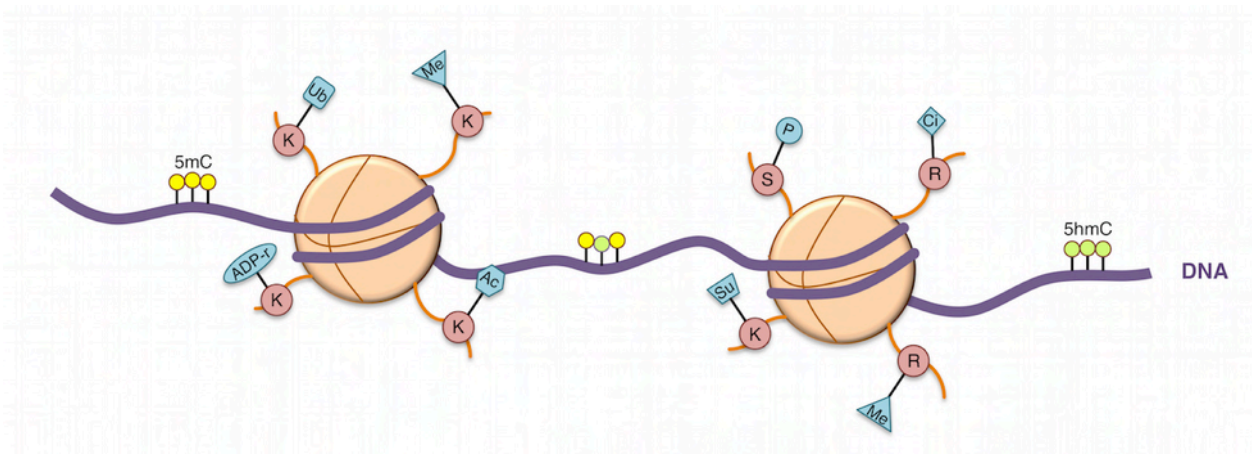

Fig. 1: Schematic illustration of epigenetic modifications.
Histones are coloured in orange, DNA in purple. DNA is wrapped approximately 1.6x around histone octamers. 5mC=5-methyl cytosine, 5hmC=5-hydroxymehtyl cytosine, K=lysine, R=arginine, S=serine, Ub=ubiquitination, Me=methylation, ADP-r=ADP-ribosylation, Ac=acetylation, P=phosphorylation, Ci=citrullination, Su=sumoylation.

PcG protein complexes were first observed in *Drosophila* as responsible factors for the silencing of *Hox*-genes (Schuettengruber et al., 2007). Proteins of the PcG form the multi-subunit repressive complexes PRC1 and PRC2 (Polycomb repressive complex 1 and 2) (Margueron and Reinberg, 2011), (Simon and Kingston, 2009). The PRC2 histone methyltransferase EZH2 (Enhancer of zeste homolog 2) mediates trimethylation of H3K27 (H3K27me3), a prominent mark in the establishment of repressive chromatin in both the adult organism and early development (Czermin et al., 2002). PRC1 unites different complexes containing the RING1A/B ubiquitin ligase and is therefore assumed to mediate silencing of its targets at least in part by ubiquitination of H2AK119 (Gao et al., 2012). However, the exact mechanism of PRC1-mediated gene repression and chromatin compaction still remains elusive (Simon and Kingston, 2013).
Finally, the incorporation of histone variants such as H3.3, H2A.Z or macroH2A can change the state of chromatin, leading to a more open or closed conformation (Gaspar-Maia et al., 2011).

1.4. ESCs display a unique epigenetic landscape

Even though a big effort still has to be undertaken to molecularly decrypt the functional entity of histone modifications, recent studies have provided genome-wide insights into how these marks might function *in vivo*. Since human and murine ESCs harbour a huge potential for biological research and medical applications, there is a big interest in mapping and understanding the epigenetic landscape of this special cell type (Voigt et al., 2013). When localizing chromatin modifications in ESCs, histone marks as H3K4me1 and H3K27ac can be found at active enhancers and H3K4me3 and H3K27me3 within active and silent promoters. These signatures are basically present in all mammalian cell types (Zhou et al., 2011) but certain features appear to be specifically more abundant in ESCs. There is a substantial fraction of genes, many of them

regulating developmental processes, carrying both the activating mark H3K4me3 and the repressive modification H3K27me3 at the same time. These on the first sight contrarious marks are termed "bivalent" domains and were mentioned for the first time in 2006 by Bernstein et al. after having performed sequential ChIP analysis against different histone modifications (Bernstein et al., 2006). Although these special domains are most abundant in ESCs they are also occurring in cell types with more restricted potency (Voigt et al., 2013).

Above observations have led to the hypothesis that bivalent domains may maintain genes in a state poised or primed for differentiation, allowing either rapid activation or silencing upon sensing appropriate stimuli. This is supported by several follow-up studies showing that on a genome wide scale, genes with bivalent profiles exhibit associated expression changes upon induction of differentiation (Pan et al., 2007), (Mikkelsen et al., 2007), (Zhao et al., 2007).

Most of the bivalent genes in ESCs are targets of PcG proteins. Thus, valuable information about their importance can be gained from knockout studies of PRC complex members. For example, in ESCs with depleted Eed protein (*Eed*$^{-/-}$), which together with Suz12 and EZH2 constitutes the essential components of PRC2, a premature expression of bivalent genes can be observed (Azuara et al., 2006), (Boyer et al., 2006). The same is true for *Suz12*$^{-/-}$-ESCs (Pasini et al., 2007). However, despite premature expression of genes related to differentiation, self-renewal capacity and cell viability are not impaired. Nevertheless, PRC2-deficient ESCs exhibit a compromised differentiation potential (Pasini et al., 2007), (Shen et al., 2008), (Chamberlain et al., 2008). In conclusion, these findings indicate that PRCs are crucial for adequate differentiation of ESCs, most likely by controlling bivalent promoters of target genes coding for proteins involved in development.

When an ESC differentiates, its bivalent promoters either undergo activation or silencing. When the expression of such a gene is activated repressive marks in the promoter region have to be removed and vice versa. Thus, activation of a bivalent gene requires erasure of H3K27me3 while repression is mediated by the removal of H3K4me3 (Voigt et al., 2013). These processes are initiated when the cell experiences developmental cues and transfers them into the nucleus via cell signalling cascades. This is often accompanied by the recruitment of specific transcription factors, leading to the activation of the target gene. At many bivalent promoters, the related transcription factors are absent or inactive in the pluripotent state (Ku et al., 2008). They are recruited upon induction of differentiation, which might be a key process in activating the transcription of these genes. In favour of this assumption, overexpression of transcription factors regulating developmental genes results in alterations of transcriptional programs and heavily affects bivalent genes (Nishiyama et al., 2009), (Sharov et al., 2011). Unlike bivalent genes, housekeeping genes do not show altered expression upon differentiation, most likely due to the presence of a persistent and sufficient amount of protein complexes activating transcription.

Finally, extrinsic signals are also able to modulate the nuclear levels of chromatin modifiers and influence the structure of the chromatin by facilitating or impeding transcription (Badeaux and Shi, 2013).

1.5. DNA methylation and mESCs

Because of their highly dynamic chromatin, mESCs are one of the most well studied systems for epigenetic changes. When mESCs differentiate, genes associated with pluripotency have to be silenced rapidly while other factors driving differentiation are activated. Surprisingly, mESCs are tolerant to global demethylation. Despite depletion of all three DNA methyltransferases *(DNMT1$^{-/-}$/3a$^{-/-}$/3b$^{-/-}$)*, the molecular signature of pluripotency is unaffected and self-renewal is not lost (Tsumura et al., 2006). Nevertheless, differentiation capacity of *DNMT* triple knockout mESCs is drastically reduced. On one hand, triple knockout cells loose the ability of upregulating markers associated with germ layers and on the other hand, they fail to efficiently shut down promoters of pluripotency genes (Jackson et al., 2004). Upon differentiation, gene promoters such as *Oct4* and *Nanog* are silenced by hypermethylation. Silencing of *Oct4*, as an example for a gene promoter of a gene associated with pluripotency, is initiated first by repressor binding and subsequent H3K9 methylation, mediated by the histone methyltransferase G9a and recruitment of heterochromatin protein 1 (HP1) and is accomplished by *de novo* DNA methylation. However, when *G9a* expression is absent silencing of *Oct4* is inefficient and reversible (Feldman et al., 2006). During the differentiation process, DNA methylation of distinct promoters occurs concomitantly with nucleosome assembly preventing further binding of transcription factors to target promoters (You et al., 2011). It is moreover shown that silencing of *Oct4* can be forced *in vitro* by artificial targeting of HP1α to the *Oct4* promoter, resulting in methylation of H3K9 and subsequent DNA methylation. When carried out in MEFs, this *de novo* silencing is stable and heritable after removal of the HP1α-targeting stimulus but in mESCs withdrawal leads to demethylation and reactivation of *Oct4*-expression (Hathaway et al., 2012).

A unique feature of mESCs that is not found in other cell types is the presence of DNA methylation in non-CpG background, most commonly in CpA dinucleotides probably reflecting a state of hyperactive *de novo* DNMT3a/b activity (Ramsahoye et al., 2000). Even though globally occurring, this non-CpG type of methylation is enriched at certain genomic loci. It co-localizes with high degrees of CpG methylation and is silenced on differentiation (Ziller et al., 2011). Furthermore, DNA methylation is exhibiting a buffer function in extraembryonic commitment (Jackson et al., 2004), (Ng et al., 2008). *DNMT1$^{-/-}$* mESCs exhibit a uniquely high potential for the trophectodermal lineage verified by the upregulation of the transcription factor *Elf5*. Together with other factors such as *Cdx2* and *Eomes*, *Elf5* takes a crucial role in trophectodermal

specification during the development of an early mouse embryo. More importantly, expression of these genes induces a competition with genes associated with the pluripotency network (Smith and Meissner, 2013). In contrast, in a *wild type (wt)* population of mESCs, promoters of these genes are methylated and only a very small fraction of cells is able to differentiate into trophectodermal tissue (Ng et al., 2008).

Taken together, how exactly DNA methylation is orchestrated with other mechanisms of gene silencing still is a complex question. It remains a challenging task to evaluate the role of CpG methylations in different developmental contexts (Smith and Meissner, 2013).

1.6. Epigenetic events during preimplantation development of the mouse embryo

The preimplantation process in the mouse starts with the fertilization of the oocyte by the sperm and ends with the implantation of the embryo in the uterus. This process can be divided into the well-organized stages ovulation (E0), fertilization (E0.5), zygotic stage (E0.5-1.5), cell cleavage (E1.5-E2.5), morula formation (E2.5-E3.5), blastocyst formation (E3.5-E4.5) and implantation (E4.5). The induction of the above stages is regulated on both the genetic and epigenetic level, and these two levels of regulation are strictly interrelated. In mammalian embryos, the oocyte stores a bunch of maternal RNAs and proteins subsequently expressed in the earliest phase of preimplantation development (Wang and Dey, 2006). Fertilization acts as a trigger for the degradation of these maternal factors, which at the 2-cell stage are almost undetectable anymore (Nothias et al., 1995). Then, the newly assembled zygotic genome initiates its expression between the 2- and the 4-cell stage and genetic patterns required for subsequent development of the embryo are established. This process is also known as zygotic genome activation (ZGA) (Wang and Dey, 2006). Preceding morula and blastocyst stage, a second wave of gene activation peaks at the 8-cell stage, the so-called mid-preimplantation gene activation (MGA), involving the activation of adhesion molecules required for blastomere polarity and compaction (Hamatani et al., 2004).

Genetic expression patterns during early embryonic development are very well characterized. Based on this knowledge research soon focused on the generation of corresponding epigenetic profiles (Shi and Wu, 2009). Every epigenetic event requires certain enzymes that need to be obligatorily expressed in advance, for example DNMTs, HDACs or HMTs or even whole chromatin remodelling complexes. Some epigenetic regulators are expressed concomitantly with ZGA. One example is HDAC1, whose expression is initiated at the single cell stage and gradually increases until blastocyst stage (Ma and Schultz, 2008). On the other hand, the expression of other regulators such as the histone methyltransferase SETB1 is not seen until the blastocyst stage when maternal SETB1 gets exhausted (Dodge et al., 2004).

Epigenetic regulation always functions in cooperation with genetic control. The early preimplantation embryo has to first differentiate into two compartments, the inner cell mass (ICM) and the trophectoderm. The ICM will give rise to the whole organism while the trophectoderm develops into extraembryonic tissues. Consequently, cells of the ICM retain their pluripotent expression profiles whereas trophectodermal tissues lose them. Thus, as described previously in chapter 1.2, the expression of *Oct4* defining the pluripotent population of cells needs to be precisely regulated. In cells of the ICM, the transcription factor Sall4 binds at the promoter region of *Oct4* and activates *Oct4*-expression (Zhang et al., 2006). Then, Oct4 is able to interact with the proximal region of *Nanog* promoter activating *Nanog* expression (Kuroda et al., 2005). In the outer cells of the morula the transcription factor TEAD4 controls the expression of Cdx2, which in turn blocks the activity of *Oct4* and *Nanog*, leading to the establishment of the trophectodermal line (Nishioka et al., 2008). At the same time, levels of DNA- and histone methylation and histone acetylation at the promoter of *Oct4* might be altered to fix the permanent shutdown of the *Oct4* gene (Hattori et al., 2004).

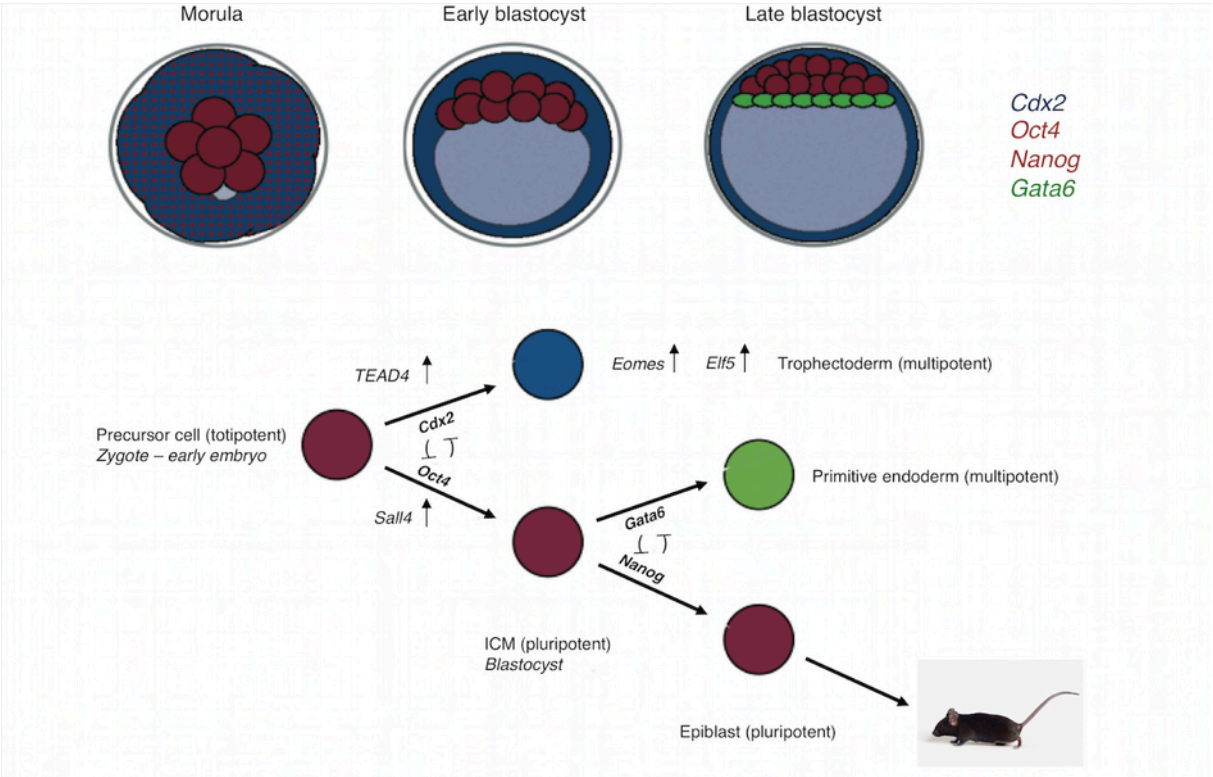

Fig. 2: Regulatory events defining the first steps of differentiation in the early mouse embryo.
In the early morula stage inner cells maintain the expression of *Sall4* and *Oct4* leading to the activation of *Nanog*. In the outer, future trophectodermal cells expression of *TEAD4* is activating *Cdx2*, antagonizing *Oct4* expression in the inner cells. Subsequent activation of *Eomes* and *Elf5* is stabilizing the trophectodermal fate. In the late blastocyst the ICM is separated in primitive endoderm, specified by the expression of *GATA6* antagonizing the expression of *Nanog* expressed in the cells of the epiblast. From Ralston and Rossant, 2005, modified.

TEAD4 and Cdx2 in concert activate the expression of *Eomes* leading to the upregulation of *Elf5*, further specifying trophectodermal fate (Sasaki, 2010). However, how exactly cells are poised for one or the other fate still remains a debate. The key regulatory processes in the development of the early embryo are illustrated in Fig. 2.

During preimplantation development, DNA methylation undergoes dynamic changes. After fertilization, maternal and paternal pronuclei are formed. Just after fertilization the murine paternal genome exchanges protamines, substitutes of histones in spermatogenesis, with maternally inherited histones (Adenot et al., 1997) and the paternal genome is actively demethylated rapidly (Mayer et al., 2000). How this active demethylation is mediated in detail is still not understood. Recent studies reveal that 5-mehtylcytosine (5mC) can sequentially be oxidized to 5-hydroxymethylcytosine (5hmC) (Tahiliani et al., 2009), 5-formylcytosine (5fC) and 5-carboxymethylcytosine (5caC) (He et al., 2011), (Ito et al., 2011) by the enzymes Tet1-3. Tet3 is highly expressed in oocytes and zygotes but downregulated at the 2-cell stage. Furthermore, 5hmC accumulates in the paternal genome while 5mC levels decrease, leading to the assumption that the active loss of 5mC in the paternal genome is at least in part due to the oxidation of 5mC by Tet3 (Iqbal et al., 2011).

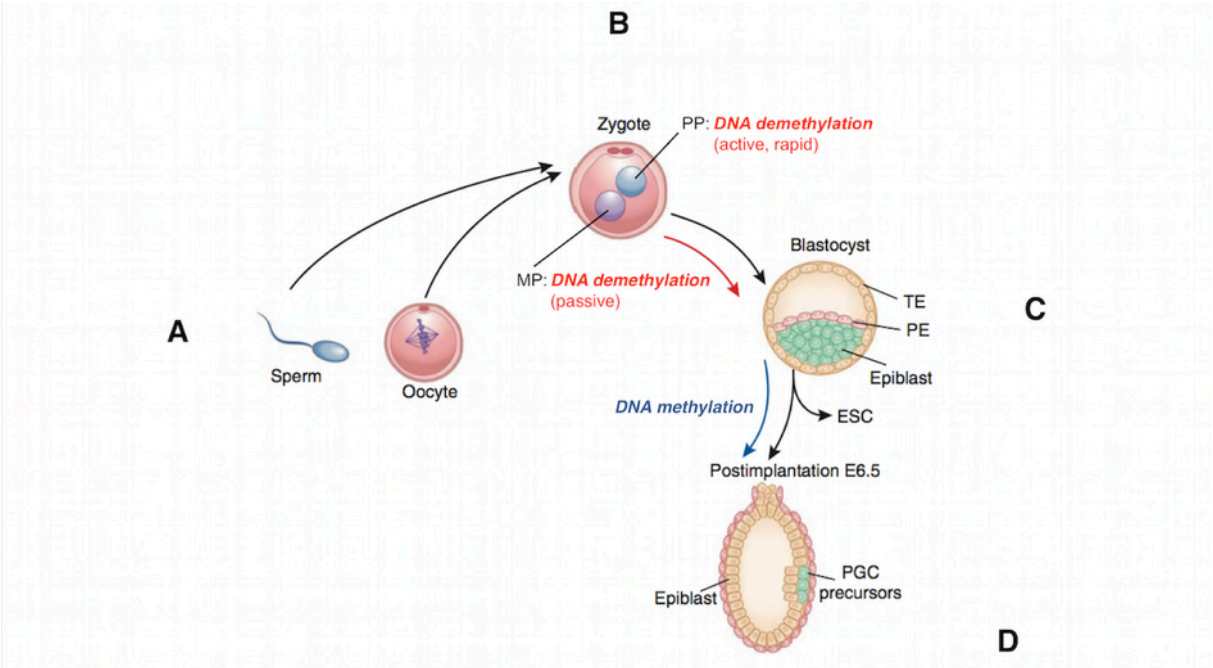

Fig. 3: Alterations in DNA-modification profiles in the early mouse embryo.
A: Fertilization of the oocyte by the sperm. **B:** Soon after fertilization protamines in the paternal pronucleus are replaced by maternally provided histones. DNA in the paternal nucleus is actively demethylated very fast. **C:** From 2 cell to the blastocyst stage the maternal genome is demethylated by a passive mechanism. In the late blastocyst the ICM is separated into epiblast and primitive endoderm (see Fig. 2). **D:** From the late blastocyst stage onwards a wave of DNA remethylation is induced. In the postimplantation epiblast primordial germ cell precursor cells are specified. PP= paternal pronucleus, MP= maternal pronucleus, TE= trophectoderm, PE= primitive endoderm, PGC= primordial germ cells. From Cantone and Fisher, 2013, modified.

In the maternal genome, the protein Dppa3 (Stella) interacts with H3K9me2 and prevents Tet3 access (Nakamura et al., 2012). Thus, the conversion from 5mC to 5hmC is less evident. The loss of 5mC in the maternal genome is thought to occur via a rather passive mechanism by repeated cell divisions resulting in an overall reduction of 5mC levels (Fig. 3) (Rougier et al., 1998), (Santos et al., 2002), (Inoue and Zhang, 2011). However, since DNMT1 is present throughout preimplantation development and is sufficient to maintain DNA methylation at imprinted regions (Hirasawa et al., 2008), the mechanism by which 5mC is passively lost still needs to be clarified. From the blastocyst stage onwards, the first differentiation processes are accompanied by *de novo* methylation mediated by DNMT3a/3b leading to silencing of genes responsible for the maintenance of pluripotency (Santos et al., 2002).

Compared to DNA methylation the situation for histone modifications and histone variants is more complex. Histone tails can be extensively modified and from the experimental data accessible no general model can be drawn so far. As for DNA methylation, there is a dramatic change in histone modifications during preimplantation development in specific stages and cell types (Shi and Wu, 2009). In addition, it is observed that within one embryo different cells can exhibit divergent mRNA expression patterns for DNMTs and HMTs, 5mC-binding proteins and other chromatin modifiers. Therefore, different cells carry different epigenetic profiles further complicating the analysis (May et al., 2009). Taken together, these findings suggest a tight temporal and spatial program orchestrating DNA- and chromatin-modifications, resulting in the establishment of the zygotic developmental program (Cantone and Fisher, 2013).

2. Preferentially expressed antigen in melanoma-like 7 (Pramel7)

2.1. PRAME, the founding member of a big gene family

The leucine-rich repeat (LRR) containing human protein PRAME (Preferentially expressed antigen in melanoma) is considered the founding member of the *Pramel (PRAME-like)* gene family (Preferentially expressed antigen in melanoma-like). PRAME was originally found as a gene coding for an antigenic peptide presented to autologous tumour-specific cytolytic T lymphocytes that were derived from a patient suffering from melanoma (Ikeda et al., 1997). Expression profiles of PRAME define it as a cancer-testis antigen (CTA). These genes are usually highly expressed in tumours while in to healthy tissues they are predominantly found in germinal cells (Haqq et al., 2005). However, specific expression of *PRAME* was also detected in adrenal tissues, placenta and endometrium (Ikeda et al., 1997). In addition, levels of PRAME in malignant tissues of breast cancer and neuroblastoma correlated with poor clinical outcome and thus acts as a useful marker for the progression of the disease (van 't Veer et al., 2002), (Oberthuer et al.,

2004). Since the exact regulatory mechanisms of PRAME are not completely understood its molecular functions in healthy tissues and malignancies still remain elusive.

In 2005 Epping et al. described PRAME as a dominant repressor of retinoic acid (RA) signalling. F9 embryonic carcinoma cells expressing PRAME were observed to be resistant to RA treatment. In general, RA signalling was shown to induce differentiation, arrest of proliferation and apoptosis, and failure in RA signalling could be linked to cancer. The authors proposed a model for healthy cells, where RA is binding to its ligand RAR (Retinoic acid receptor) inducing the expression of RA target genes. This cascade is ultimately leading to differentiation of cells and growth arrest. In contrast, in PRAME-positive tumour cells, PRAME is interacting with RAR. This leads to the recruitment of PcG proteins such as the histone methyltransferase EZH2. As a consequence, RA targets are silenced, RA-dependent features cannot be triggered and uncontrolled proliferation is provoked (Epping et al., 2005). A comparable effect could be observed in myelogenous immortalized leukemia cells (K562) where inhibition of *PRAME* caused growth arrest and apoptosis (Tanaka et al., 2011). Finally, *PRAME*-knockdown in Hodgkin lymphoma cells induced an increase in retinoic acid signalling and cytotoxic drug sensitivity (Kewitz and Staege, 2013).

On the molecular level, a recent study states that PRAME is able to act as a substrate recognition subunit of a Cullin2-based Cullin-RING ligase (CRL) targeting substrates for proteasomal degradation. The authors found that many members of the large *PRAME* gene family harbour conserved BC- and Cullin2-boxes and stated that they might function as recognition components, with different levels of specificity in substrate selection. Furthermore, chromatin immunoprecipitation-based experiments revealed enriched levels of PRAME at active promoters that were also bound by the nuclear transcription factor Y (NFY). Recruitment of PRAME was linked to high transcriptional activation of these NFY-loci. Nevertheless, how these novel molecular features of PRAME are implicated in the progression of malignant tumours still remains elusive (Costessi et al., 2011).

2.2. Pramel7 and other PRAME-like proteins

Arisen from gene duplications, 18 *PRAME-like (Pramel)* genes and 15 pseudogenes were predicted in a gene cluster-region on mouse chromosome 4 in the mouse (Birtle et al., 2005). Two members of the *Pramel*-family (*Pramel1* on chromosome 4 and *Pramel3* on the X-chromosome) are described as a group of proteins exclusively expressed in male germ cells of an adult mouse (Wang et al., 2001). A recent work focusing on the expression of *Pramel1* in spermatogenesis shows that its expression in testis starts from week 3 onwards. Developing spermatids exhibit a positive staining in the acrosome and parts of the flagellum, suggesting a hypothetical role for *Pramel1* in the acrosomal development and sperm maturation (Mistry et al., 2013).

In 2003, Bortvin et al. asked why cloned embryos were not surviving as efficiently as normal embryos and hypothesized that cloned embryos may not correctly reactivate certain pluripotency-related genes as *Oct4*. To assess this, the authors aimed at identifying genes in cloned embryos in comparison to normal embryos displaying similar expression changes as *Oct4* and found that a majority of ten identified candidates were not correctly expressed in cloned embryos. Indeed, correct reactivation of *Oct4*-related genes correlated with the efficiency of the embryonic development of blastocysts cloned from either somatic cells or mESCs. Intriguingly, four out of ten candidates encoded proteins of the *Pramel*-family, *Pramel4*, *Pramel5*, *Pramel6* and *Pramel7* whose expression in early embryonic cleavage stages could be shown (Bortvin et al., 2003).

A study from Cinelli et al. demonstrated the generation of germ line competent ESCs from the non-permissive mouse strain *FVB*. These cells ectopically expressed *STAT3*, the key transcription factor crucial for the maintenance of mESCs *in vitro* activated by the cytokine LIF. When comparing the transcriptome of *STAT3*-overexpressing and *wt* FVB ESCs in a microarray experiment a set of 26 differentially regulated genes were isolated including *Pramel7*, exhibiting an upregulation of 8.5-fold in *STAT3*-overexpressing cells. When examining the expression of Pramel7 in the early mouse embryo positive *in situ* hybridization signals were detected in the central part of the morula and the ICM of the blastocyst, the pluripotent compartments of the early embryo. In addition, upon overexpression of Pramel7, mESCs could be maintained in a pluripotent state even in the absence of LIF (Cinelli et al., 2008).

Similar to *STAT3-overexpressing* mESCs, *Pramel7*-expression was also observed to be upregulated also in *Smad4*$^{-/-}$ mESCs. In the early embryo, Smad4 is required for axis patterning. *Smad4-null* embryos arrest shortly after implantation and have a shortened proximodistal axis, a reduced epiblast and a thickened visceral endoderm layer. Concomitantly, *Smad4* mutant mESCs and embryoid bodies display reduced nascent mesoderm markers and enhanced expression of other non-canonical pluripotency markers as *Zscan4* and *Tbx3* whose functions are not precisely defined (Costello et al., 2009).

To confirm that the expression of *Pramel7* is regulated by LIF/STAT3 and to examine the role in self-renewal of mESCs in general, Casanova et al. provided evidence that *Pramel7* is mediating LIF/STAT3-dependent self-renewal in mESCs. Upon ablation of *Pramel7* mESCs began to differentiate, whereas its overexpression blocked the capacity of mESCs to differentiate *in vitro* and *in vivo*. Consequently, *Pramel7*-overexpressing mESCs were not able to participate in the generation of chimeric mice. Interestingly, after transgenic excision of *Pramel7*, mESCs regained this feature. When assessing the differentiation ability of mESCs overexpressing *Pramel7 in vivo* a similar outcome was observed. Upon injection of cells into immuno-deficient mice no teratoma could be generated. On the molecular level, the expression of *Pramel7* was found to be con-

trolled by LIF-signalling via both STAT3-dependent regulation on the transcriptional level and via phosphorylation of glycogen synthase kinase 3ß (GSK3ß), dependent on phosphatidylinositide 3-kinase (PI3K) signalling. Furthermore, upon induced knockdown of Pramel7 mESCs started to differentiate even in the presence of LIF and enforced activation of STAT3. These findings suggest that *Pramel7* is an important and essential gene in the molecular circuitry of the pluripotency maintenance network (Casanova et al., 2011). However, the exact mechanism and the role of the protein Pramel7 *in vitro* and *in vivo* still need to be understood.

3. Ubiquitin-like, containing PHD and RING finger domains, 1 (UHRF1): An important regulator of epigenetic patterning

Before initiating this project we were interested in the molecular function of Pramel7 within the cell. Analysis of the amino acid composition of the protein sequence indicated the absence of DNA-binding domains suggesting that Pramel7 is unlikely to act as a transcription factor. Nevertheless, it was possible to identify the presence of leucine rich repeats (LRRs) implying a role of Pramel7 in protein-protein interaction. As a next step, using the yeast two-hybrid approach, we identified the protein ubiquitin-like, containing PHD and RING finger domains, 1 (UHRF1) as a potential binding partner. The following chapter tries to summarize the most important benchmark data from the last years on UHRF1 describing this multi-functional epigenetic regulator protein.

3.1. Nomenclature and protein architecture

It was in 1998 when Fujimori et al. described NP95 (95kDa Nuclear Protein) as the first member of the UHRF protein family in mouse. After detection of differential expression patterns throughout different stages of the cell cycle it was defined as a "novel nuclear protein in cell cycle progression and/or in DNA replication" (Fujimori et al., 1998). Two years later, Hopfner et al. discovered the human UHRF1 counterpart ICBP90 (Inverted CCAAT-binding protein 90), a 90kDa protein with similar domains as NP95. By yeast one-hybrid screening, ICBP90 was shown to bind the promoter region of topoisomerase IIα and thereby regulate topoisomerase IIα expression. Since the modulation of this gene was thought to enhance the sensitivity to anti-topoisomerase II drugs ICBP90 was selected with the intention to find new anti-cancer drugs and new markers for proliferation. Thus, UHRF1 was assumed to have potential roles in cell proliferation processes and cancer mechanisms (Hopfner et al., 2000). According to the comparable composition of domains, the Human Genome Organization (HUGO) nomenclature committee then assigned the term UHRF1 (Ubiquitin-like, containing PHD and RING finger domains) to both the human and the mouse protein variants. In

the following years additional family members were described (UHRF2 and UHRF3) but up to now the main scientific focus has been on UHRF1.

UHRF1 is a multi-domain protein thought to be involved in cellular processes such as epigenetic control, cell cycle progression or ubiquitination. A schematic overview showing the structure of UHRF1 is illustrated in Fig. 4. The UBL (ubiquitin-like) domain is located the most N-terminally of all UHRF1 domains and can be found in almost all members of the UHRF protein family. The domain *per se* shares 35% homology with ubiquitin. UBL comprises a typical alpha/beta ubiquitin fold. The two surface lysine residues K33 and K52 are structurally conserved with lysine residues of ubiquitin (K29 and K48), which is the key signal for degradation in the proteasome when attached to a target protein in several copies. However, the role of UBL is unclear. Since a transfer of UHRF1's UBL to another protein is unlikely, the domain may rather have a structural role or be involved in protein-protein interactions than actively polyubiquitinating other proteins (Bronner et al., 2007).

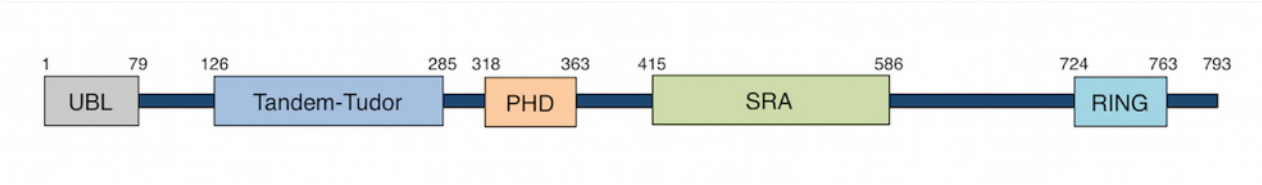

Fig. 4: UHRF1 domain architecture.
UHRF1 is composed of an N-terminal UBL-domain, followed by a Tandem-Tudor and a PHD domain. SRA and RING domains are located most C-terminally. UBL=Ubiquitin-like, PHD=Plant homeodomain, SRA=SET and Ring finger-associated, RING=Really interesting new gene.

Tandem-Tudor and PHD (Plant homeodomain) domains are involved in the recognition of the H3-tail (see Introduction chapter 3.4.1). The SRA (SET and Ring finger associated) domain is able to act as a reader unit for hemimethylated DNA during DNA replication leading to the recruitment of DNMT1 to particular sites and enabling a faithful propagation of DNA methylation (see Introduction chapter 3.4.2). Finally the RING (Really Interesting New Gene) domain possesses E3 ubiquitin ligase activity and might be involved in processes concerning protein degradation (see Introduction chapter 3.3).

3.2. UHRF1 is involved in the maintenance of DNA methylation

3.2.1. UHRF1 is essential for the maintenance of global DNA methylation

Two independent research groups uncovered the biological key function of UHRF1 around the same time in 2007. They proposed a model describing UHRF1 mediating the faithful propagation of DNA methylation patterns from mother to daughter cells during DNA replication. The studies in detail showed that in *Uhrf1*$^{-/-}$ mESCs a substantial global loss of DNA methylation is observed. This loss could not be explained by concomitant reduction of DNA methyltransferases since the

amounts of DNMT1, DNMT3a and 3b were not lowered. In addition, UHRF1 was shown to be physically associated with DNMT1 and a reduction of UHRF1 deleted the association of DNMT1 with chromatin. However, depletion of DNMT1 did not reduce the interaction of UHRF1 with chromatin. Finally, DNMT1 enrichment in heterochromatin could not be observed anymore during the S-phase of the cell cycle in *Uhrf1*$^{-/-}$ mESCs. These findings suggest that UHRF1 has a role in guiding DNMT1 to chromatin (Bostick et al., 2007), (Sharif et al., 2007).

Besides binding to DNMT1, UHRF1 was also shown to interact with the *de novo* DNA methyltransferases DNMT3 and 3b. Meilinger et al. made use of the fact that the CMV promoter is rapidly silenced in mESCs und used the feature as a model for studying the importance of the three molecules in silencing of CMV. First, *DNMT3a*$^{-/-}$*/3b*$^{-/-}$ double and *DNMT1*$^{-/-}$*/3a*$^{-/-}$*/3b*$^{-/-}$ triple knockout mESCs were unable to silence CMV. Knockout of *DNMT1* resulted in only weak CMV silencing indicating a major importance of the de novo methyltransferases DNMT3a and 3b in this process. Surprisingly, complete loss of CMV silencing was observed in *UHRF1*$^{-/-}$ mESCs despite the presence of a full set of functional DNA methyltransferases. These observations emphasize the importance of UHRF1 and DNMT3a/b in the silencing process. In *wt* cells CMV silencing preceded the emergence of DNA methylation. Based on this finding the authors hypothesized that other factors such as the histone methyltransferase G9a may mediate immediate silencing. Indeed, *G9a*$^{-/-}$ cells were unable to induce silencing of the CMV promoter. In consideration of the fact that UHRF1 is able to interact with DNMT3a, DNMT3b and as well G9a these factors might be involved in a common immediate silencing pathway independent of DNA methylation (see Introduction chapter 3.2.3) (Meilinger et al., 2009).

3.2.2. The SRA domain mediates the recognition of hemimethylated DNA

Shortly after Avvakumov et al., Hashimoto et al. and Arita et al. independently deciphered the molecular reading mechanism by which the SRA domain of UHRF1 recognizes hemimethylated CpG (hemCpG) sites emerging during the synthesis of new DNA strands. By doing so, UHRF1 hands over the DNA to DNMT1 by direct interaction ensuring the accurate copy of methylation marks during S-phase of the cell cycle (Arita et al., 2008). In addition, besides hemCpG recognition the SRA domain was shown to be responsible for the mediation of the interaction of UHRF1 with DNMT1 (Achour et al., 2008). The mechanism works by flipping out the methylated CpG from the double helix, placing it into a binding pocket specific for hemCpG and finally filling the resulting gaps in major and minor grooves of the DNA with two specialized SRA loops. The so-called "NKR finger" (Asn-Lys-Arg are present at this specific site) fills the gap in the major groove and is capable of reading the residual opposite nucleotides of the CpG duplex. The resulting gap in the minor groove is filled by the "thumb" which shows no direct interaction with the nucleotides but is linked to the NKR finger via Van der Waals interactions, resulting in a kind of "finger-thumb" grasping

(Avvakumov et al., 2008). As a conclusion, a model for a faithful transfer of the methylation patterns from mother to daughter strands was described in which the SRA domain recognizes a hemCpG-duplex and interacts with the methylated cytosine residue by base-flipping.

3.2.3. Subsequent studies characterizing the epigenetic function of UHRF1

When looking more closely at intracellular UHRF1 dynamics it was found that after photobleaching UHRF1 recovery between *DNMT1*$^{-/-}$ single- and *DNMT1*$^{-/-}$/*3a*$^{-/-}$/*3b*$^{-/-}$ triple-knockout mESC was comparable. This observation indicates that the prevalence of methylated DNA and DNA methyltransferases does not influence the overall binding kinetics of UHRF1 to chromatin. Moreover, recovery after photobleaching was more efficient for DNMT1 than for UHRF1 what was explained with the tight association of UHRF1 with hemCpGs (Rottach et al., 2010).

The histone methyltransferase G9a (EHMT2) is a potent epigenetic regulator involved in transcriptional silencing (Tachibana et al., 2002). G9a was seen to interact with RING and SRA domains of UHRF1, with a higher affinity for RING. As seen in *UHRF1*$^{-/-}$ mESCs lack of UHRF1 lead to decreased amounts of G9a on chromatin, suggesting a role for UHRF1 in the recruitment of G9a to chromatin (Kim et al., 2009). This observation might also affect transcriptional silencing and the generation of heterochromatin.

In a very recent study, Nishiyama et al. found that recruitment of DNMT1 during S-phase is not conveyed solely by direct interaction between DNMT1 and UHRF1, but requires ubiquitination of H3K23 (H3K23ub) mediated by the RING domain of UHRF1. In *Xenopus* egg extracts, depletion of UHRF1 firstly caused a decrease in the recruitment of DNMT1 to chromatin and secondly, reduced DNA methylation. Intriguingly, efficiency and timing of DNA replication were not affected. Reduced amounts of DNMT1 enhanced the presence of UHRF1 on chromatin, most likely due to increased amounts of hemimethylated DNA. Furthermore, it was shown that the RING domain of UHRF1 mediates the ubiquitination of H3 at lysine 23 and DNMT1 specifically interacts with H3K23ub, whereas neither unmodified H3 nor UHRF1 displayed a binding with H3K23ub. In addition, despite a RING-deficient mutant of UHRF1 was seen to co-localize with the replication complex and to form nuclear foci in *UHRF1*$^{-/-}$ HeLa cells, the RING mutant was not able to restore the correct distribution of DNMT1 at nuclear foci. Taken together, ubiquitination of H3 by UHRF1 provides the platform for recruiting DNMT1 to sites of DNA replication (Nishiyama et al., 2013).

3.3. The C-terminal RING domain and its function as an E3 ubiquitin ligase

RING domains are small Zn-binding domains frequently linked with ubiquitin ligase activity (Freemont, 2000), (Pickart, 2001). Ubiquitin (Ub) is a 76AA protein and has pivotal roles in protein degradation, transcriptional regulation or gene transcription when attached to other proteins in one

or several copies (Sun, 2003), (Kerscher et al., 2006). Its activation occurs through the formation of a thiol ester bond with the Ub-activating enzyme (E1) followed by the transfer to an E2-Ub-conjugating enzyme and finally its attachment to the substrate by an E3 ubiquitin ligase complex (Haas et al., 1982). E3 ligase complexes assign specificity to the reaction since they are able to recognize and select for different substrates (Citterio et al., 2004). The biological consequences of ubiquitination processes are diverse and depend on the number of Ub molecules added to the target protein. Monoubiquitination of histones for example can lead to chromatin remodelling causing alterations in transcription. However, the most common ubiquitin modification is polyubiquitination where several Ub molecules are added to a substrate, leading to its degradation in the 26S proteasome (Jenkins et al., 2005), (Kerscher et al., 2006).

UHRF1 was observed to ubiquitinate all core histones, with a preference towards H3 (Citterio et al., 2004). Previous to this, ubiquitination of histones had only been described for elongating spermatids where it was thought to relax the nucleosome structure facilitating the access for the transcription machinery or restructuring chromatin (Chen et al., 1998). Jenkins et al. later on described autoubiquitination activity of UHRF1 mediated by the RING domain (Jenkins et al., 2005).

As mentioned above, UHRF1 recruits DNMT1 to hemimethylated DNA at replication forks. Interestingly, UHRF1 is also able to ubiquitinate DNMT1 priming it for proteasomal degradation. In this interplay, a protein called USP7 (HAUSP, Ubiquitin carboxyl-terminal hydrolase 7) holds an important role. USP7 was demonstrated to first interact with and then deubiquitinate DNMT1 and thus preventing DNMT1 from proteasomal degradation. In addition, acetylation of DNMT1 by the acetyltransferase Tip60 was illustrated to stimulate proteasomal degradation of DNMT1. Based on these findings, it was hypothesized that during DNA replication DNMT1 is guided to hemimethylated DNA by UHRF1. In this time frame, the activity of UHRF1-RING is inhibited either by direct interaction with USP7 or indirectly by continuous deubiquitination of DNMT1 by USP7. The whole mechanism is thought to proceed as follows. During DNA replication DNMT1 is found associated with UHRF1, Tip60 and USP7, in which the latter two stabilize DNMT1 by deacetylation and deubiquitination. After completion of DNA replication, USP7 dissociates from the complex and Tip60 acetylates DNMT1 serving as a stimulus for UHRF1 to polyubiquitinate DNMT1, inducing proteasomal degradation of DNMT1 in G2 (Fig. 5) (Du et al., 2010). Felle et al. later confirmed the interactions between UHRF1, USP7 and DNMT1. However, when performing DNA digestion preceding immunoprecipitation, the binding of USP7 to UHRF1 was significantly reduced, in contrast to USP7-DNMT1 that remained very stable, even in a soluble environment. Thus, when detached from chromatin USP7 was suggested to be found in a stable dimeric complex with only DNMT1 whereas when present on chromatin a trimeric complex including USP7, DNMT1 and UHRF1 is formed. Furthermore, USP7 can deubiquitinate UHRF1 leading to reduced proteasomal degradation and stabilization of UHRF1 levels. Therefore, USP7 might act as an amplifying and

supporting module in the stabilization and faithful maintenance of DNA methylation patterns within the trimeric complex USP7-DNMT1-UHRF1 (Felle et al., 2011).

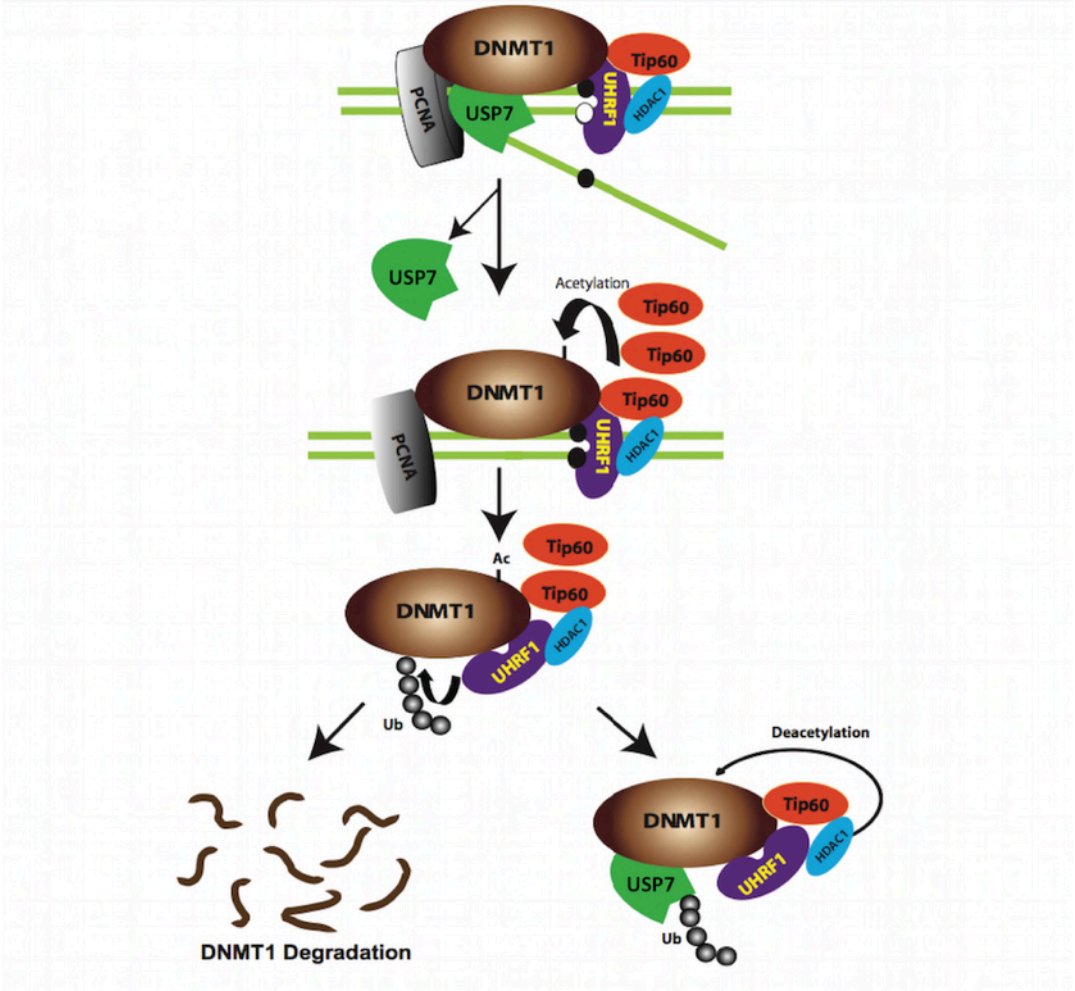

Fig. 5: Mechanistic model describing a complex mediating the faithful propagation of DNA methylation patterns during the S-phase of the cell cycle.
During DNA replication DNMT1 is associated with UHRF1, Tip60 and USP7. USP7 and Tip60 stabilize DNMT1 by deacetylation and deubiquitination. After completion of DNA replication USP7 dissociates from the complex and Tip60 acetylates DNMT1, stimulating UHRF1 to polyubiquitinate DNMT1, inducing proteasomal degradation of DNMT1 in G2. From Du et al., 2010, modified.

How UHRF1 is molecularly targeted for degradation was clarified in a more recent work. The respective study identified the $SCF^{ß\text{-}TrCP}$ E3-ligase complex to be responsible mediating the ubiquitination and subsequent proteasomal degradation of UHRF1. In addition, in the N-terminal region of UHRF1, a phosphodegron was identified and phosphorylation of S108 was found to be crucial for UHRF1 ubiquitination by $SCF^{ß\text{-}TrCP}$. A phosphodegron is defined as a protein site that gets unstructured upon phosphorylation, what is the sign for the degradation process to initiate (Schrader et al., 2009). When UHRF1 S108 was not phosphorylated, no interaction of UHRF1 and $SCF^{ß\text{-}TrCP}$ could be observed. The kinase responsible for the phosphorylation was deciphered as CK1∂ (Casein kinase isoform ∂) triggering UHRF1 ubiquitination by $SCF^{ß\text{-}TrCP}$ (Chen et al., 2013). CK1∂ is an essential serine/threonine-protein kinase regulating various cellular growth and survival processes in-

cluding Wnt-signalling, DNA repair and circadian rhythms (Peters et al., 1999), (Hoekstra et al., 1991), (Etchegaray et al., 2009). To summarize, the interplay between protein-protein interactions and ubiquitination reactions maintain a correct homeostasis of the molecular participants involved in the faithful maintenance of DNA methylation and possibly histone modifications. Nevertheless, the exact mechanisms modulating the levels of UHRF1 are still unclear.

3.4. PHD- and Tandem-Tudor domains are recognizing the N-terminal tail of H3

3.4.1. PHD fingers can read the histone code

PHD fingers consist of a conserved zinc finger motif and exist in numerous chromatin regulators. Moreover, they were shown to play a role in many biological processes like reading of the histone code (Shi et al., 2006) or E3 ubiquitin binding (Dul and Walworth, 2007). For a long time this particular structure was thought to be involved in protein-protein interactions until it was demonstrated that the PHD finger of the histone acetyltransferase p300 interacts with its neighbouring bromodomain in binding histones. Both domains were observed to interact with nucleosomes while also interconnect with each other (Ragvin et al., 2004). Nowadays a reasonable number of works have been published linking PHD fingers to interactions with differentially modified H3 tails and thus to gene repression, transcriptional activation and chromatin dynamics (Eberharter et al., 2004), (Martin et al., 2006), (Vermeulen et al., 2007), (Palacios et al., 2008). Many H3 binding proteins carrying a PHD finger are macromolecules with own catalytic activity (e.g. histone methyltransferases or demethylases). Other PHD proteins function as scaffolding molecules linking enzymatic complexes with other subunits to particular regions in the genome. Therefore, many of these proteins are able to induce changes in the chromatin state. Even though most publications describe interactions of PHD domains with H3, there are studies demonstrating the ability of PHD fingers to bind to non-histone proteins. This increases the complexity of biological effects mediated by PHD domains. Moreover, most of the PHD domains are found in molecules containing more than one PHD finger or other features capable of reading the epigenetic code, for example chromodomains, bromodomains or the Tandem-Tudor domain of UHRF1. Taken together, PHD domains are manifold elements changing chromatin state and thus rule crucial intracellular DNA-based processes such as transcription or epigenetic silencing (Musselman and Kutateladze, 2011).

3.4.2. The Tandem-Tudor domain recognizes modifications of the H3-tail

When screening databases it became evident that the sequence between UHRF1 UBL- and PHD domains contains a conserved region with high structural similarity to the family of Tudor domains (Rottach et al., 2010). Hallmarks of this class of domains are two subdomains (Tandem-Tudor) creating an aromatic cage formed by three highly conserved amino acids (Phe152, Tyr188 and Tyr191 in UHRF1) resulting in a hydrophobic pocket able to place an H3K9me3 N-terminal tail. A similar

feature is shown for the chromodomain of heterochromatin protein 1ß (HP1ß), which also interacts with H3K9me and is important in the establishment of pericentric heterochromatin. One of the structurally resolved Tandem-Tudor domains is incorporated in the Lysine-specific demethylase 4A (KDM4A, JMJD2A), a member of a histone demethylase superfamily (Tsukada et al., 2006). This specific hybrid Tandem-Tudor domain possesses the capacity of interacting with two distinct peptides, H3K4me3 and H4K20me3, with the same affinity while two adjacent arginine residues, R2 and R19, are stabilizing the binding (Lee et al., 2008). These findings imply that the Tandem-Tudor domain can potentially recognize different combinations of H3 modifications at one time what highlights the complexity of methyl-lysine recognition (Adams-Cioaba and Min, 2009).

3.4.3. UHRF1 in targeting the N-terminal H3-tail

In 2004 Citterio et al. showed that UHRF1 is able to interact with histones showing a strong preference for histone H3, followed by histone H1 and histone H2B. Interactions were mediated by the N-terminal tails of histones (Citterio et al., 2004).

There are numerous proteins with known methyltransferase activity against H3K9, including G9a, SUV39H1, SUV39H2, ESET/SETDB1 or EuHTMase1 (O'Carroll et al., 2000), (Ogawa et al., 2002), (Rea et al., 2000), (Schultz et al., 2002), (Yang et al., 2002). Although they recognize the same PTM, there are relevant differences concerning their distribution, chemistry and molecular roles. PTMs catalysed by the above enzymes can in turn be removed by specific histone demethylases like Kdm4c, Jmid2b or Jhdm3a (Cloos et al., 2006) (Fodor et al., 2006), (Klose et al., 2006).

Karagianni et al. could localize UHRF1 to heterochromatic regions enriched in H3K9me3. Indeed, this PTM was shown to be required for proper heterochromatic localization of UHRF1. MEFs deficient for the histone methyltransferase *Suv39h*$^{-/-}$ or NIH3T3 cells overexpressing the histone demethylase JMJD2A, both exhibiting defects in the methylation of H3K9, lost the typical heterochromatic pattering of the chromatin and the signal intensity for UHRF1 was lowered. In addition, Bartke et al. showed that in the context of mCpG, UHRF1 interaction with nucleosomes carrying H3K9me3 methylation was much stronger than with H3K9me3 in unmethylated DNA regions (Bartke et al., 2010) indicating a supportive effect of H3K9me3 on the localization of UHRF1.

When UHRF1 Tandem-Tudor is isolated from the full-length protein, in comparison to other H3 PTMs a highly significant preference for H3K9me3 was observed (Rottach et al., 2010). However, this effect was less prominent for the full-length version of the protein. Interestingly, the presence of acetylated H3K9 (H3K9ac, activation mark) inhibited the interaction with Tandem-Tudor. It also became evident that the binding of Tandem-Tudor and H3K9me3 additionally required H3K4 in an unmodified or monomethylated state whereas di- or trimethylated H3K4 (activation mark) fully abolished the interaction. These findings suggest that UHRF1 is enriched at genomic sites harbouring the H3K4/H3K9me3 signature. The enrichment is potentiated by the presence of methylated

DNA (Nady et al., 2011). Nonetheless, it is difficult to draw conclusions from assays using only single UHRF1 domains since in context of the full-length protein observed effects might be altered by the presence of other functional domains. Follow-up studies revealed that the PHD domain specifically recognizes unmodified H3R2 while Tandem-Tudor targets H3K9me3. Different experiments showed that Tandem-Tudor is necessary but not sufficient for the recognition of the whole H3 tail. Summarizing, it is assumed that the PHD domain by interacting with unmodified H3R2 mediates the overall binding activity of the whole protein and that Tandem-Tudor confers binding specificity by targeting H3K9me3 (Cheng et al., 2013), (Liu et al., 2013).

A recent study systematically tried to assess to what extent the H3-binding Tandem-Tudor and the hemCpG-binding SRA domains are providing binding strength to the interaction of UHRF1 to chromatin. Moreover, it was of interest how strong the two domains influence the targeting of DNMT1 to the replication fork and the maintenance of DNA methylation in general. To achieve this, different mutants were generated either defective in H3K9 recognition (Tandem-Tudor mutant) or hemCpG binding (SRA-mutant). Surprisingly, when transfected in *UHRF1*$^{-/-}$ mESCs, both mutants were able to partially rescue heterochromatin association, DNMT1 recruitment and even DNA methylation. However, when expressing a Tandem-Tudor/SRA double mutant in *UHRF1*$^{-/-}$ mESCs, rescue of neither of the above features was observed. This leads to the conclusion that in *UHRF1*$^{-/-}$ mESCs UHRF1 can at least partially target DNMT1 to DNA replication sites through unconnected recognition of the H3-tail on the newly assembled nucleosomes and/or hemCpG on the nascent DNA (Liu et al., 2013).

Aim of the work

To shed light into the molecular role of Pramel7 in the maintenance of pluripotency, following aims are addressed.

- Confirm the interaction between Pramel7 and UHRF1 and identify other potential binding partners.

- Characterize domains of UHRF1 and Pramel7 necessary for the formation of a complex between the two proteins.

- Study potential epigenetic effects induced by *Pramel7* overexpression in HEK293T cells and pluripotent and differentiating mESCs.

- Characterize the function of Pramel7 in the maintenance of pluripotency *in vitro* and draw conclusions for the mouse development *in vivo*.

B. Results

1. Discovering interaction partners of Pramel7

The novel protein Pramel7 is found expressed in the central part of the morula and the inner cell mass of the blastocyst exclusively, the pluripotent compartments of the early embryo (Cinelli et al., 2008). Moreover, for *Pramel7*-overexpression a supportive effect on the maintenance of pluripotency is described in murine embryonic stem cells (mESCs) (Casanova et al., 2011). However, the exact molecular function of Pramel7 remains unclear.

1.1. Screening for potent interaction partners

An initial search for conserved protein motifs in the open reading frame of Pramel7 using the *LRR finder* software revealed the existence of three leucine rich-repeat (LRR) structures (Fig. 6A, 1-3). However, additional re-screening with the *LRR search* programme uncovered three other potentially important LRRs (Fig. 6A, 4-6). Re-screening was made after analysing the outcome of immunoprecipitation experiments described in chapter 1.5 (Results).

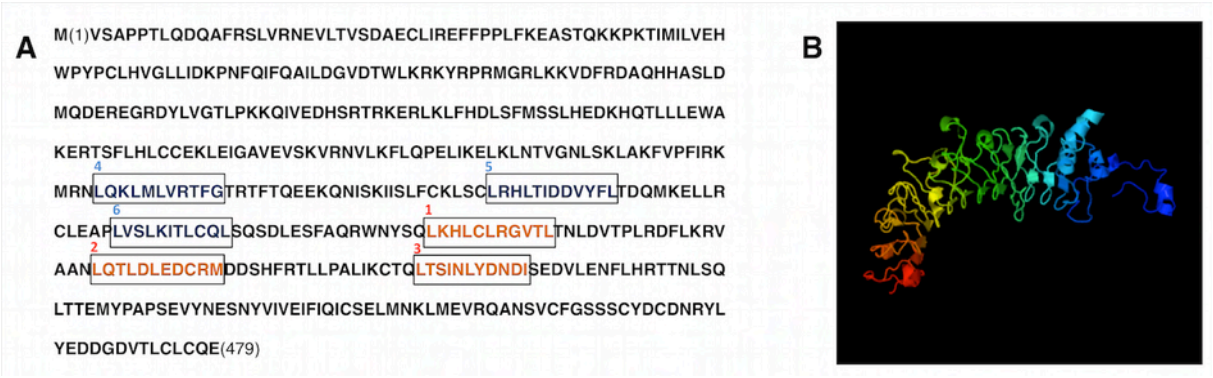

Fig. 6: Pramel7 protein sequence with predicted LRRs and protein model.
A: Pramel7 protein sequence with predicted LRRs. LRRs discovered in the initial screening are labelled in orange (1-3) (www.lrrfinder.com). LRRs identified by re-screening are coloured in blue (4-6) (www.lrrsearch.com). **B:** Predicted protein model designed with the Phyre2 software (Kelley and Sternberg, 2009). LRR=leucine rich repeat.

LRRs are 20-30 amino acids long sequence motifs and consist of a N-terminally conserved sequence of eleven residues rich in leucines at defined positions (LxxLxLxxNxL, x is any amino acid). The asparagine and the leucine residues can be substituted by any hydrophobic amino acid. This conserved N-terminal region of the LRR is forming a ß-sheet and a loop-region leading to the C-terminal part that is more variable in structure and sequence. LRRs are present in many proteins and participate in protein-protein interactions in various cellular processes and locations (Kobe and Deisenhofer, 1994), (Kajava, 1998). Moreover, since no DNA-binding domain typical for transcription factors was identified, Pramel7 and other members of the family of PRAME-proteins might be involved in protein-protein interactions rather than regulate the

transcription of genes by direct binding to the DNA. In order to identify a specific interaction partner of Pramel7, a yeast two-hybrid assay was performed. A bait consisting of the full-length Pramel7-LexA fusion protein was used to screen a library containing cDNA generated from the whole transcriptome of *wt E14* mESCs. After successful isolation of five clones, sequence analysis of three of the clones revealed that all represented the coding sequence of a protein involved in epigenetic regulation, UHRF1 (Fig. 7). The lacZ signal from UHRF1-clones was substantially stronger than the signal of the two residual clones suggesting that UHRF1 might be a potent interaction partner of Pramel7. Since this interaction had never been shown before, the binding of Pramel7 and UHRF1 had to be verified in a less artificial system than yeast two-hybrid.

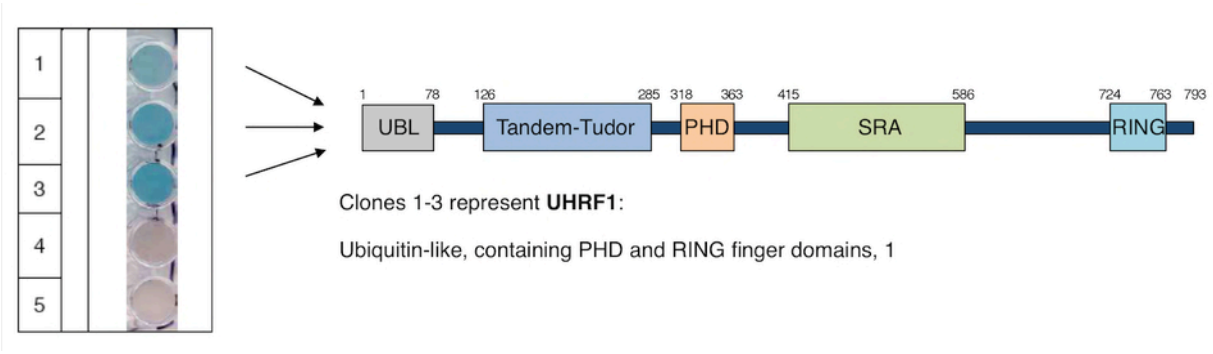

Fig. 7: A yeast two-hybrid screen reveals UHRF1 as a possible binding partner of Pramel7.
Yeast two-hybrid assay: Bait: Pramel7. Bait vector: Full-length & truncated pLexA-dir. Prey: cDNA library of *E14* mESCs. Prey vector: pGAD-HA. Plasmid isolation: 5 clones. Successful plasmid rescue: 5 clones. 3 clones (1-3) represent UHRF1.

1.2. Generation of a polyclonal antibody specifically recognizing Pramel7

Because of lack of commercial availability, we next decided to generate an antibody recognizing Pramel7 as a tool for immunodetection of the protein (in collaboration with Pineda Antikörper Service, Berlin, Germany). In a sequence alignment of Pramel7 and other members of the *PRAME*-gene family we screened for unique sequences suitable as epitopes for the antibody, revealing peptide sequences 4b and 5 as most convenient (Fig. 8A).

Three rabbits were immunized with either peptide and the final antibody fraction of animal 2 immunized with peptide 5 was successfully tested using Western Blotting and immunohistochemistry on HEK293T cells transfected with a plasmid ectopically expressing *Pramel7* (Fig. 8B). However, the antibody was not able to recognize endogenously expressed Pramel7 in *wt E14* mESCs. This is most likely due to endogenous expression levels under a detection threshold. Nevertheless, a new tool in the analysis of Pramel7 has become available.

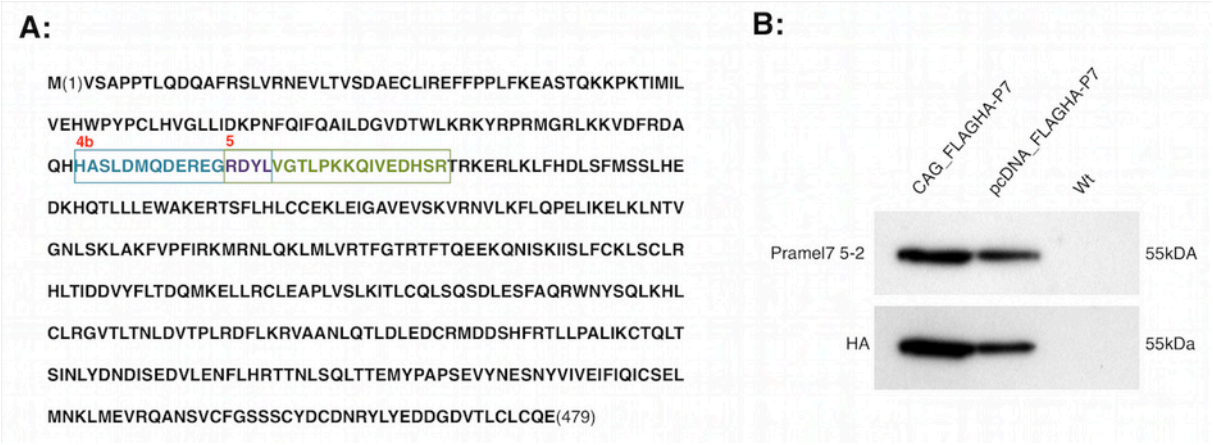

Fig. 8: Selected epitopes for antibody generation and testing of final antibody fraction.
A: Pramel7 protein sequence with selected epitopes 4b and 5. **B:** After immunization of 3 animals with either peptide the final antibody fraction of animal 2 immunized with peptide 5 (Ab 5-2) was selected and successfully tested by Western blotting. (Ab=antibody).

1.3. Pramel7 is interacting with UHRF1 in HEK293T cells and mESCs

To prove the interaction of Pramel7 and UHRF1 not only with the artificial yeast two-hybrid approach but also in a living mammalian cell, we made use of HEK293T cells. First a *FLAGHA*-tagged version of *Pramel7* was cloned into an expression plasmid driven by a CMV promoter *(pcDNA3.1_FLAGHA-P7)*. Expression of the plasmid was successfully tested using Western blotting of protein lysate from HEK293T cells transfected with the plasmid. While co-expressing mouse UHRF1 *(pCMV_Sport6_UHRF1)*, subsequent co-immunoprecipitation (co-IP) against FLAG-Pramel7 followed by SDS-PAGE and Western blotting revealed a strong interaction of the two proteins (Fig. 9A). To confirm these results, *FLAGHA* was cloned in front of the N-terminus of *UHRF1* and expressed under the *pcDNA3.1* expression plasmid backbone. In turn, in agreement with the previous Western blot, upon co-transfection with a plasmid expressing untagged *Pramel7* followed by co-IP anti-FLAG, a strong co-precipitation of FLAG-UHRF1 and Pramel7 was obtained (data not shown). Moreover, in a third assay, Pramel7 was able to precipitate endogenous human UHRF1 from HEK293T cells. This suggests a high specificity and a cross-species conservation of the protein domain in UHRF1 responsible for this interaction (Fig. 9C). After these observations in HEK293T cells, we were interested if the interaction could also be shown in mESCs. To achieve this, *E14* mESCs cultivated in complete medium +LIF (CM+LIF) and in parallel *129* mESCs grown in N2B27 medium +2i +LIF were electroporated with a construct expressing *FLAGHA-Pramel7* (*CAG* promoter driven) and positively selected clones were expanded. After determining the expression levels of *Pramel7* by RTQ-PCR and Western blotting, clones with the highest *Pramel7* overexpression levels were selected for the experiment. However, subsequent IP anti-FLAG-Pramel7 did not reveal a positive signal for UHRF1 in the output fractions from both cell types, *E14* and *129*. Therefore, we decided to change the

Pramel7-expression plasmid and replaced the *CAG* with an *EF1* promoter *(EF1_FLAGHA-P7)*. *Wt E14* mESCs were again electroporated and positive clones selected and expanded. After characterization, *wt E14* and *EF1_HAFLAG-P7* mESCs were cultivated in self-renewing conditions (CM+LIF) and collected. After IP anti-FLAG-Pramel7 low levels of UHRF1 could be detected in the output fractions of *Pramel7*-overexpressing mESCs (Fig. 9B). Why the interaction was not detected in *E14 CAG_FLAGHA-P7* and in *129 CAG_FLAGHA-P7* mESCs remained elusive.

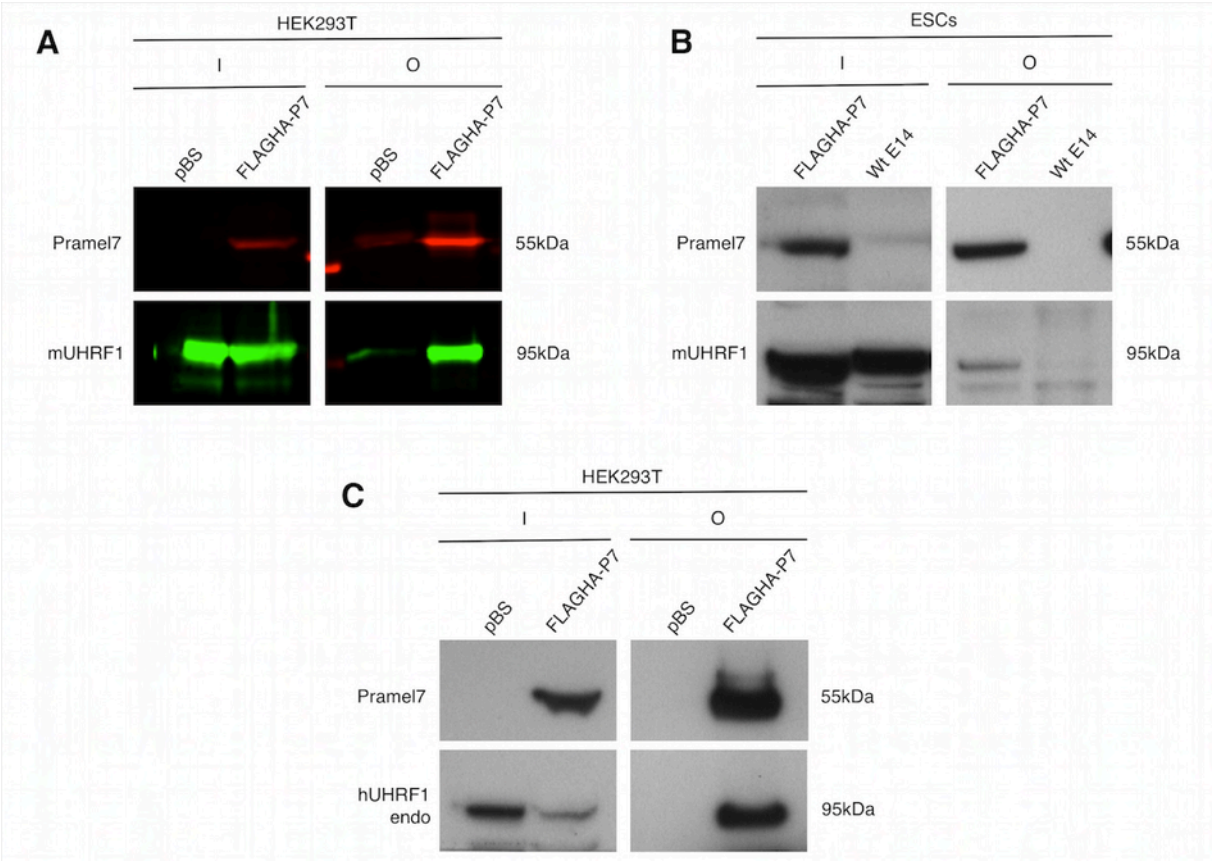

Fig. 9: Pramel7 interacts with UHRF1 in HEK293T cells and mESCs.
A: FLAGHA-Pramel7 was co-expressed with murine UHRF1 in HEK293T cells and IP was performed anti-FLAG. **B:** FLAGHA-Pramel7 was stably overexpressed in wt E14 mESCs (*EF1* promoter), IP was performed anti-FLAG-Pramel7 and endogenous UHRF1 was detected in the output. **C:** FLAGHA-Pramel7 was expressed in HEK293T cells, IP was performed anti-FLAG-Pramel7 and endogenous UHRF1 was detected in the output. P7=Pramel7, I=input, O=output.

Taken together, for the first time, this novel interaction could be demonstrated in the mammalian system. The specific binding of the two proteins suggests a hypothetical role for Pramel7 in modifying the epigenetic regulation of the cell.

1.4. Mass spectrometry reveals additional binding partners of Pramel7-UHRF1

As the interaction of Pramel7 and UHRF1 could successfully be verified in HEK293T and mESCs, we were next interested if other proteins could be identified in the complex. After transfection of *pcDNA3.1_FLAGHA-P7* in HEK293T cells and subsequent IP anti-FLAG-Pramel7, the

protein fractions from the outputs were eluted. After precipitation of eluates with TCA, dried protein fractions were finally analysed by mass spectrometry. Interesting candidates are listed in Tab. 2. First, confirming the data obtained in 1.3, we were able to identify the endogenous human form of UHRF1 from HEK293T cells in the output of the IP. Furthermore, various types of histones were detected, such as H3.3, a histone variant of the canonical H3 and marker for transcriptional activation, and canonical histones H2A and H4. In addition, a protein named Transcription elongation factor B polypeptide 1 (TCEB1) could be identified. Its alternative name is ElonginC, which was reported to either be involved in the activation of transcription elongation (Garrett et al., 1994) or, by directly interacting with PRAME, to potentially act as a component of a Cullin-RING ligase complex (CRL), targeting substrate proteins for proteasomal degradation via attachment of Polyubiquitin peptides (Costessi et al., 2011). Finally, Polyubiquitin itself was detected in the FLAG-Pramel7 precipitate, giving evidence that Pramel7 could have a similar role in recognizing a specific substrate that is subsequently targeted for proteasomal degradation. The detection of histones may indicate a possible presence of Pramel7 at the chromatin.

Tab. 2: Mass spectrometry data IP anti-FLAG-Pramel7 in HEK293T cells.
Eluted IP-outputs were TCA-precipitated and fractions of FLAG-Pramel7 and pBS-control IPs were analysed by mass spectrometry. Pept.=number of peptide hits. Probability: over 95%. Mass spectrometry was performed at the Functional Genomics Center, Zurich (FGCZ).

Protein name	Protein ID	FLAG-Pramel7 (pept.)	pBS control (pept.)	database
E3 ubiquitin-protein ligase UHRF1	sp Q96T88	3	0	swiss human
Histone H2A type 2	sp A1A4R1	2	0	swiss human
Histone H3.3	sp A2XHJ3	1	0	swiss human
Histone H4	sp P08436	3	0	swiss human
BTB/POZ domain-containing protein KCTD5	sp Q9NXV2	4	0	swiss human
Transcription elongation factor B (SIII) (ElonginC)	gi 109495363	3	0	swiss human
Heterogeneous nuclear ribonucleoprotein U	gi 125991756	4	0	swiss human
Polyubiquitin	gi 2627129	6	0	ncbi

Next, we intended to elucidate if the presence of Pramel7 might lead to differential binding of UHRF1 to its interactor proteins. Therefore, IP and co-IP anti-FLAG-UHRF1 was performed either in presence (co-transfection with *CAG_P7*, untagged) or absence of Pramel7. The different outputs were analysed by mass spectrometry. As visible in Tab. 3, Pramel7 was pulled down in the corresponding sample. In both fractions (+/- Pramel7), independent of the presence of Pramel7, various histones and histone complexes could be found. Therefore, these proteins most likely represent binding partners of UHRF1. Moreover, Poly (ADP-ribose) polymerase 1 PARP1 (ARTD1) was detected in both approaches, a multifunctional protein managing the structure and the function of high-order chromatin by on one hand binding to core histones and on the other hand poly-ADP-ribosylating other proteins that govern transcriptional processes (Pinnola et al., 2007). This leads to a supportive effect on heterochromatin formation and thus to prevention of gene transcription. XRCC5 (X-ray repair cross-complementing protein 5, Ku80) and XRCC6 (X-ray repair cross-complementing protein 6, Ku70) together are building dimers with major functions in DNA repair, in the regulation of transcription of specific genes, apoptosis, regulation of the cell cycle and telomere maintenance (Tuteja and Tuteja, 2000). SMARCA5 (SWI/SNF-related matrix-associated actin-dependent regulator of chromatin subfamily A member 5) was seen to have an essential role in chromatin remodelling complexes (CHRAC, RSF, ACF/WCRF, WICH). The WICH complex for example was reported to regulate the transcription of various genes. In addition, roles in RNA polymerase I- and RNA polymerase III-mediated transcription and in the maintenance of chromatin structures during DNA replication were reported (Dirscherl and Krebs, 2004).

Tab. 3: Mass spectrometry data IP anti-FLAG-UHRF1 (+/- Pramel7) in HEK293T cells (1).
Eluted IP-outputs were TCA-precipitated and fractions of FLAGHA-Pramel7 and pBS-control IPs were analysed by mass spectrometry. Pept.=number of peptide hits. Probability: over 95%. Numbers in (): probability <95%. Mass spectrometry was performed at the Functional Genomics Center, Zurich (FGCZ).

Protein name	Protein ID	FLAG-UHRF1/P7 (pept.)	FLAG-UHRF1/pBS (pept.)	pBS control (pept.)	Database
E3 ubiquitin-protein ligase UHRF1	Q96T88	5	12	0	swiss human
PRAMEl7	Q810Y8	1	0	0	uniref
Poly (ADP-ribose) polymerase 1 PARP1	P09874	9	11	0	swiss human
Histone H1.3	P16402	5	9	0	swiss human
Histone H2A type 1-C	Q93077	6	22	(1)	swiss human

Tab.3: Mass spectrometry data IP anti-FLAG-UHRF1 (+/- Pramel7) in HEK293T cells (2).

Protein name	Protein ID	FLAG-UHRF1/P7 (pept.)	FLAG-UHRF1/pBS (pept.)	pBS control (pept.)	Database
Histone H2A.Z	P0C0S5	2	5	0	swiss human
Histone 3.1	P68431	10	15	(1)	swiss human
Histone H4	P62805	7	17	0	swiss human
X-ray repair cross-complementing protein 5 (XRCC5)	P13010	11	19	0	swiss human
X-ray repair cross-complementing protein 6 (XRCC6)	P12956	9	19	0	swiss human
Polyadenylate-binding protein 1 PABP1	P11940	7	7	(1)	swiss human
DNA-dependent protein kinase catalytic subunit PRKDC	P78527	6	11	0	swiss human
Probable ATP-dependent RNA helicase DDX5	P17844	3	2	0	swiss human
ADP/ATP translocase 2 SLC25A5/ADT2	P05141	2	3	0	swiss human
Single-stranded DNA-binding protein, mitochondrial	Q04837	3	2	0	swiss human
Transcription factor A, mitochondrial (TFAM)	Q00059	2	2	0	swiss human
SWI/SNF-related matrix-associated actin-dependent regulator of chromatin subfamily A member 5 SMARCA5/SMCA5	O60264	2	1	0	swiss human
FACT complex subunit SPT16/SUPT16H	Q9Y5B9	3	0	0	swiss human
Nuclear migration protein nudC	Q9Y266	1	(1)	0	swiss human
Chromobox protein homolog 3 CBX3 (HP1γ)	Q13185	3	0	0	swiss human
Chromodomain-helicase-DNA-binding protein 4 CHD4	Q14839	2	0	0	swiss human
Transcription elongation factor B polypeptide 1 TCEB1 (ElonginC)	Q15369	2	0	0	swiss human

Tab.3: Mass spectrometry data IP anti-FLAG-UHRF1 (+/- Pramel7) in HEK293T cells (3).

Protein name	Protein ID	FLAG-UHRF1/P7 (pept.)	FLAG-UHRF1/pBS (pept.)	pBS control (pept.)	Database
Eukaryotic translation initiation factor 3 subunit I EIF3I	Q13347	1	0	0	swiss human
RNA-binding protein 39 RBM39	Q14498	1	0	0	swiss human
DNA topoisomerase 2-alpha TOP2A	P11388	1	0	0	swiss human
Elongation factor 2 EF2/EEF2	P13639	0	1	0	swiss human
Puromycin N-acetyltransferase (CAG-vector)	P13249	3	0	0	uniref
Polyubiquitin-B	P0CG47	2	3	(1)	swiss human

Following candidates were exclusively isolated in the protein fraction containing co-expressed *Pramel7*. Thus, their presence could hypothetically be dependent on the presence of Pramel7. SPT16 is one of two subunits assembling the FACT complex (SPT16 & SSRP1). FACT was shown to alleviate the transition of RNA polymerase II along the DNA by removing an H2A-H2B dimer, facilitating transcription (Orphanides et al., 1998). In addition, the FACT complex was reported to interact with PARP1. PARP1 poly-ADP-ribosylates SPT16, leading to enhanced dissociation of FACT from the chromatin and therefore reduced transcriptional activity (Huang et al., 2006). CBX3 (heterochromatin protein 1 homolog γ, HP1γ) represents another interesting candidate. The family of HP1 proteins is generally linked to support the formation of heterochromatin (Grewal and Moazed, 2003). However, other studies shed light on a different function where HP1γ is observed to predominantly localize to euchromatic regions (Fanti et al., 2003). Moreover, HP1γ is found to associate with a set of transcribed genes. In mammalian cells, the protein is enriched at coding regions of transcribed genes (Vakoc et al., 2005). Interestingly, even a direct link between HP1γ and FACT complex was described wherein HP1γ links FACT complex to RNA Polymerase II, resulting in transcription elongation in a subset of genes (Kwon et al., 2010). All these findings suggest that HP1γ might function not only in the formation of heterochromatin and thus silencing of genomic regions but also has a crucial role in euchromatic regions, supporting active gene transcription. When screening all factors identified in the IP anti-FLAG-UHRF1 with co-expressed Pramel7, TCEB1 (ElonginC) was the only protein also detected in the IP anti FLAG-Pramel7 (Tab. 2), providing further evidence that this

factor could specifically be dependent on the presence of Pramel7. Furthermore, we identified Polyubiquitin in the output fractions from both FLAG-UHRF1 IPs (+/- Pramel7). To in part verify the data of this proteomic mass spectrometry assay the outputs of an IP anti-FLAG-Pramel7 in HEK293T cells were loaded on an SDS gel and two of the identified candidates, H3 and PARP1, were successfully detected of by Western blotting (Fig. 10).

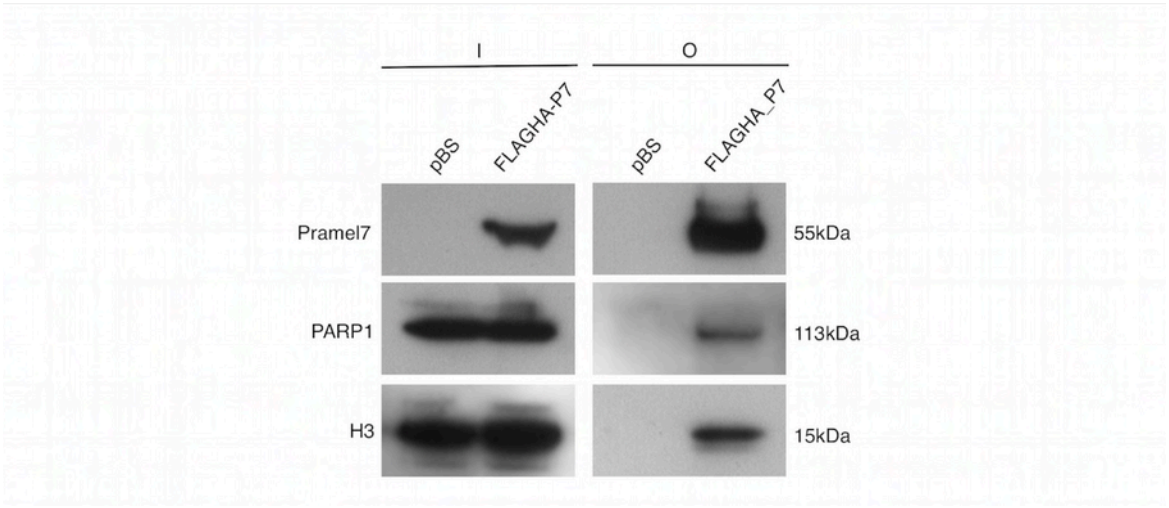

Fig. 10: Verifying binding partners of Pramel7-UHRF1 identified in the mass spectrometry assay. FLAG-Pramel7 was expressed in HEK293T cells, IP was performed anti-FLAG-Pramel7 and endogenous PARP1 and H3 were detected in the output fractions. I=input, O=output, pBS=pBluescript.

1.5. Mutated forms of Pramel7 show impaired binding to UHRF1

To assess the impact of the region in Pramel7 containing the three identified LRRs on the interaction with UHRF1, three different *FLAGHA*-tagged expression constructs with major and minor deletions in the LRR area were generated. The smallest deletion has a length of 33 amino acids (AA) covering one LRR (Fig. 11B). The 61AA deletion lacks two LRRs (Fig. 11C). The largest deletion affects three potential LRRs and is 82AA long (Fig. 11D). Co-IP anti FLAG-Pramel7 and identification of UHRF1 levels in the output fractions revealed that all three mutations, regardless if 33, 61 or all 82AA were deleted, showed a substantial decrease in bound UHRF1 protein at similar levels, leading to the conclusion that the LRR crucial for the interaction most likely is located within the smallest 33AA protein fragment (Fig. 12, left). To verify this, a control construct lacking 63AA located N-terminally of the deletion area was generated (Fig. 11E). Interestingly, the control mutant could only partly restore, but not completely rescue the interaction (Fig. 12, right). An additional round of screening using another software (*LRR search*, www.lrrsearch.com) revealed three other LRRs located in the control region (Fig. 11, LRRs 4-6). This explains the only partial recovery of precipitated UHRF1 levels by the control mutant.

Fig. 11: Generation of mutated forms of Pramel7 containing deletions in the predicted LRR region.
A: Full-length Pramel7 (FLAGHA-FL). **B:** 33AA deletion (FLAGHA-33) (green area deleted). **C:** 61AA deletion (FLAGHA-61) (green and red areas deleted). **D:** 82AA deletion (FLAGHA-82) (green, red and orange areas deleted). **E:** 63AA control mutation (FLAGHA-63 C) (blue area deleted). Blue area: N-terminal control deletion. LRRs are marked by rectangles labelled with red numbers (blue numbers for additionally identified LRRs in the control region). Dotted rectangles indicate partially deleted LRRs.

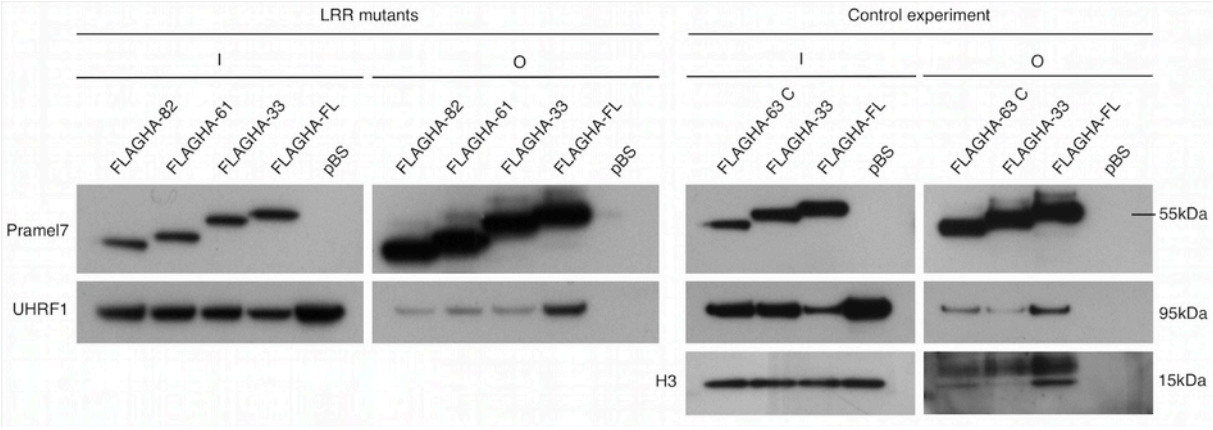

Fig. 12: UHRF1 binding ability of mutated forms of Pramel7 described in Fig. 11.
Left: IP with LRR mutants. FLAGHA-tagged mutant forms of Pramel7 were co-expressed with UHRF1 in HEK293T cells and IP was performed anti-FLAG. Compared to full-length Pramel7 (FLAGHA-FL) all mutants showed drastically lowered binding ability to UHRF1. **Right:** Control IP. The FLAGHA-tagged control mutation (FLAGHA-63C) of Pramel7 was co-expressed with UHRF1 in HEK293T cells and IP was performed anti-FLAG. The 33AA LRR mutant (FLAGHA-33) was used as a control. FLAGHA63-C partly restored the interaction between Pramel7 and UHRF1. Co-binding of histone 3 (H3) showed the same pattern as UHRF. I=input, O=output, pBS=pBluescript.

When furthermore analysing co-precipitated levels of H3 (endogenous) this protein was following the binding pattern of UHRF1 (Fig. 12, right). This suggests that, of LRRs detected in the first screening (LRRs 1-3), LRR 1 (LKHLCLRGVTL) is critical in mediating the interaction between

Pramel7 and UHRF1. However, it is likely that LRRs 4-6 from the second screening contribute to the interaction as well.

1.6. Mutant forms of UHRF1 interact with Pramel7 at different strength

As seen above, the region in Pramel7 rich in LRRs is involved in mediating the interaction with UHRF1. To gain insight into which domains of UHRF1 are contributing to the binding to Pramel7, six different FLAG-tagged human UHRF1 mutants were co-expressed with Pramel7 (untagged) in HEK293T cells and co-IP was performed anti-FLAG. The constructs were kindly provided by Jiemin Wong from East China Normal University, Shanghai (Liu et al., 2013). A schematic illustration of full-length and mutated forms of UHRF1 and a successful expression test is depicted in Fig. 13.

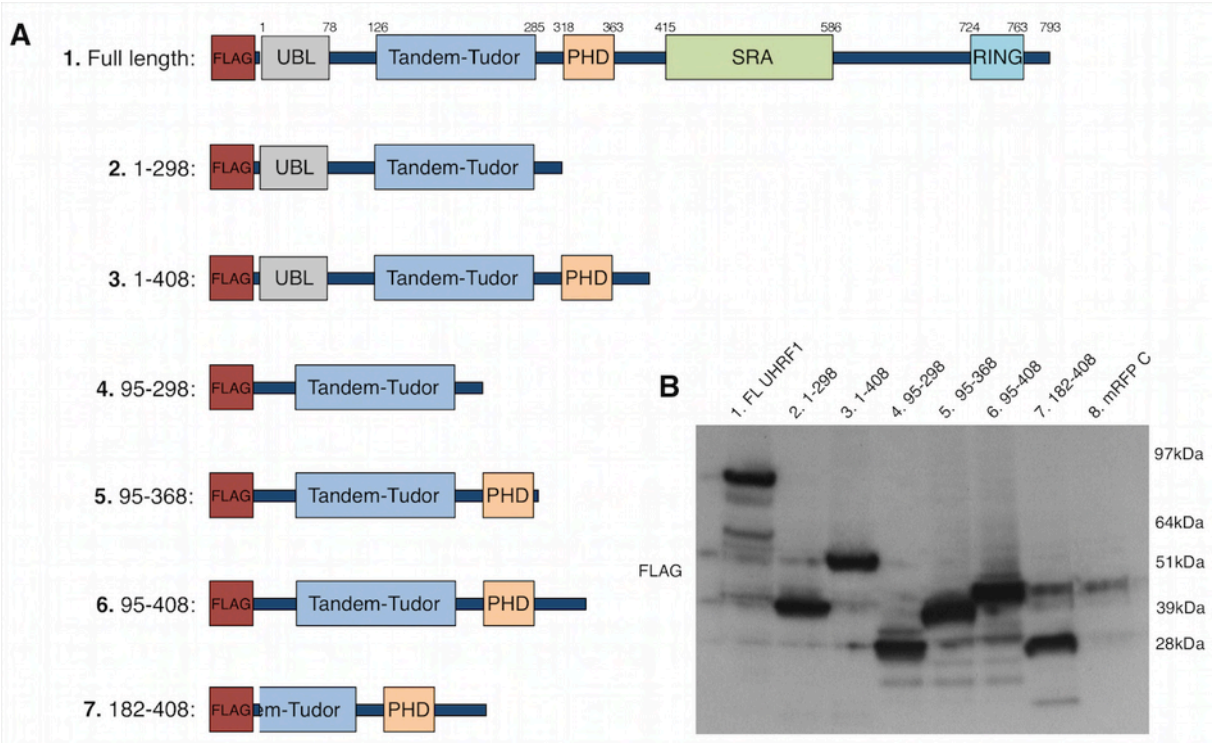

Fig. 13: FLAG-tagged forms of UHRF1 with different deletions.
A: Schematic illustration of seven FLAG-tagged UHRF1 expression constructs. Numbers in front indicate the range of amino acids present related to the full-length protein. **B:** Expression test anti-FLAG. FL=full-length. mRFP C (lane 8): HEK293T cells expressing red fluorescent protein were used as a transfection control and as a negative control for Western blotting.

All six mutants are completely lacking the C-terminal part of the protein comprising SRA and RING domains and exhibit different appearances in UBL, Tandem-Tudor and PHD domains. After IP anti-FLAG, levels of Pramel7 in the output fractions were determined. As visible in Fig. 14, by far most Pramel7 could be detected together with full-length UHRF1, followed by UHRF1_1-298 containing UBL- and intact Tandem-Tudor domains and UHRF1_182-408 consisting of a partial Tandem-Tudor and a full PHD domain. These two forms of UHRF1 were displaying considerably reduced levels of Pramel7 compared to full-length UHRF1. Very weak

Pramel7 signals could be observed for UHRF1_1-408 (full UBL, Tandem-Tudor and PHD domains), UHRF1_95-368 (full Tandem-Tudor and PHD domains, short tail at C-terminus) and UHRF1_95-408 (full Tandem-Tudor and PHD domains, long tail at C-terminus). The shortest form, UHRF1_95-298 (Tandem-Tudor domain only), was unable to give any signal for Pramel7. These results indicate that SRA and RING domains deleted in all the mutants significantly contribute to the interaction of UHRF1 and Pramel7.

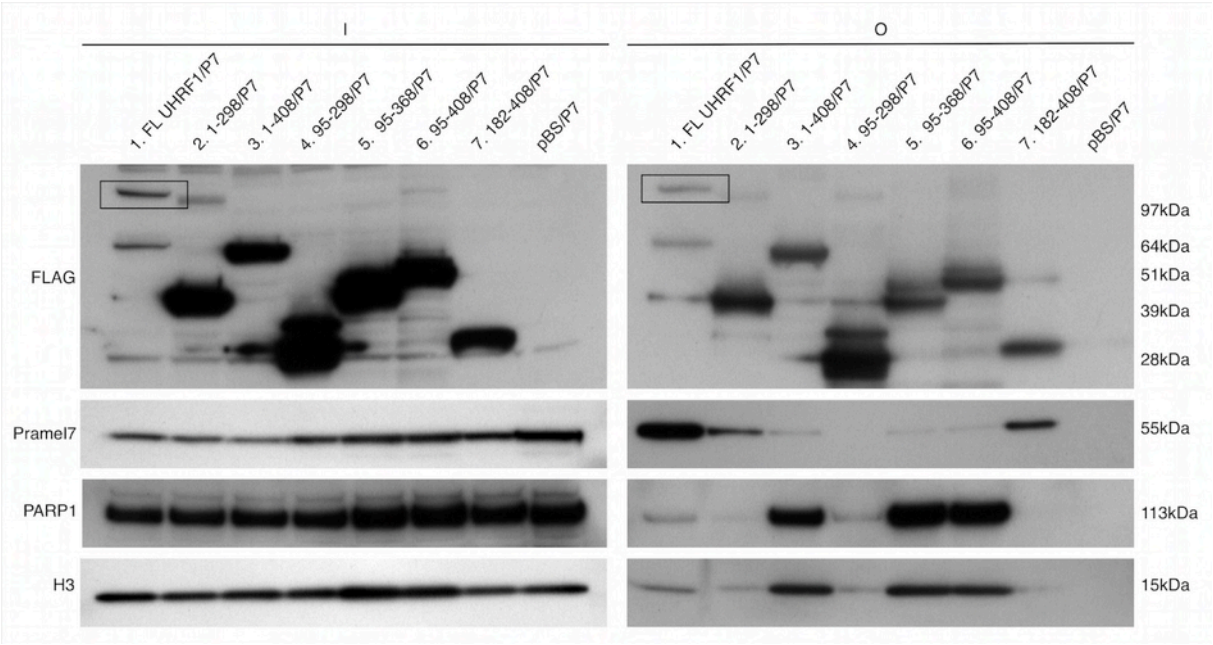

Fig. 14: Interaction capacities of mutant forms of UHRF1 in presence of Pramel7 co-expression.
FLAG-tagged UHRF1 mutations were co-expressed with Pramel7 in HKE293T cells and IP was performed anti-FLAG. Outputs were analysed for the presence of Pramel7, PARP1 and H3. Bands in rectangles: Signals of full-length UHRF1 in input and output fractions (lanes 1). I=input, O=output, FL=full-length, pBS=pBluescript.

To elucidate if H3 and PARP1 show a differential binding pattern among UHRF1 mutants, we additionally analysed outputs of different IPs for these two candidates under ectopic expression of Pramel7. Interestingly, in comparison with Pramel7, opposite binding patterns could be observed (Fig. 14). In mutations UHRF1_1-408, UHRF1_95-368 and UHRF1_95-408, all exhibiting a comparably low interaction with Pramel7, a significantly higher affinity for PARP1 and H3 could be shown. The two UHRF1 forms with a more efficient Pramel7 interaction, UHRF1_1-298 and UHRF1_182-408, did show very low signals for PARP1 and H3. UHRF1_95-298, the shortest of UHRF1 fragments, did not exhibit any significant signals for any of the three binding partners Pramel7, H3 and PARP1.

Remarkably, by looking more closely at the full-length form of UHRF1, almost no PARP1 and H3 could be precipitated, whereas a high amount of Pramel7 was present in the output (Fig. 14 lane 1). Since it is known that UHRF1 is a potent interaction partner of PARP1 and H3 in *wt* conditions, the presence of Pramel7 might thus prevent the interaction of UHRF1 with PARP1

and H3. Therefore, the experiment was repeated in complete absence of Pramel7 (Fig. 15). While binding between the deletion-mutants and H3/PARP1 remained similar as in the presence of Pramel7, in the case of full-length UHRF1 a clearly higher binding affinity for PARP1 and a drastically higher interaction with H3 was observed when Pramel7 was absent. Interestingly, determination of input and output fractions of full-length UHRF1 revealed that in the presence of Pramel7, full-length UHRF1 protein levels were drastically reduced already prior to being loaded for the IP (see bands in rectangles in Fig. 14 and Fig. 15, left). In contrast, in the absence of Pramel7, input amounts of full-length UHRF1 were not significantly lowered when compared to input levels of other UHRF1 versions.

This remarkable finding might explain the differential interactions of full-length UHRF1 in presence or absence of Pramel7. The following chapters will focus on the explanation of this phenomenon.

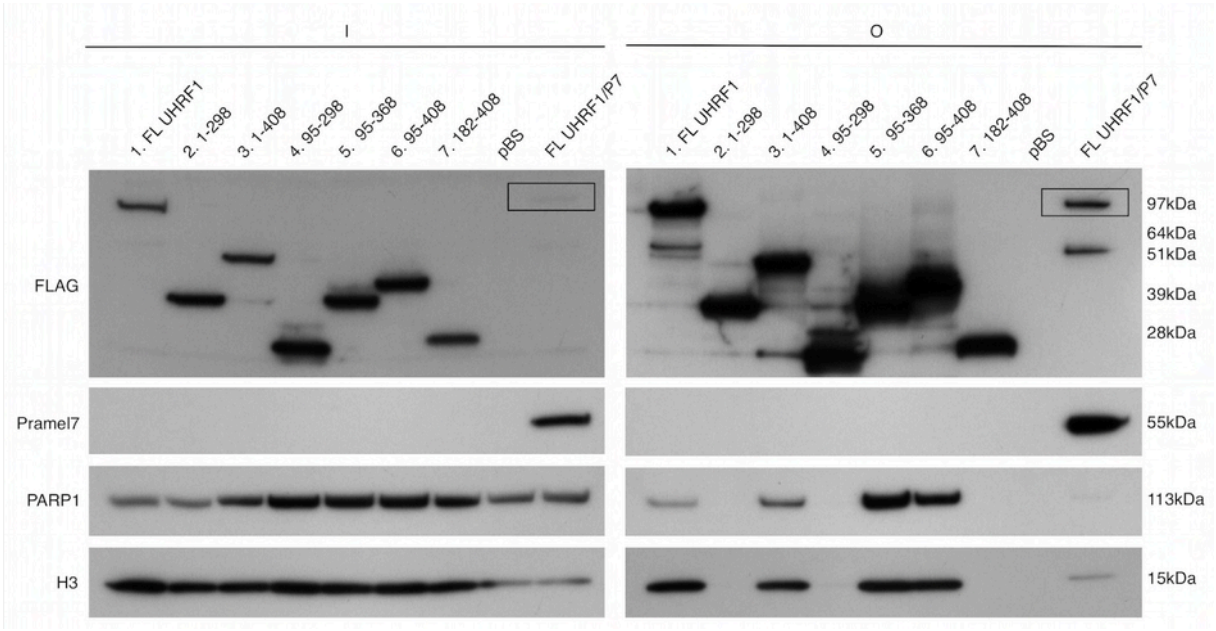

Fig. 15: Interaction capacities of mutant forms of UHRF1 in absence of Pramel7 co-expression.
FLAG-tagged UHRF1 mutations were co-expressed in absence of Pramel7 protein (except lanes 9) in HKE293T cells and IP was performed anti-FLAG. Outputs were analysed for the presence of Pramel7, PARP1 and H3. UHRF I=input, O=output, FL=full-length. Bands in rectangles: Full-length UHRF1 signals in input and output fractions with co-expression of Pramel7 (lanes 9).

2. Molecular effects caused by the interaction between Pramel7 and UHRF1

2.1. Pramel7 as a potential recognition subunit of an E3-ligase complex

After proving the interaction of the two proteins in HEK293T and mESCs, we next aimed to decipher its biological consequence. Under consideration of the data obtained in 1.6 and knowing that PRAME is potentially able to participate as a substrate recognition subunit in an E3 CRL complex, we wondered if Pramel7 could act the same way and UHRF1 could be its specific substrate (see introduction chapter 2.1). Furthermore, when screening the amino acid sequence of Pramel7, potential protein motifs strengthening this hypothesis could be identified in the N-terminal region, a BC-Box required for the interaction with ElonginC and a Cullin2-box mediating the binding to the Cullin scaffold protein (Fig. 16). However, in the Cullin2-box of Pramel7, the canonical proline (P) at position 31 and a canonical leucine (L)/isoleucine (I) at position 34 are mutated. In addition, we showed that the LRR-region located in the C-terminal part of Pramel7 is responsible for the interaction with the potential substrate, UHRF1. According to data published for PRAME, ElonginC is further coupled to ElonginB. The Cullin scaffold protein links the complex to the E3 ubiquitin protein ligase Rbx1, catalysing the polyubiquitination of the target substrate and subsequent degradation in the 26S-proteasome (Costessi et al., 2011) (see also Fig. 37).

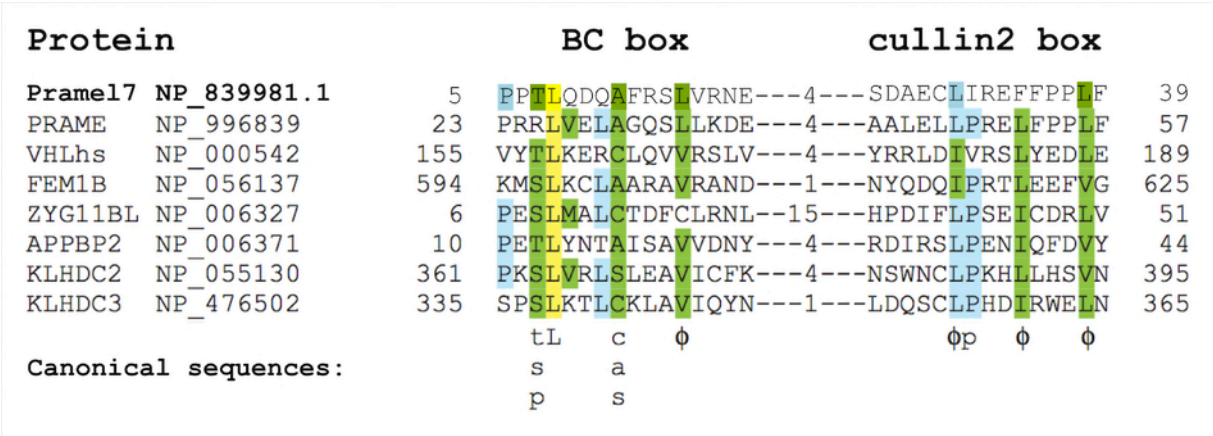

Fig. 16: Conserved features in BC and Cullin2 boxes of Pramel7 and other proteins.
Pramel7 shows canonical landmarks of the BC box. The canonical proline of the Cullin2 box is absent and the conserved leucine/isoleucine residue is replaced by phenylalanine. Yellow=identical amino acids, blue=very similar amino acids, green=similar amino acids. Canonical BC and Cullin2 box sequences are depicted below protein sequences. Alignment of candidate proteins (without Pramel7) was made by (Costessi et al., 2011) using the blosum62 mt2 alignment matrix with the AlignX program of the Vector NTI software package. Colour coding is based on the AlignX default similarity table. From Costessi et al., 2011, modified.

2.2. HEK293T and mESCs overexpressing *Pramel7* display drastically reduced levels of UHRF1

To assess if ectopic expression of *Pramel7* is sufficient to lead to a degradation of UHRF1 and thus, to corroborate the above model, we first expressed *Pramel7* in HEK293T cells for 48h and analysed UHRF1 levels in *Pramel7*-overexpressing, *pBS*-transfected control cells (to exclude transfection artefacts) and untransfected HEK293T cells. Strikingly, after 48h of *Pramel7*-expression, UHRF1 levels were drastically and efficiently reduced, whereas in both control samples, UHRF1 levels remained comparably high. The murine protein Pramel7 was thus sufficient to lead to this remarkable and efficient degradation of the human isoform of UHRF1, suggesting a high degree of conservation also across species. To see if this is true for mESCs as well, UHRF1 levels of *wt E14* mESCs and a mESC-line stably overexpressing *CAG_FLAGHA-P7* were determined. Consistent with the data from HEK293T cells, levels of murine UHRF1 were significantly lower also in *Pramel7*-overexpressing mESCs (Fig. 17A).

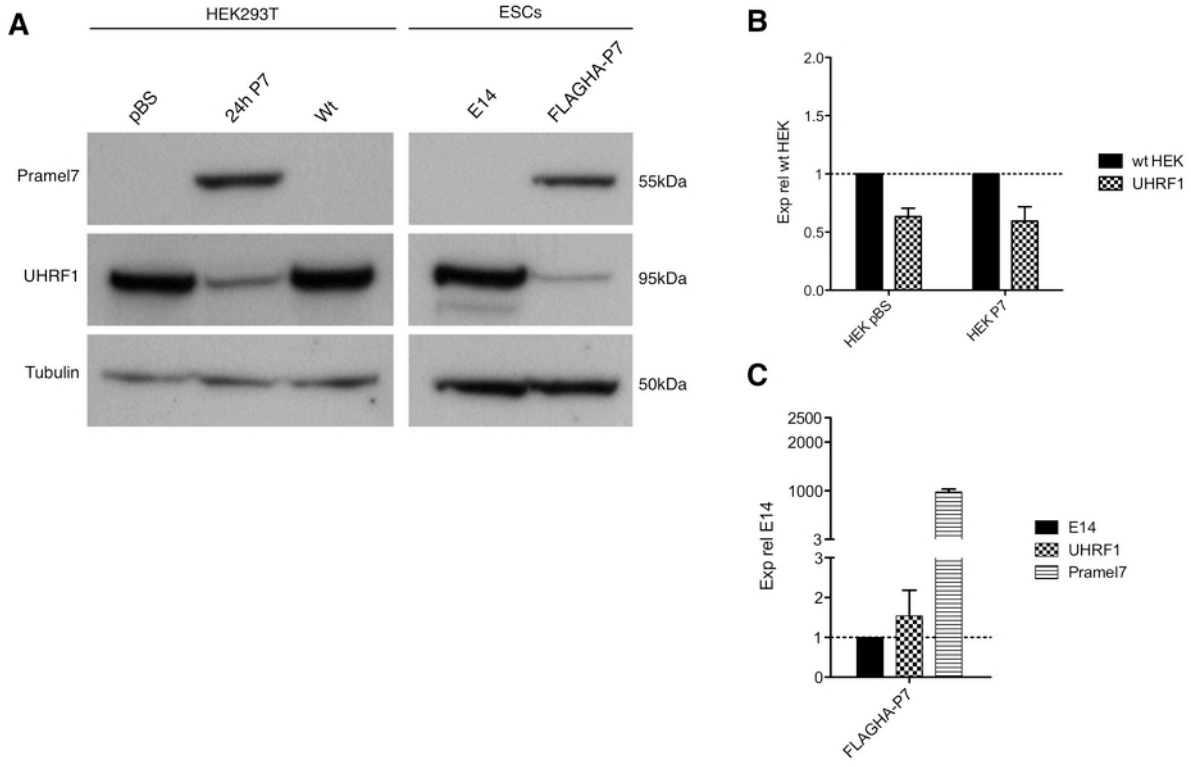

Fig. 17: Protein levels and gene expression of UHRF1 in HEK293T and mESCs upon overexpression of *Pramel7*.

A: Western Blot analysis displaying protein levels of *Pramel7*-overepxressing and control HEK293T (transient overexpression, untagged) and mESCs (stable overexpression, FLAGHA-tagged), respectively. **B:** Analysis of *UHRF1* gene expression in *Pramel7*-overexpressing and control HEK293T cells. **C:** Analysis of *UHRF1* and *Pramel7* gene expression in *FLAGHA-Pramel7* overexpressing (stable overexpression) and *wt E14* mESCs. pBS=pBluescript, P7=Pramel7. Exp rel=Expression relative to.

We next wanted to verify if the decrease of UHRF1 protein levels is mediated through the inhibition of *UHRF1* gene expression, mRNA degradation or protein degradation. To achieve this, amounts of *UHRF1*-mRNA in *Pramel7*-overexpressing and *wt* HEK293T cells and mESCs were determined. RTQ-PCR analysis revealed that levels of *UHRF1*-mRNA were not altered in *Pramel7*-overexpressing HEK293T or mESCs indicating that the decline of UHRF1 protein level is mediated on the protein level (Fig. 17B/C)

Finally, by confocal microscopic analysis after immunofluorescent labelling, the amounts and the cellular distribution of UHRF1 were assessed in *wt E14* and *Pramel7*-overepxressing *(CAG-FLAGHA-Pramel7)* mESCs. Consistent with the above observations, *Pramel7*-overexpressing mESCs exhibited a significantly weakened UHRF1 signal. Moreover, association of UHRF1 with DAPI-dense pericentric heterochromatin regions could easily be detected in *wt E14* mESCs whereas in *Pramel7*-overexpressing these signals were drastically reduced or completely absent (Fig. 18).

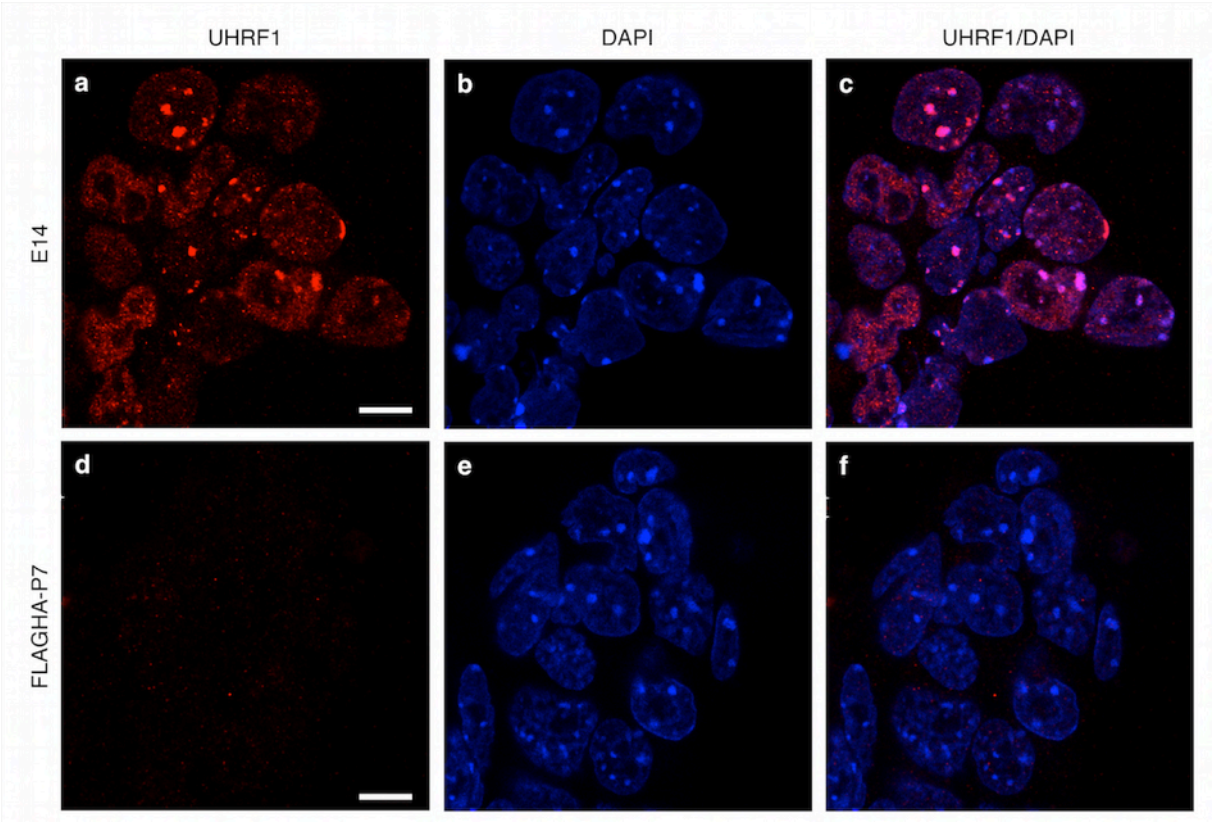

Fig. 18: Confocal microscopic analysis of UHRF1 levels in *wt E14* and *FLAGHA-Pramel7* overexpressing mESCs.

a-c: *Wt E14* mESCs. **d-f:** *FLAGHA-Pramel7* overexpressing mESCs. **a/d:** Anti UHRF1 staining. **b/e:** DAPI signal. **c/f:** DAPI/UHRF1 overlay. Confocal microscopy was performed at the Center for Microscopy and Image Analysis of the University of Zurich (ZMB). Scale bar: 10µm. P7=Pramel7.

Summing up, the expression of the protein Pramel7 is efficiently reducing the amount of UHRF1 in HEK293T cells and mESCs. Moreover, mouse Pramel7 is able to induce a degradation of both mouse and human UHRF1.

2.3. When ectopic expression of *Pramel7* is lost, UHRF1 amounts are restored to *wt* levels

To gain further evidence if the degradation of UHRF1 is indeed caused by the expression of Pramel7, we wondered if *wt* UHRF1 levels could be restored after loss of transiently expressed *Pramel7*. Therefore, a one week time course analysis in HEK293T cells was carried out and cells were collected at different time points ranging from 8h post transfection with *CAG_P7*, earliest, and 120h (5 days) post transfection, latest.

In Fig. 19 it can be seen that Pramel7 protein became detectable 24h post transfection and expression peaked at 36h-48h. Remarkably, a simultaneous reduction of UHRF1 protein could be identified at these time points. After one passage and 72h of cultivation, *Pramel7* expression was decreasing and expression was finally lost after 96h and second passaging of cells. Concomitant with the disappearance of Pramel7, UHRF1 levels were restored to control amounts, leading to the conclusion that the pure presence of Pramel7 indeed results in the drastic decrease of UHRF1.

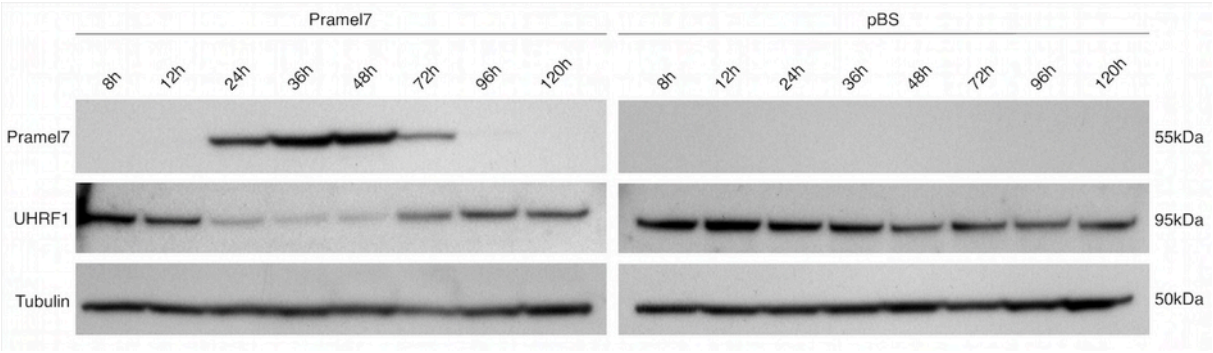

Fig. 19: Transient overexpression of *Pramel7* in HEK293T cells for five days (120h).
HEK293T cells were transfected with *CAG_Pramel7* (left) and *pBS* (control, right). Cells were harvested at indicated time points and UHRF1 levels were determined by Western blotting. pBS=pBluescript.

To verify these observations also in mESCs, we made use of our *E14* cell line stably overexpressing *FLAGHA-Pramel7*. The overexpression construct was designed as seen in Fig. 20A, containing a *FLAGHA-Pramel7-IRES-Puro* cassette flanked by *loxP* sites followed by an *EGFP* (Casanova et al., 2011). *Pramel7*-overexpressing mESCs were electroporated with *cre-recombinase*, *FLAGHA-P7-IRES-Puro* was floxed out and expression of EGFP was induced in recombined cells. We seeded the electroporated cells and selected the emerging clones based on intensity and homogeneity of the EGFP signal. EGFP-positive clones were finally picked and expanded. At this step, we immunofluorescently labelled the electroporated cells from the primary dishes with an antibody recognizing UHRF1. When comparing signal intensity and distribution, a remarkable difference between EGFP-positive, recombined, and EGFP-negative, non-recombined mESCs could be observed. While EGFP-positive colonies displayed an UHRF1 signal similar to *wt E14* cells (strong nuclear appearance), in EGFP-negative cells still carrying

the *Pramel7*-overexpression cassette firstly, UHRF1 signal intensity was much lower and secondly, we were unable to detect a clear nuclear expression pattern (Fig. 20B).

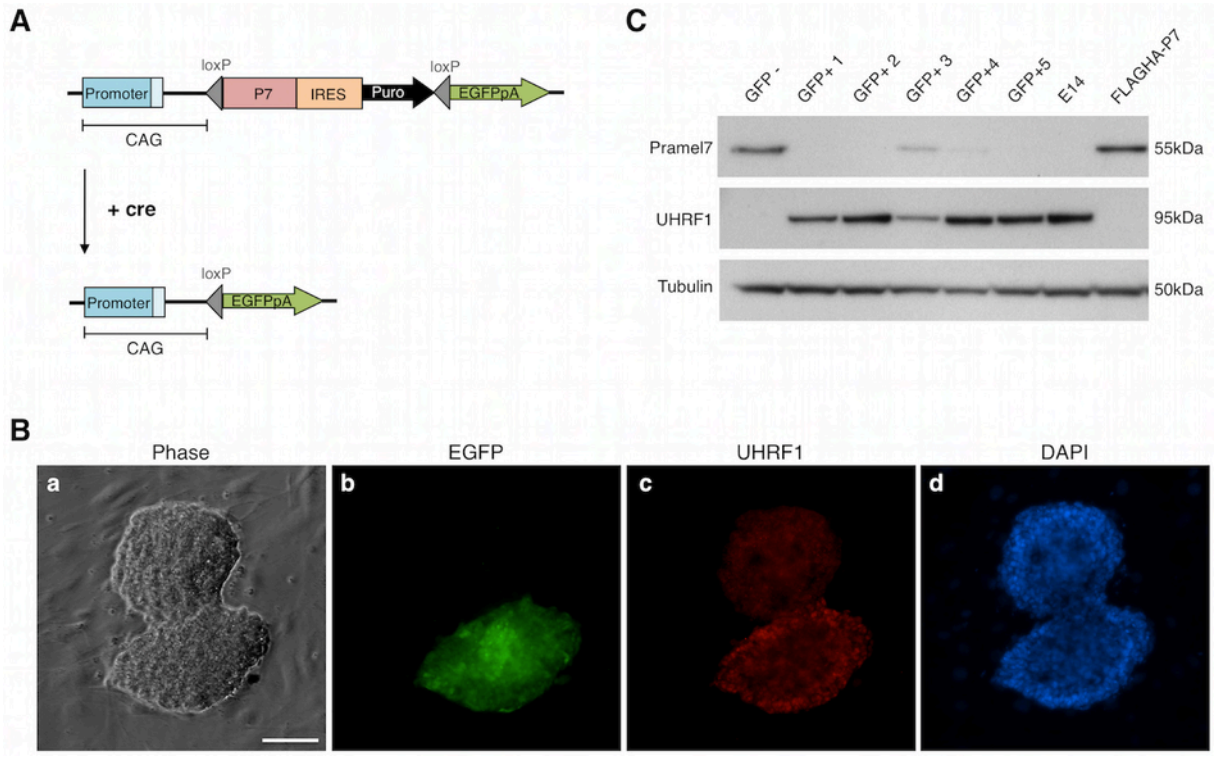

Fig. 20: Cre-mediated excision of the *Pramel7*-expression cassette in mESCs.
A: Schematic illustration of the *CAG_FLAGHA-Pramel7* expression vector. Pramel7 (P7) carries the FLAGHA-tag on the N-terminus. Upon transfection of *cre-recombinase* the expression of *Pramel7* is lost and expression of *EGFP* is activated. **B:** ***a:*** Phase contrast image showing mESC colonies after electroporation. ***b:*** The top colony did not undergo cre-recombination (EGFP-negative) whereas the bottom colony lost the expression of *Pramel7* indicated by a strong EGFP signal. ***c:*** UHRF1 staining. The recombined colony with lost *Pramel7* expression (bottom) exhibits a strong nuclear *wt*-like expression pattern. ***d:*** DAPI signal. Scale bar: 100µm. **C:** Pramel7 and UHRF1 protein levels of expanded clones with recombined (GFP+, Pramel7-) or non-recombined Pramel7 (GFP-, Pramel7+).

Next, five EGFP-positive and one EGFP-negative control clone from the electroporation fraction were expanded for three to four passages and further characterized by Western blotting. Indeed, five recombinant, EGFP-positive clones showed restored *wt*-like UHRF1 levels, whereas a control clone retained undetectable UHRF1. Interestingly, the clone *GFP+3* (Fig. 20C) still exhibited a weak signal for Pramel7, indicating a composition of a mixed population of recombined EGFP-positive and EGFP-negative cells. Nevertheless, even this weak Pramel7 signal was sufficient to cause a partial decrease in UHRF1 levels. This indicates that the intensity of the degradation is dependent on the dosage of Pramel7 protein. Moreover, the degradation is reversible as soon as the expression of Pramel7 is below a critical threshold.

2.4. Is Pramel7 inducing the degradation of UHRF1 through the 26S-proteasome?

The 26S-proteasome mediates the final step in the degradation of Polyubiquitin-tagged proteins. As seen above, the decrease of UHRF1 protein was not mediated on the mRNA level and is thus likely to be regulated on the protein level. To assess if the degradation process is mediated via the 26S-proteasome, *Pramel7* was overexpressed in HEK293T cells and cells were cultured in the presence of the proteasome inhibitor MG132 for 4, 8 and 12h. It is noteworthy that the expression of *Pramel7* was induced 24h prior to the addition of MG132. In accordance with the above data, 24h after transfection of *Pramel7* the cells already displayed very low levels of UHRF1. 4, 8 and 12h after the addition of MG132, levels of endogenous UHRF1 were gradually increasing. In *pBS*-transfected control cells no significant change in UHRF1 levels could be observed throughout the whole experiment. These data indicate that degradation of UHRF1 resulting from *Pramel7* expression may occur via the 26S-proteasome (Fig. 21A).

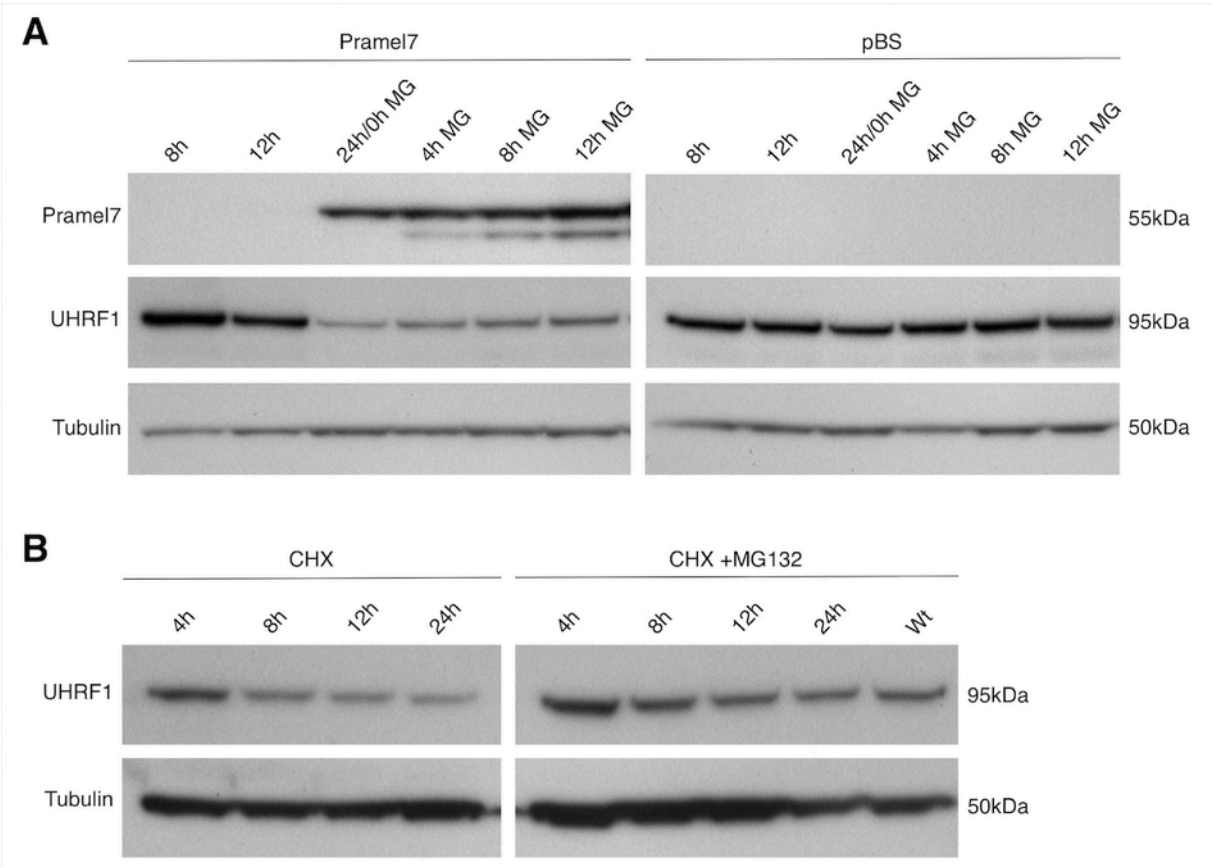

Fig. 21: Cultivation of HEK293T cells overexpressing Pramel7 in presence of MG132 and cycloheximide.

A: MG132 was added 24h after transfection of *CAG_Pramel7* and *pBS* (control). Cells were incubated for 4, 8 and 12h and levels of UHRF1 were determined by Western blotting. **B:** Functionality of MG132 was assessed by cultivating untransfected HEK293T cells in presence or absence of MG132 in medium containing the inhibitor of translation cycloheximide for different time spans and UHRF1 levels were determined. pBS=pBluescript, MG=MG132, CHX=cycloheximide.

To verify the functionality of MG132, we incubated HEK293T cells in the presence of firstly the inhibitor of translation cycloheximide and secondly of both cycloheximide and MG132 for

different periods. In steady-state culture conditions UHRF1 is reported to be gradually degraded by the proteasome via ubiquitination by the $SCF^{\beta\text{-}TrCP}$ E3-ligase (Chen et al., 2013). Therefore, lowered UHRF1 levels were expected in cells cultivated in cycloheximide only, whereas in cells supplemented with cycloheximide and MG132, UHRF1 levels should remain comparable. Indeed, UHRF1 levels were decreased already after 8h in presence of only cycloheximide. In contrast, upon addition of MG132, no significant change in UHRF1 levels could be observed (Fig. 21B). Another indicator for a correct function of MG132 is the gradual increase of overexpressed Pramel7 with time (Fig. 21A).

2.5. Forms of Pramel7 mutated in the LRR-region cannot induce the degradation of UHRF1

It was shown above that IP against FLAG-tagged forms of Pramel7 with deletions in the LRR-region significantly reduced the potential of pulling down co-expressed UHRF1 (see Results 1.5). In accordance with the reduced binding between the two proteins we were interested, if also the potential of inducing the degradation of UHRF1 is impaired or abrogated. To achieve this, full-length and mutant forms of *Pramel7* (33AA, 62AA, 84AA, 62AA control, described in 1.5) were expressed in HEK293T cells and effects on endogenous human UHRF1 levels were assessed. Indeed, only full-length Pramel7 was able to cause a decrease in UHRF1 (Fig. 22 lane 1). In contrast, UHRF1 levels stayed comparably high in cells expressing the three LRR mutants (33AA, 62AA, 84AA). Interestingly, the expression of the 62AA control mutation affecting only one out of six potential LRRs induced a weak decrease of UHRF1 protein level (Fig. 22). Taken together, to mediate the degeneration of UHRF1, Pramel7 requires an intact LRR region. Deletion of only 33AA is sufficient to completely inhibit the reduction of UHRF1 protein levels.

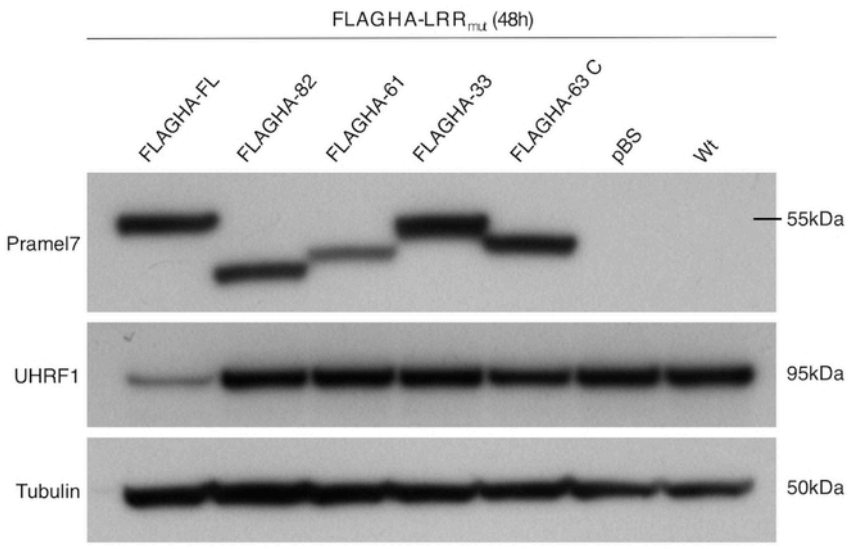

Fig. 22: Degradation of UHRF1 by different variants of Pramel7 mutant in the LRR region.
HEK293T cells were transfected with different constructs coding for the LRR mutants described in 1.5 and protein levels of UHRF1 were analyzed by Western blotting after 48h. FL=Full-length, pBS=pBluescript.

2.6. Pramel7 is unable to degrade different mutant forms of UHRF1

We then wondered which mutant forms of UHRF1 (described in 1.6) could be primed for degradation by full-length Pramel7. To assess this, Pramel7 was co-expressed with full-length UHRF1 and six UHRF1 mutants for 48h in HEK293T cells. Interestingly, only full-length UHRF1 protein was reduced, whereas all the mutant forms did not display any difference to the controls (Fig. 23). Thus, the C-terminal part of UHRF1 comprising RING and SRA domains deleted in all mutants plays a crucial role in enabling the degradation of the protein. It was described in 1.6 (Results) that Pramel7 is able to best interact with full-length UHRF1 by far. The fact that the capacity of the mutants to bind Pramel7 was ranging from low to completely absent and that in addition, Pramel7 was seen to heavily reduce intracellular levels of only full-length UHRF1 emphasizes the significance of a proper interaction between Pramel7 and UHRF1.

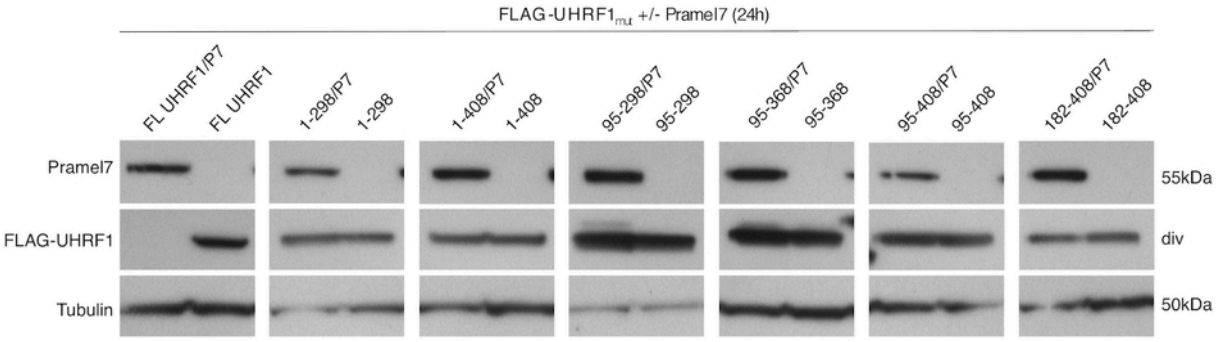

Fig. 23: Pramel7-induced degradation of different variants of UHRF1.
HEK293T cells were co-transfected with *CAG_Pramel7* and different FLAG-tagged versions of UHRF1 (described in 1.6). Cells were cultivated for 24h and protein levels assessed by Western blotting. P7=Pramel7.

2.7. Reduction of UHRF1 results in decreased levels of DNA methylation

During the S-phase of the cell cycle, UHRF1 guides DNMT1 to sites of hemimethylated DNA and ensures faithful propagation of the overall DNA methylome from mother to daughter cells. A very recent study goes one step further by demonstrating that UHRF1 is not only guiding DNMT1 but also increasing its activity (Bashtrykov et al., 2013). Two key publications in UHRF1 research state that a decrease or even full abolishment of UHRF1 levels in cycling mammalian cells leads to a gradual reduction of overall DNA methylation (Bostick et al., 2007), (Sharif et al., 2007). We hence wondered if this effect could be caused by ectopic expression of *Pramel7* as well.

2.7.1. Digestion of genomic DNA from mESCs with methylation-sensitive restriction enzymes

To get a first impression if DNA methylation in *Pramel7*-overexpressing mESCs or HEK293T cells is reduced, we extracted genomic DNA (gDNA) from either HEK293T cells transiently

overexpressing *Pramel7* for 48h or from mESCs stably overexpressing *FLAGHA-Pramel7* for at least ten passages. Methylation of gDNA was compared by digestion with the methylation sensitive restriction endonuclease HpaII, an enzyme unable to digest methylated DNA. In HEK293T cells, no obvious difference in the amount of gDNA digested by HpaII could be observed between cells transfected with *Pramel7* and untransfected cells (data not shown). This was most likely due to a too short time span of *Pramel7* expression (48h) since DNA methylation is thought to decrease in a replication-coupled manner and thus requires a certain number of cell divisions. In contrast, in mESCs, a substantially higher amount of gDNA was digested in *Pramel7*-overexpressing cells than in *wt E14* cells (Fig. 24A, left).

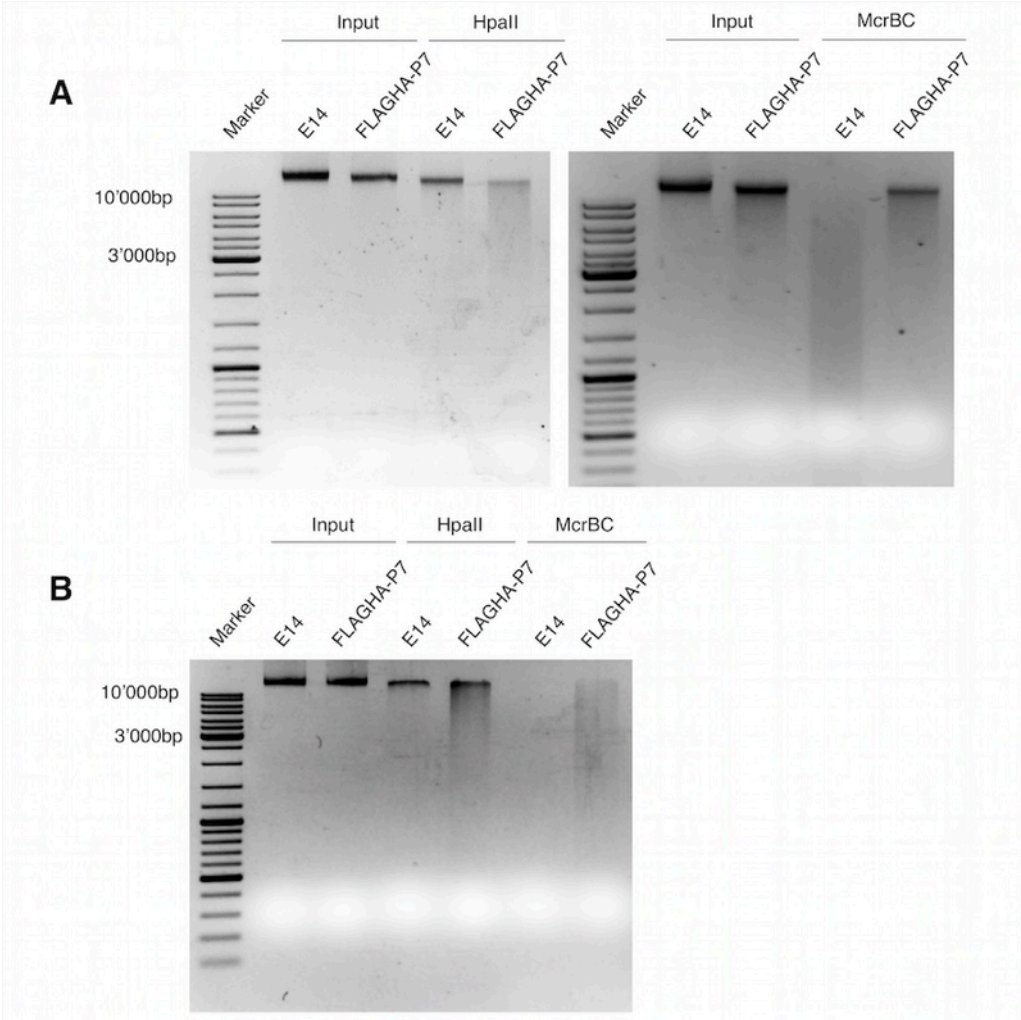

Fig. 24: Digestion of genomic DNA (gDNA) with methylation-sensitive restriction enzymes HpaII and McrBC.

A: gDNA of *wt E14* and *FLAGHA-Pramel7* overexpressing mESCs cultivated in self-renewing conditions. **B:** gDNA of *wt E14* and *FLAGHA-Pramel7* overexpressing mESCs after 10d of differentiation. P7=Pramel7. Digestion experiments were performed by Eva Vollenweider, Santoro lab, Institute of Veterinary Biochemistry and Molecular Biology, University of Zurich.

To corroborate this finding, gDNA of mESCs was digested with McrBC, a restriction enzyme requiring DNA in a (hemi-) methylated state for activity (Fig. 24A, right). Indeed, while *E14* cells showed a high degree of digestion, DNA of *Pramel7*-overexpressing mESCs was still pre-

sent in larger fragments, indicating reduced digestion. In mESCs, it is widely recognized that the degree of methylation is increasing upon differentiation. Consequently, we were interested if the reduction in DNA methylation induced by Pramel7 is still detectable in mESCs differentiated for 10 days in feeder-free conditions and deprived from LIF. Indeed, comparable results could be observed also after differentiation, indicating that the presence of Pramel7 on one hand can be maintained and on the other hand is able to keep UHRF1 and thus DNA methylation on a low level throughout the process of differentiation (Fig. 24B).

2.7.2. Confocal microscopy reveals reduced signals for 5mC in mESCs overexpressing *Pramel7*

To further confirm the above findings, we immunofluorescently labelled *Pramel7*-overexpressing and *wt E14* mESCs with an antibody recognizing 5mC and analysed the signals by confocal microscopy. Whereas *E14* cells displayed positive signals of nuclear heterochromatic foci rich in DNA methylation and thus 5mC, in *Pramel7*-overexpressing cells 5mC signals at DAPI-dense pericentric heterochromatin regions were reduced or absent. Taken together, over a certain number of passages low UHRF1 levels caused by the expression of *Pramel7* lead to massively reduced DNA methylation in mESCs (Fig. 25).

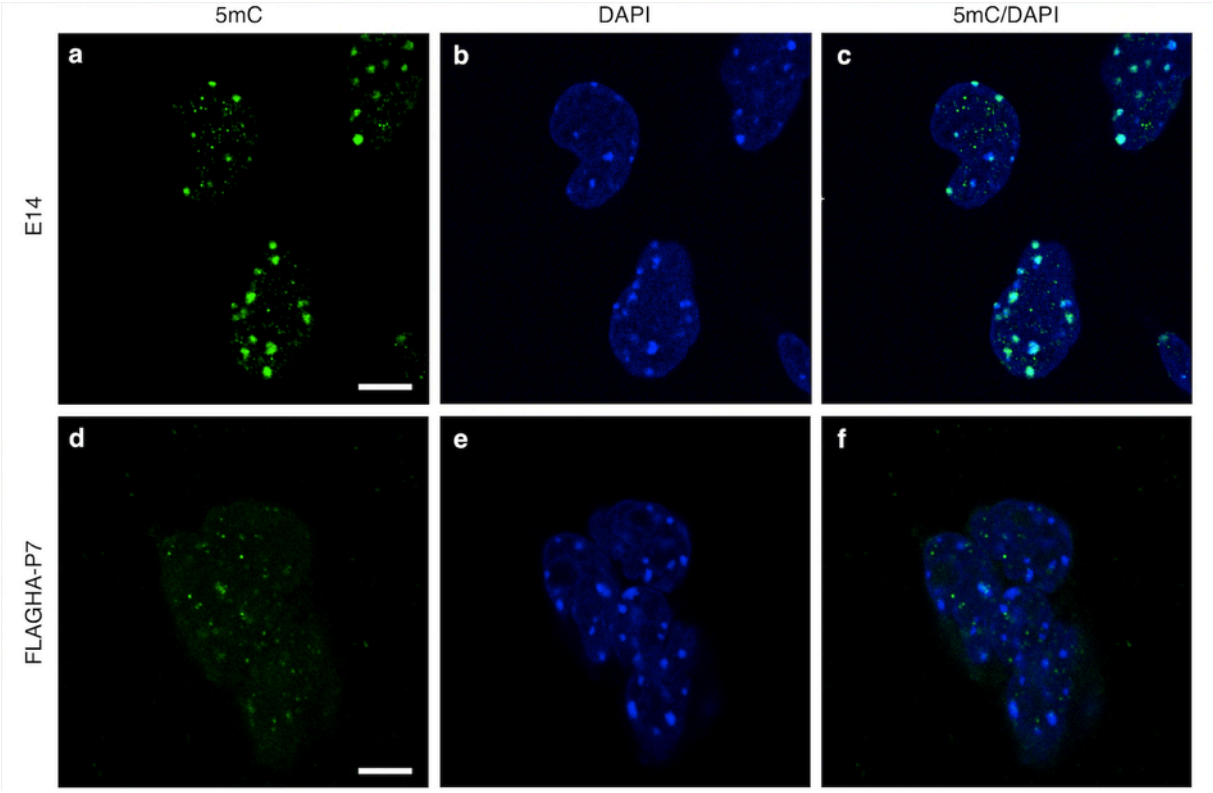

Fig. 25: Confocal microscopy analysis of 5mC levels in *wt E14* and *FLAGHA-Pramel7* overexpressing mESCs.

a-c: *Wt E14* mESCs. **d-f:** *FLAGHA-Pramel7* overexpressing mESCs. **a/d:** Anti 5mC staining. **b/e:** DAPI signal. **c/f:** DAPI/5mC overlay. Confocal microscopy was performed at the Center for Microscopy and Image Analysis of the University of Zurich (ZMB). Scale bar: 10µm. P7=Pramel7.

2.7.3. Pramel7-overexpressing mESCs exhibit elevated expression levels of the trophectodermal marker *Elf5*

Embryonic stem cells with depleted DNMT1 (*DNMT1*$^{-/-}$) exhibit a uniquely high potential for the trophectodermal lineage illustrated by the upregulation of the transcription factor *Elf5*. *Elf5* together with *Cdx2* and *Eomes* take an important role in trophectodermal specification during the development of an early mouse embryo. Its aberrant upregulation is caused by inefficient methylation at promoters of trophectodermal genes (see Introduction chapter 1.5). To test if this side effect can also be observed in *Pramel7*-overexpressing mESCs, we analysed the expression levels of *Elf5* in *wt E14* and *Pramel7*-overexpressing mESCs (Fig. 26). Samples from various experiments described in the figure legend of Fig. 26 were used. Indeed, amounts of *Elf5* mRNA were significantly higher in all mESC samples overexpressing *Pramel7* than in the corresponding *wt E14* samples. In samples representing mESCs cultured in self-renewing culture conditions (Fig. 26A) the upregulation effect of Elf5 caused by the overexpression of *Pramel7* was 7.5-12.5-fold. Upon differentiation of mESCs, the upregulation in *Pramel7* overexpressing cells increased to 55-fold (d10 diff) and 255-fold (d14 diff), respectively (Fig. 26B). These data further confirm that via degradation of UHRF1 overexpression of *Pramel7* in leads to impaired DNA methylation mESCs and therefore, resembling *DNMT1*$^{-/-}$ mESCs, aberrant expression of the trophectodermal marker *Elf5*.

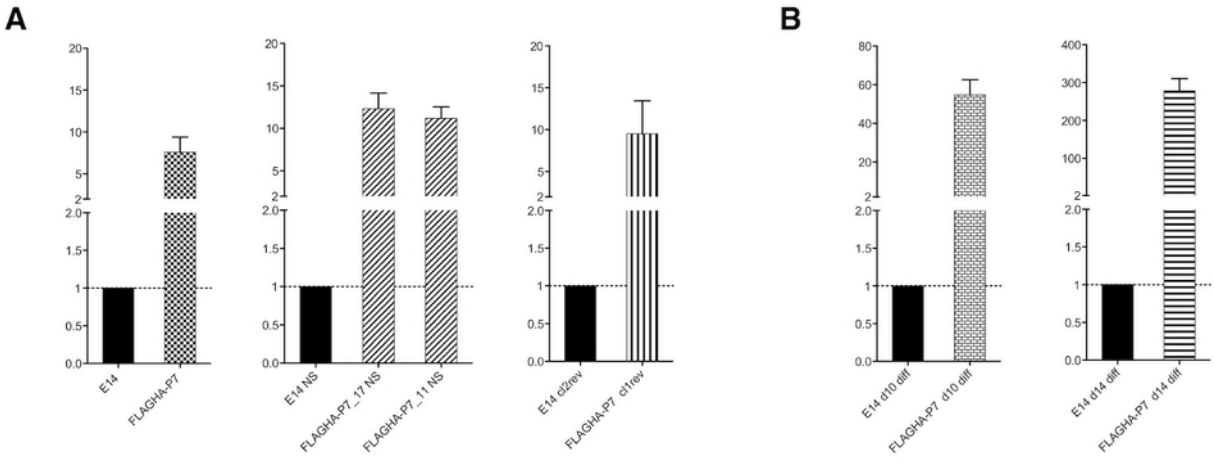

Fig. 26: RTQ-PCR analysis for the trophectodermal marker *Elf5* in self-renewing and differentiated *Pramel7*-overexpressing mESCs.

Expression levels are compared to *wt E14* cells in the corresponding condition/experiment. **A:** Samples from mESCs cultivated in self-renewing conditions (CM+LIF). *Left: Wt E14* and *Pramel7*-overexpressing mESCs (FLAGHA-tagged) routinely used in this work. *Middle: Wt E14* and two *Pramel7*-overexpressing clones (11&17) adapted to a new fetal bovine serum (NS) for 3 passages. *Right:* A *wt E14* and a *Pramel7*-overexpressing clone reconverted to pluripotency after differentiation (see experiment described in Results chapter 3.1.5). **B:** Samples from differentiated mESCs (CM-LIF, no feeders). *Left:* mRNA from d10 differentiated mESCs (see Results chapter 2.7.1). *Right:* mRNA from d14 differentiated mESCs (see Results chapter 3.1.1).

2.8. Chromatin of *Pramel7*-overexpressing mESCs is enriched in activating histone marks

Modifications of the N-terminal tail of histones can indicate an active or inactive chromatin state. By quantifying and comparing the expression of different histone marks in *wt E14* and *Pramel7*-overexpressing mESCs we wanted to examine if the reduction in DNA methylation might have an effect on the prevalence of histone modifications. Using antibodies against different histone marks representing an either active or inactive chromatin state, whole cell lysates were analysed by Western blotting. Fig. 27 shows elevated levels of the activating histone marks H3K9ac, H3K27ac, H3K4me3 and H4ac in *Pramel7*-overexpressing cells when comparing to *E14* mESCs, whereas the repressive mark H3K27me3 was more abundant in *wt* cells. This is leading to the assumption that the reduction in DNA methylation caused by Pramel7-induced degradation of UHRF1 results in a generally more open and thus more active transcriptional state of the chromatin.

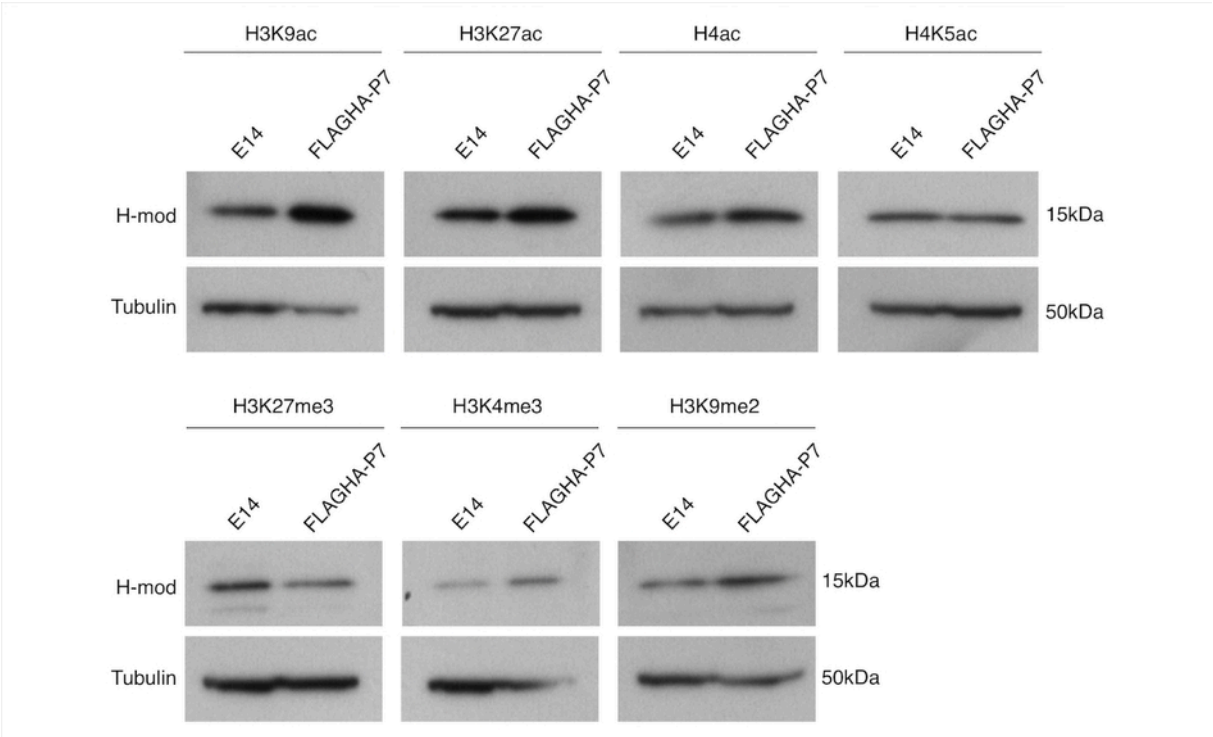

Fig. 27: Levels of different histone modifications in *wt E14* and *Pramel7*-overexpressing mESCs.
Prevalence of histone modifications was analyzed from whole cell lysates from mESCs cultivated in self-renewing conditions. P7=Pramel7. H-mod=histone modification.

2.9. Overexpression of *Pramel7* is not altering cell cycle profiles of HEK293T and mESCs

Previous works showed that in some mammalian cell lines a reduction of UHRF1 is influencing the distribution of cells in different phases of the cell cycle (Bonapace et al., 2002), (Jenkins et al., 2005). We therefore tested if this is also the case for both mESCs stably overexpressing *Pramel7* and HEK293T cells ectopically expressing *Pramel7* for 48h. After harvesting and fixation cells were subjected to PI-FACS analysis (Fig. 28). Neither in HEK293T nor in mESCs a significant difference between *Pramel7*-overexpressing and *wt E14* cells could be observed, assuming that *Pramel7* expression is not altering the distribution of cells in different phases of the cell cycle in these two particular mammalian cell types.

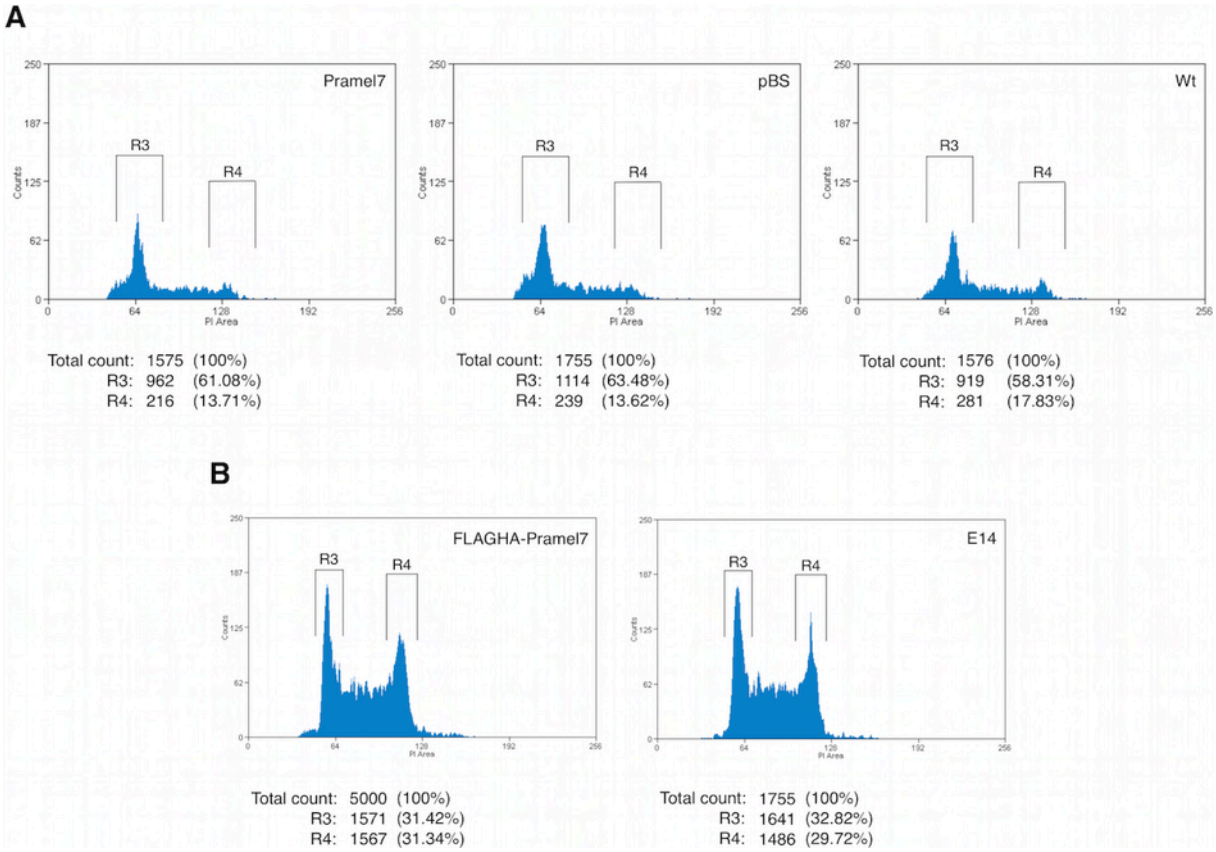

Fig. 28: PI-FACS profiles of HEK293T and mESCs in presence or absence of *Pramel7*-overexpression.
A: HEK293T cells. After transfection cells were cultivated for 48h and analyzed for PI intensity (left: *Pramel7*-tranfected; middle: *pBS*-transfected; right: untransfected). **B:** mESCs. Cells were cultivated in self-renewing conditions and analyzed for PI intensity (left: *FLAGHA-Pramel7* overexpressing; right: *wt E14*).

2.10. Localization of Pramel7 in the cell

To obtain further information about the localization of Pramel7 within the cell, several experiments were executed. First, HEK293T cells were $CaCl_2$-transfected with *CAG_FLAGHA-Pramel7*, cultivated for 48h and immunofluorescently labelled for Pramel7 and HA, respectively. As visible in Fig. 29A, Pramel7 exhibited different localization patterns in HEK293T cells. In one fraction of cells the protein was detected in the cytoplasm exclusively, whereas in other cells a nuclear enrichment was observed. However, many cells with nuclear enrichment were as well exhibiting a positive cytoplasmic signal. These observations could be made in immunofluorescence experiment using both anti-HA (data not shown) and anti-Pramel7 antibodies. To exclude a detrimental side effect caused by transfecting too high amounts of plasmid DNA and thus excessive overproduction of the protein, transfected DNA was diluted from 1µg to 50ng. Even at these low dilutions a similar distribution pattern was observed (data not shown).

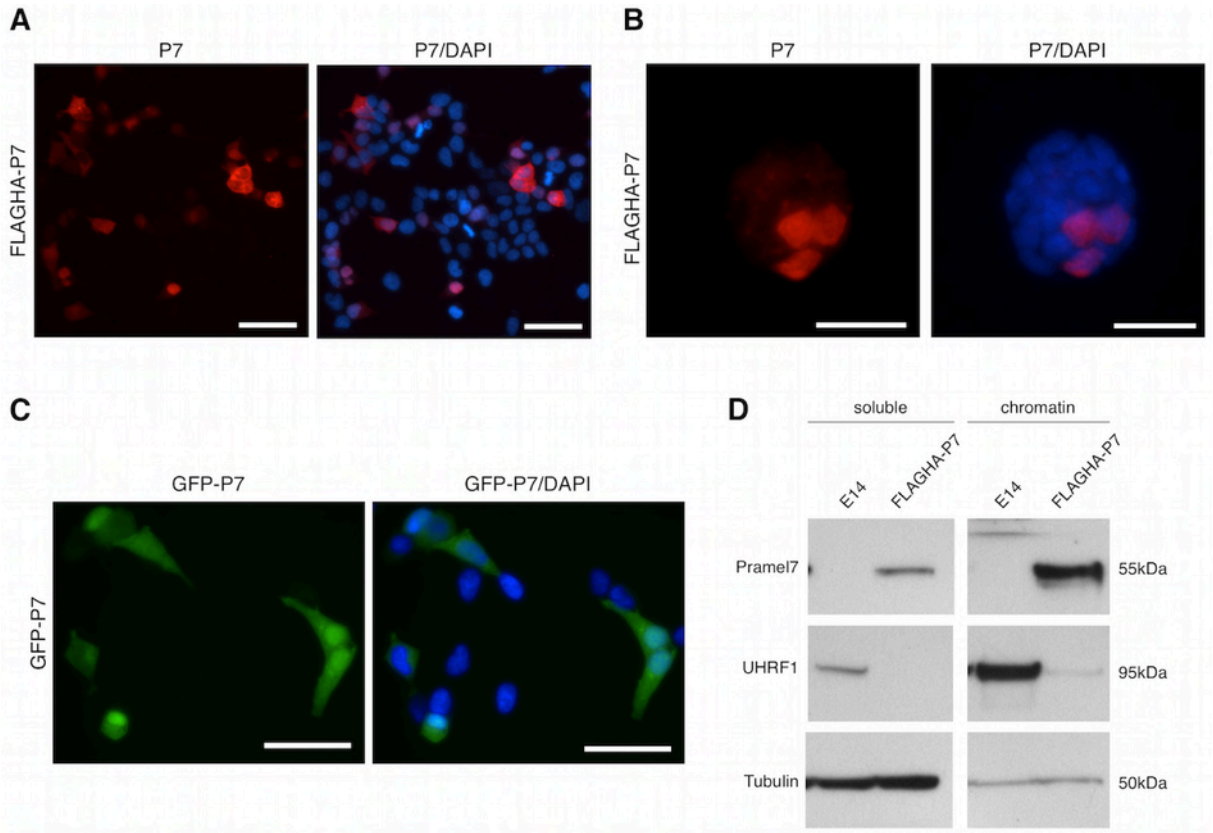

Fig. 29: Localization of Pramel7 in the cell.
A: HEK293T cells transfected with *FLAGHA-Pramel7* and stained for Pramel7. Scale bar: 50µm. **B:** *Wt 129* mESCs transfected with *CAG_FLAGHA-Pramel7* and stained for Pramel7. Scale bar: 30µm. **C:** HEK293T cells transfected with *pEF_GFP-Pramel7*. Scale bar: 50µm. **D:** Separation of chromatin and soluble fractions of *wt E14* and *FLAGHA-Pramel7* overexpressing mESCs cultivated in self-renewing conditions. P7=Pramel7.

Next, *129* mESCs cultivated on gelatin in defined serum-free conditions (2i+LIF) were transiently transfected with *CAG_FLAGHA-Pramel7*, cultured for 48h and immunofluorescently labelled for Pramel7. As to expect, transfection efficiency was lower compared to HEK293T cells. Nev-

ertheless, in all cells positive for FLAGHA-Pramel7 the signal was covering the whole cell and was not restricted to a particular subcellular region as cytoplasm or nucleus in both anti-HA (data not shown) and anti-Pramel7 assays (Fig. 29B).

We then constructed a *GFP*-tagged version of *Pramel7 (pEF_GFP-Pramel7)*, transfected it into HEK293T cells and analysed the GFP signal after 24-48h. Confirming the above data, GFP-Pramel7 was restricted to the cytoplasm in one fraction of cells whereas in other cells an accumulation in the nucleus coinciding with a cytoplasmic signal was detected (Fig. 29C). Taken together, these approaches show that in HEK293T cells Pramel7 is exhibiting a miscellaneous localization pattern. Pramel7 is either present in the cytoplasm exclusively or accumulates in the nucleus without completely losing its cytoplasmic localization. In *129* mESCs, no distinction between cytoplasmic and nuclear localization could be made when ectopically expressing *Pramel7*.

We were also curious to see if and to what extent the protein is capable of interacting with the chromatin of mESCs. Therefore, we separated the chromatin from the soluble fraction (nucleo- and cytoplasm) of *wt E14* and *Pramel7*-overexpressing mESCs and detected Pramel7 and UHRF1 by Western blot (Fig. 29D). Interestingly, in *Pramel7*-overexpressing cells a significantly higher amount of Pramel7 was detected in the chromatin fraction whereas levels in the soluble fraction were lower. As expected, by looking at the distribution of UHRF1, in *wt E14* cells the major bulk of UHRF1 was associated with chromatin and only very few protein could be detected in the soluble fraction. In contrast, confirming our previous findings, in the soluble fraction of *Pramel7*-overexpressing cells, no UHRF1 could be observed and only a very faint band was detected in the chromatin fraction, representing degraded UHRF1 caused by the expression of *Pramel7*.

2.11. Compared to Pramel7, PRAME exhibits a similar expression pattern in HEK293T cells

As *PRAME* was described to be the founder gene of the *PRAME-like* family, we wanted to examine if the expression patterns of this gene are comparable to those of *Pramel7*. To verify this, a *FLAGHA*-tagged version of *PRAME* was cloned into a *pcDNA3.1*-expression plasmid. HEK293T cells were transfected with the construct, cells were cultivated for 24h and finally immunofluorescently labelled anti-HA (Fig. 30). Indeed, PRAME and Pramel7 proteins exhibited similar expression patterns. The signal was detected either exclusively in the cytoplasm or accumulating in the nucleus. Thus, these data are not excluding similar mechanistic roles for the two proteins and probably also for other members of the *PRAME-like* gene family.

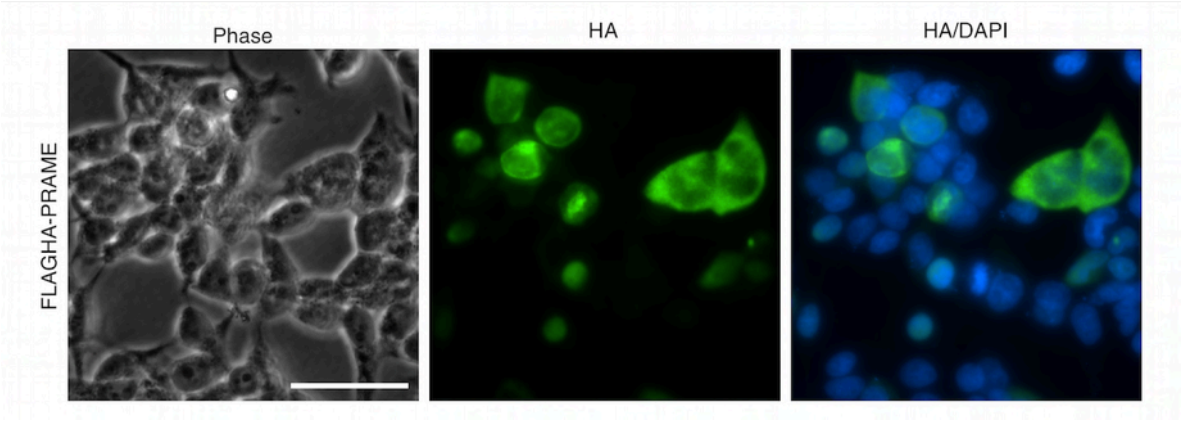

Fig. 30: Expression of FLAGHA-PRAME in HEK293T cells.
HEK293T cells were transfected with *FLAGHA-PRAME*, cells were cultivated for 24h and localization of PRAME analyzed by immunofluorescent labeling anti-HA. Scale bar: 50µm.

2.12. PRAME and Pramel6 are not able to reduce UHRF1 levels after ectopic expression

In context of the comparable subcellular localization of PRAME and Pramel7, it was assessed if expression of PRAME and Pramel6, a member of the PRAME-like family highly conserved to Pramel7, might also lead to a decrease in UHRF1 levels. Western blot analysis in Fig. 31A shows that in contrast to Pramel7, PRAME and Pramel6 were not able to induce a significant degradation of UHRF1 after 24h and 48h. Since no antibody recognizing Pramel6 is commercially available, the expression of the plasmid was verified by RTQ-PCR, indicating a massive expression of the plasmid (Fig. 31B). Considering the conservation of the two proteins Pramel6 and Pramel7 and the inability of Pramel6 to induce a degradation of UHRF1, it is to assume that the interaction between Pramel7 and UHRF1 is highly specific. This strengthens the hypothesis that every member of the PRAME-like protein family might efficiently recognize and target a particular substrate for subsequent degradation with high specificity.

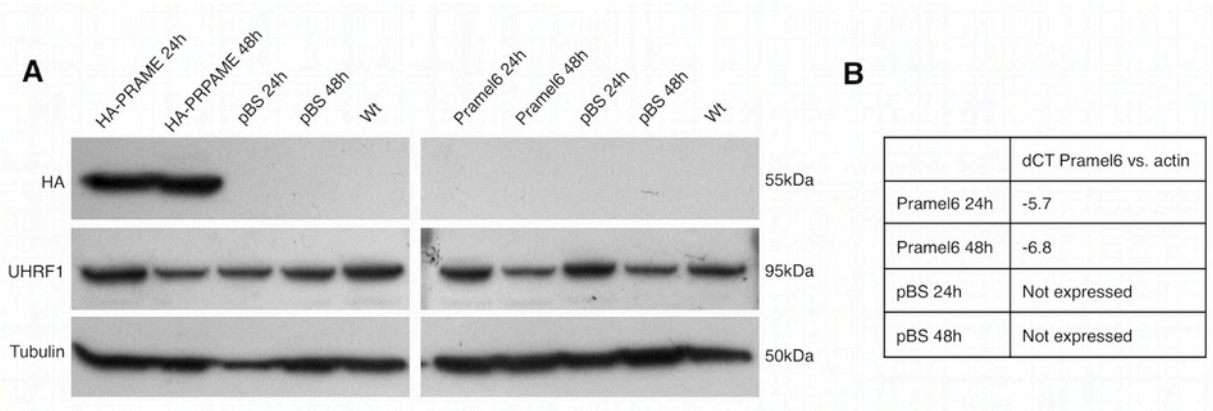

	dCT Pramel6 vs. actin
Pramel6 24h	-5.7
Pramel6 48h	-6.8
pBS 24h	Not expressed
pBS 48h	Not expressed

Fig. 31: Capability of PRAME and Pramel6 to induce the degradation of UHRF1
A: *HAFLAG-PRAME* and *CAG-Pramel6* were expressed in HEK293T cells and cells were cultivated for 48h. UHRF1 protein levels were determined by Western blotting. **B:** Verification of *Pramel6* expression by determining dCT values (compared to actin). pBS=pBluescript.

3. A biological consequence of *Pramel7* expression in mESCs

Terminal differentiation of mESCs requires the establishment of DNA methylation and repressive histone modifications at promoters of pluripotency-related genes such as *Oct4*, *Nanog* or *Rex1* to ensure a faithful shutdown and to prevent their reactivation.

Taking into account that Pramel7 maintains UHRF1 levels constantly low leading to loss of global methylation, we wondered if the presence of Pramel7 disturbs terminal differentiation of mESCs and facilitates the reactivation of a pluripotent state.

3.1. mESCs overexpressing *Pramel7* show impaired terminal differentiation

3.1.1. After 14 days of differentiation, *Pramel7*-overexpressing mESCs exhibit a drastically elevated expression of pluripotency-related genes

To assess if mESCs overexpressing *Pramel7* are capable to undergo terminal differentiation or if the lack of global methylation prevents robust silencing of pluripotency-associated genes, we cultivated *wt E14* and *Pramel7*-overexpressing mESCs in feeder-free conditions in complete medium deprived from LIF for 14 days. During this period, cells should not grow over confluence ensured by passaging them twice. When comparing the two differentiated mESC lines in terms of physical appearance, *wt E14* mESCs developed into a homogeneous layer of cells whereas *Pramel7*-overexpressing mESCs were rather assembled into smaller groups and spots without any attached cells were visible (Fig. 32A/C). Differentiated cells were next subjected to analysis of protein levels by Western blotting to guarantee that *Pramel7* overexpression was maintained during the whole process of differentiation. When looking at Fig. 32B, the expression of Pramel7 was still detectable after two weeks of differentiation, although at slightly reduced levels. UHRF1 amounts in *Pramel7*-overexpressing cells were comparably low in undifferentiated and 14d-differentiated mESCs. As expected, UHRF1 levels in *E14* control cells were drastically decreasing during differentiation, reflecting low proliferation of cells in the differentiated state. Nevertheless, slightly more UHRF1 could be detected in control cells than in *Pramel7*-overexpressing cells. This indicates that UHRF1 levels in *Pramel7*-overexpressing mESCs were still affected by the expression of *Pramel7* after two weeks of differentiation.

Next, expression levels of the pluripotency-related genes *Oct4*, *Nanog* and *Rex1* were determined from total mRNA of differentiated cells. Remarkably, when using mRNA levels of differentiated *E14* control cells as a baseline, expression levels of all three candidates were significantly enhanced in differentiated mESCs overexpressing *Pramel7*. This suggests that in *Pramel7*-overepxpressing mESCs, promoters of *Oct4*, *Nanog* and *Rex1* could not be silenced as efficiently as in control mESCs (Fig. 32 D).

Differentiated mESCs were also immunofluorescently labelled for the pluripotency marker Oct4. In accordance with the observations from RTQ-PCR analysis, the number of cells expressing detectable levels of Oct4 was drastically higher in *Pramel7*-overexpressing than in *E14* control cells (Fig. 32 C). These data strongly suggest that during differentiation of mESCs, reduced amounts of UHRF1 caused by the expression of *Pramel7* lead to a less robust silencing of *Oct4*, *Nanog* and *Rex1*.

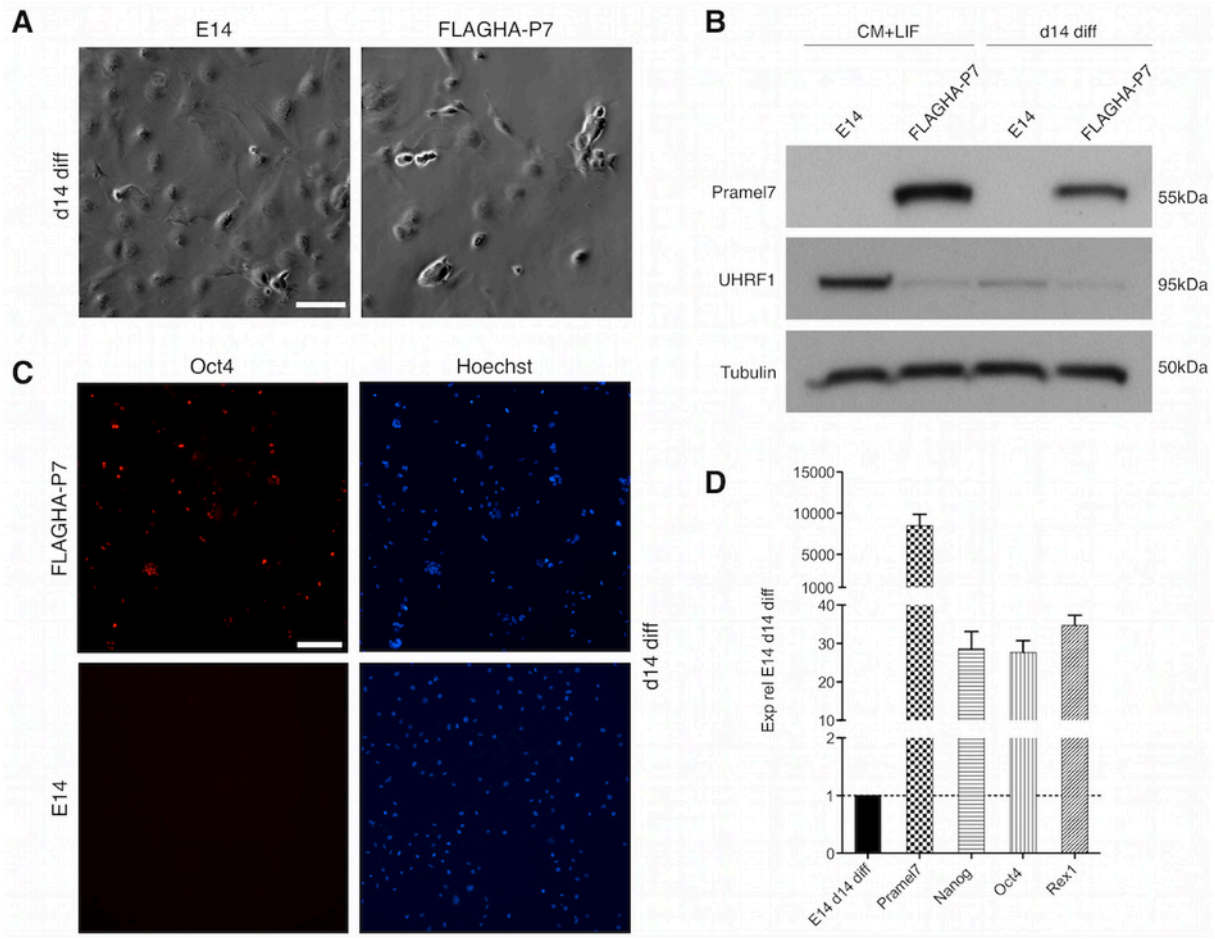

Fig. 32: *Wt E14* and *Pramel7*-overexpressing mESCs after 14d of differentiation.
A: Phase contrast images of *wt E14* and *FLAGHA-Pramel7* overexpressing mESCs after 14d of differentiation in CM-LIF -feeders. Scale bar: 100µm. **B:** UHRF1 and Pramel7 protein levels of *wt E14* and *FLAGHA-Pramel7* overexpressing mESCs in self-renewing conditions (CM+LIF, left) and after 14d of differentiation (CM -LIF -feeders, right) **C:** Immunofluorescent Oct4-labeling of *wt E14* and *FLAGHA-Pramel7* overexpressing mESCs differentiated for 14d in CM-LIF -feeders. Scale bar: 200µm. **D:** Gene expression analysis of different pluripotency markers in d14 differentiated mESCs overexpressing *FLAGHA-Pramel7*. Expression is compared to differentiated *wt E14* mESCs. P7=Pramel7, Exp rel=expression relative to.

3.1.2. Upon addition of LIF, differentiated mESCs overexpressing *Pramel7* rapidly regain features associated with pluripotency

To elucidate to what extent differentiated mESCs are capable to be reconverted to a pluripotent state when re-exposed to culture conditions supporting pluripotency, we diluted 14d-

differentiated *wt E14* and *Pramel7*-overexpressing cells and seeded them at a density of 10 cells/well in two 96-well plates (per cell type) containing feeder cells. After seven days of cultivation in self-renewing conditions (CM +LIF), wells were screened for colonies displaying a round, pluripotent morphology. In 96-well plates with *Pramel7*-overexpressing cells approximately 9/10 wells contained colonies, whereas in only around 1/10 of control wells mESC-like colonies could be observed. As a next step, 10 promising wells were passaged to 24-well plates for further expansion. Residual 182 wells were fixed and analysed for the expression of the pluripotency marker alkaline phosphatase (AP) (Fig. 33 A/D). The number of wells containing AP-positive colonies was quantified in Fig. 33 B/C. In 5/182 (2.7%) wells containing control cells one or more AP-positive colonies could be identified, whereas the number of wells with positive colonies in *Pramel7*-overexpressing cells was 147/182 (80.8%).

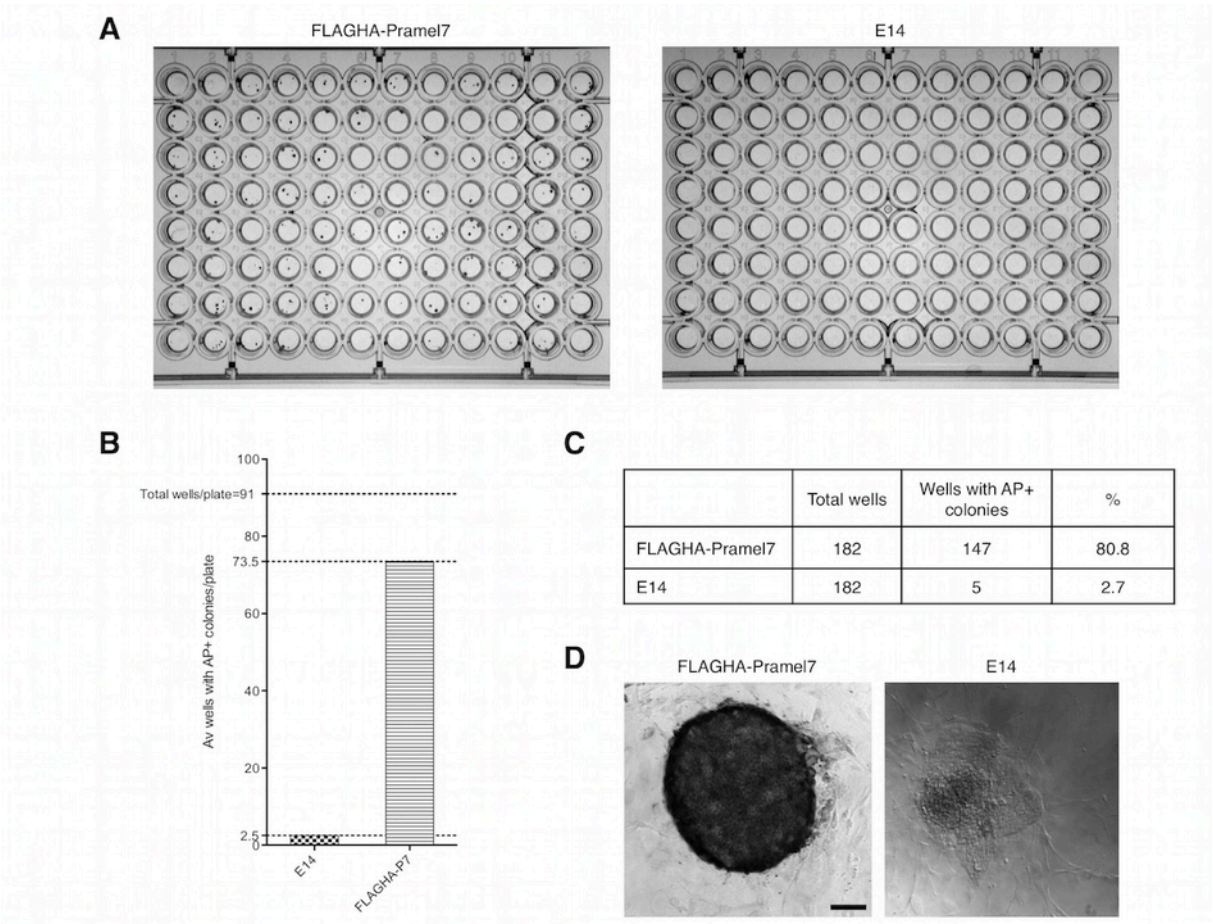

	Total wells	Wells with AP+ colonies	%
FLAGHA-Pramel7	182	147	80.8
E14	182	5	2.7

Fig. 33: Re-cultivating d14 differentiated mESCs in self-renewing conditions.
A: 96-well plates after re-cultivating d14 differentiated cells for 7d in self-renewing conditions followed by alkaline phosphatase (AP) staining. **B/C:** Numbers of wells containing AP-positive colonies after re-cultivation for 7d in self-renewing conditions. A graphic illustration showing the average number of wells with AP-positive colonies (B) and a table (C) displaying total numbers and percentages. 5 promising wells/plate were previously passaged on 24-well plates for expansion. Av= average, P7= Pramel7. **D:** Example for AP-positive and AP-negative colonies. Scale bar: 100µm.

3.1.3. Expansion of reconverted *E14*-clones requires a longer cultivation period than of reconverted mESCs overexpressing *Pramel7*

Next, we were interested if the clones from the 96-well plates could successfully be expanded without loss of pluripotency-associated features. Moreover, we wondered if the duration of expansion might vary between *Pramel7*-overexpressing and *wt E14* mESCs. After passaging 10 selected clones from 96-well plates, cells were first cultivated on 24-well plates for one passage and further expanded on 3.5cm culture dishes four two passages. At this stage, cells were collected for different experimental approaches. As schematically visible in Tab. 4, 9 out of 10 *Pramel7* clones could successfully be expanded over 3-4 passages within only 6 days. 5 of these clones were harvested for further characterization by Western blotting, RTQ-PCR and immunofluorescence. Remarkably, only one out of ten clones from 96-well plates was not successfully expanded. In contrast, all *wt E14* clones showed a delayed growing behaviour. Firstly, no colony-like phenotype was detectable during the first 3 days in 24-well and on day 4, only 2 clones could be passaged the second time. Other 8 clones had to be transferred 1:1 to new 24-wells. Finally, 10 or 11 days after initial passaging, 5 clones were harvested for further analysis. 4 out of 10 clones were lost. Thus, *E14* clones required almost double amount of time for the same steps of expansion. Taken together with data obtained in the last chapter, after addition of LIF, *Pramel7*-overexpressing cells reconvert to pluripotency at much higher frequency and consequently, expansion of these clones was more efficient than in control cells.

Tab. 4: Expansion time of d14 differentiated mESCs re-cultivated in self-renewing conditions (7d).
Expansion duration is representing the number of days after which cells exhibited a pluripotency-like phenotype ready for further analysis or freezing. OE=overexpressing, NR=not rescued.

	Clone	Expansion duration		Clone	Expansion duration
FLAGHA-Pramel7-OE mESCs	1	**d6**	*Wt E14* mESCs	1	**d10**
	2	**d6**		2	**d10**
	3	**d6**		3	**d11**
	4	**d6**		4	**d11**
	5	**d6**		5	**d11**
	6	**d5** (backup)		6	**d11** (backup)
	7	**d5** (backup)		7	NR
	8	**d5** (backup)		8	NR
	9	**d7** (backup)		9	NR
	10	NR		10	NR

3.1.4. Reconverted *Pramel7*-clones still exhibit downregulated UHRF1 and ectopic expression of *Pramel7*

After 14 days of differentiation, *Pramel7*-overexpressing mESCs still expressed detectable amounts of ectopic Pramel7 protein and slightly reduced UHRF1 levels (Fig. 32). Therefore, it had to be verified if Pramel7 protein was detectable also in reconverted clones and as a consequence, if amounts of UHRF1 protein were still reduced. Indeed, Western blot analysis revealed that reconverted *Pramel7*-clones all expressed Pramel7 at similar levels. Also UHRF1 amounts were comparable to control mESCs (original *Pramel7*-overexpressing mESC line in CM +LIF), indicating that during the whole process of differentiation and subsequent reconversion to pluripotency, ectopic expression of *Pramel7* is sufficient to keep UHRF1 at low levels (Fig. 34 A). Moreover, immunofluorescence of one selected reconverted clone of each cell type (*wt E14* & *FLAGHA_Pramel7*-overexpressing) revealed positive signals for the pluripotency markers Oct4 and SSEA1, indicating a correct re-activation of these particular two genes (Fig. 34 B).

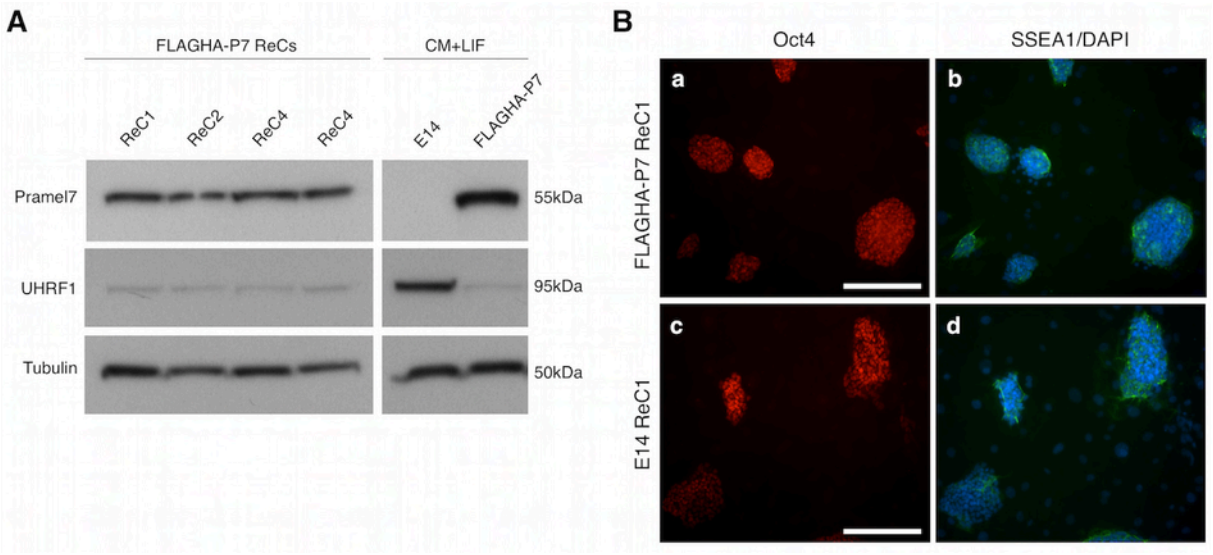

Fig. 34: Analysis of reconverted cones.
A: Western blot analysis showing protein levels of 4 reconverted clones overexpressing *FLAGHA-Pramel7*. Controls are represented by mESCs cultivated in self-renewing conditions (CM+LIF). **B:** Immunohistochemical staining for Oct4 ***(a/c)*** and SSEA1 ***(b/d)*** of one reconverted clone overexpressing *FLAGHA-Pramel7* **(a/b)** and one reconverted *wt E14* clone ***(c/d)***. Scale bar: 200µm. ReC=reconverted clone, P7=Pramel7.

3.1.5. Reconverted *E14*-clones fail to reactivate the expression of the pluripotency-related genes *Rex1* and *Pramel7*

To examine the pluripotent state of reconverted and expanded clones, expression levels of pluripotency-associated genes *Oct4*, *Nanog* and *Rex1* were analysed. RTQ-PCR data from Fig. 35 shows that both *Pramel7*-overexpressing and *wt E14* clones, although with delayed kinetics (Tab. 4), succeeded in reactivating the expression of *Oct4* and *Nanog*. Reconverted *Pramel7*-

clones also displayed amounts of *Rex1* mRNA comparable to initial levels of control mESCs. In remarkable contrast, all *E14*-clones analysed were unable to reactivate the expression of firstly *Rex1* and secondly, endogenous *Pramel7*. These findings strongly suggest that in contrast to *Pramel7*-overexpressing clones, *E14* clones cannot be fully reconverted to a pluripotent state after two weeks of differentiation.

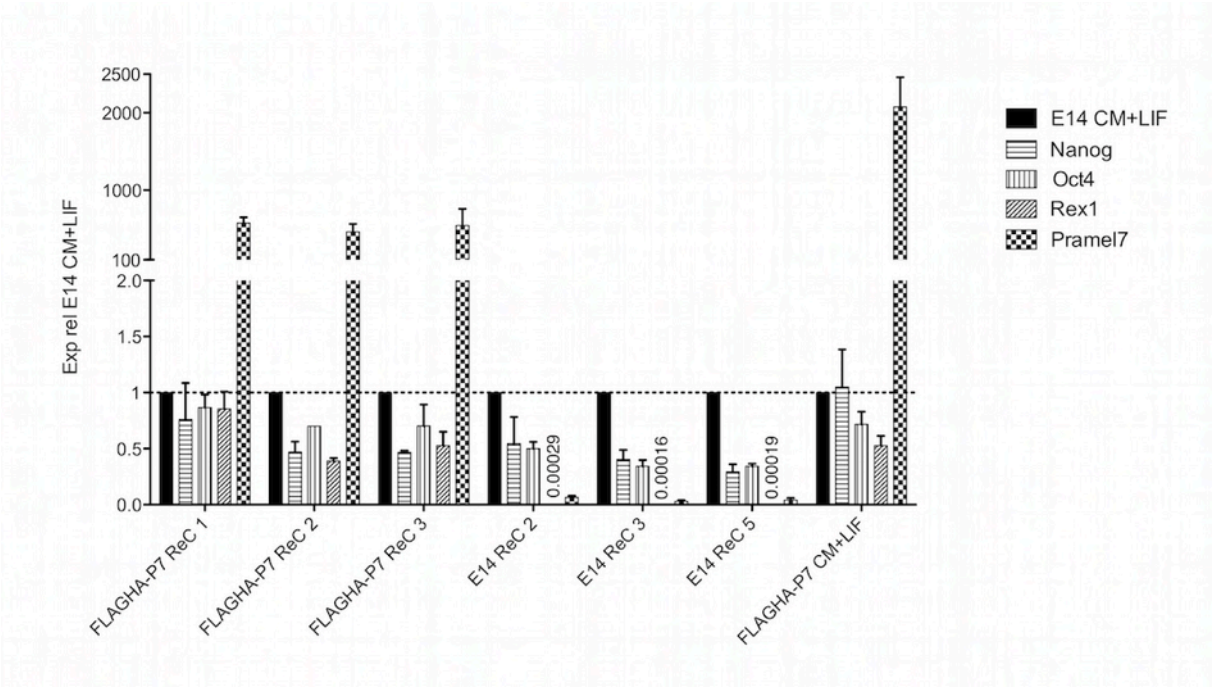

Fig. 35: Reconverted clones: expression of pluripotency markers.
Expanded reconverted clones were harvested and expression levels of pluripotency markers were assessed. Expression levels are compared to *wt E14* cultivated in self-renewing conditions (CM +LIF). ReC=reconverted clone, P7=Pramel7, Exp rel=expression relative to.

3.2. *Pramel7*-overexpressing mESCs are able to differentiate into cells positive for smooth muscle actin (SMA)

We then wanted to clarify if mESCs overexpressing *Pramel7* are able to adopt a differentiated phenotype. We exposed *E14* and *Pramel7*-overexpressing cells to a feeder-free environment, cultivated them in smooth muscle differentiation medium for 9 days and analysed their expression for SMA, a marker for smooth muscle tissue, and for UHRF1. Fig. 36 reveals differentiated smooth muscle cells highly positive for SMA in both cell lines. As to expect, resulting from the differentiated state, no UHRF1 signal was obtained in either cell line. These data show that mESCs overexpressing *Pramel7* are able to react to differentiation stimuli at least *in vitro*. Furthermore, they are able to activate the expression of differentiation markers such as SMA. However, if *Pramel7*-overepxressing mESCs are indeed capable to terminally differentiate and how stable pluripotency-related genes are silenced, remains to be clarified.

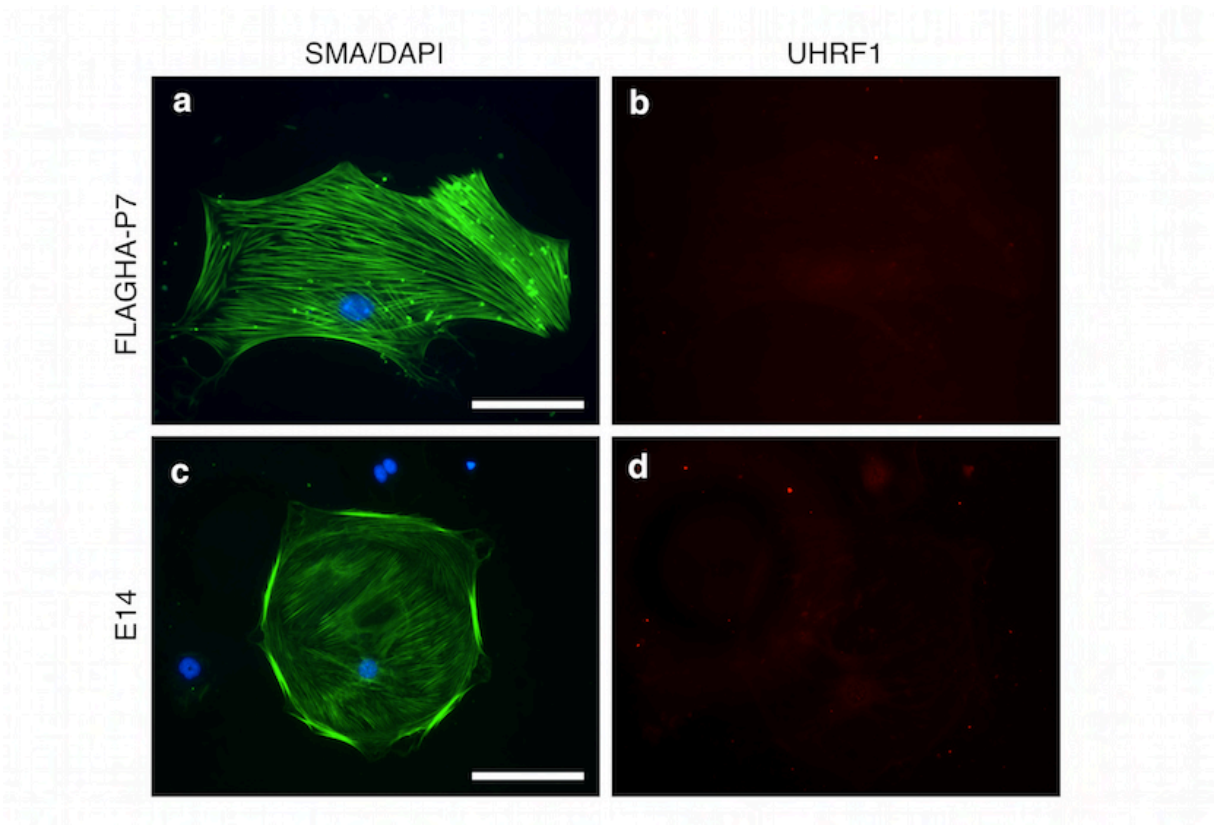

Fig. 36: Differentiation of *FLAGHA-Pramel7* overexpressing and *wt E14* mESCs into smooth muscle cells for 9d.

Differentiated (9d) smooth muscle cells from *FLAGHA-Pramel7* overexpressing **(a/b)** and *wt E14* mESCs **(c/d)** were immunohistochemically stained for smooth muscle actin (SMA) **(a/c)** and UHRF1 **(b/d)**. Scale bar: 100µm.

C. Discussion

This work for the first time identifies the functional role of a member of the PRAME-like gene family, *Pramel7*, that was originally found expressed in the pluripotent compartment of morula and blastocyst in the early mouse embryo (Cinelli et al., 2008). UHRF1 is a multi-domain protein mainly responsible for the recognition of hemimethylated DNA sites. Through guidance of DNMT1 to these sites UHRF1 mediates a faithful propagation of whole genome methylation during replication. After screening for possible binding partners we found that Pramel7, via its LRR-region, specifically interacts with the epigenetic regulator UHRF1 in HEK293T cells and mESCs. As a consequence, Pramel7 induces a rapid degradation of UHRF1 in a dose-dependent manner. The reduction of UHRF1 levels induced by the expression of *Pramel7* lead to severe global loss of genomic methylation in mESCs concomitant with a global enrichment of activating histone marks and enhanced expression of the trophectodermal marker *Elf5*. Moreover, after 14 days of differentiation mESCs overexpressing *Pramel7* were efficiently re-converted to the pluripotent state within 7 days. Finally, in this work we identified possible binding partners of the Pramel7-UHRF1 complex and set up a hypothetical model for a working mechanism of Pramel7 and possibly, other members of the *PRAME*-like gene family.

1. UHRF1, a new interaction partner of Pramel7

We identified UHRF1 as a binding partner for Pramel7 by a yeast two-hybrid assay (Fig. 7), a very suitable system to obtain initial hints for potential interaction partners. Nevertheless, this assay has certain limitations. First of all, the reliability is approximately 50% (Sprinzak et al., 2003) since the rate of false-positive hits is very high. This may be due to the following reasons. Firstly, transcription of the reporter gene is induced spontaneously by factors bound to the DNA binding domain in absence of the interaction partner (Hamdi and Colas, 2012). Secondly, since the approach occurs in the nucleus, candidates interacting in natural conditions might be found non-interacting e.g. if one of the two proteins contained a different, non-nuclear localization signal (Overington et al., 2006). Finally, the yeast cell might not be able to set up correct post-translational modifications as phosphorylation required for specific interactions in mammalian cells (Ngounou Wetie et al., 2014).

To confirm that UHRF1 was indeed interacting with Pramel7, we verified this interaction in a mammalian system where we could show a strong binding of the proteins after co-IP experiments in HEK293T cells (Fig. 9A). However, only a very weak signal of UHRF1 could be detected in mESCs (Fig. 9B). One possible explanation is that mESCs, even upon stable electroporation of an expression vector containing suitable promoters as *CAG* or *EF1,* hardly reach

expression levels as high as the ones obtained in HEK293T cells (Thomas and Smart, 2005). Therefore, the ratio between recombinant FLAG-Pramel7 and total protein used as input for the IP is reasonably less in mESCs than in HEK293T cells. Furthermore, while in mESCs we pulled down the endogenous UHRF1, in HEK293T cells UHRF1 was co-expressed with FLAG-Pramel7 resulting in more or less equal and high levels of bait and prey proteins. Furthermore, the constant degradation of UHRF1 by Pramel7 leads to strongly reduced levels of pulled-down UHRF1 in the IP when using mESCs, complicating the detection of UHRF1.

Interestingly, we were able to detect precipitated UHRF1 only when using mESCs expressing *FLAG-Pramel7* driven by the *EF1*- but not by the *CAG*-promoter (Fig. 9). A study of Chen et al. compared the activities of different promoters driving a stably integrated luciferase reporter at the *ROSA26* locus in mESCs. The authors found that the luciferase intensity in cells containing the construct driven by the *CAG* promoter was around 4 times higher than signals from cells containing the *EF1* plasmid (Chen et al., 2011). Generally, HEK293T cells produce higher amounts of proteins from exogenously integrated constructs than mESCs. Moreover, in our case we need to consider the rapid decrease in UHRF1 levels upon *Pramel7* overexpression (Fig. 17). These aspects finally lead to a reduced efficiency of the IP. We interpret that through enhanced activity of *CAG_FLAG-Pramel7* more UHRF1 is degraded already prior to the performance of the IP than in mESCs expressing *EF1_FLAG-Pramel7*. This leads to the conclusion that for a successful demonstration of this interaction in mESCs, FLAG-Pramel7 should be expressed at levels sufficiently low to prevent excessive degradation of UHRF1 but high enough to enable a detectable precipitation of UHRF1. Thus, a successful demonstration of the interaction in mESCs requires a tight balance of Pramel7 and UHRF1 levels.

Initial analysis of the Pramel7 protein sequence using the *LRR finder* software revealed three potential LRRs (Fig. 6). LRRs are patterns of repetitive sequences forming curved solenoid structures, which are particularly convenient for protein-protein interactions. These protein domains exhibit a huge structural and functional variability (Bella et al., 2008). Focusing on the region containing potential LRRs we wanted to narrow down the regions in Pramel7 mediating the interaction with UHRF1. For Pramel7, we cloned three different FLAG-tagged LRR deletion mutants of various lengths covering the predicted three LRRs and one control deletion located N-terminally of the LRRs (Fig. 11, Fig. 41/Fig. 42). Subsequent IP revealed all deletion mutants showed a drastically impaired potential of pulling down UHRF1. Interestingly, the control mutant could partly restore but not completely rescue the interaction (Fig. 12). Indeed, additional screening using another LRR detection software (*LRR search*) revealed additional three potentially important LRR located in the control region (Fig. 6). This indicates that the LRR with the sequence LKHLCLRGVTL is critical for the interaction. However, the three LRRs in the control area of Pramel7 identified in the second screening might also contribute to the interaction. The

shortest LRR deletion was 33AA in size. Hence, one could not rule out that the impaired ability in binding UHRF1 observed in all LRR mutants is originating from inappropriate protein folding. Nonetheless, in comparison with the LRR mutants, more UHRF1 was precipitated with the control deletion construct (62AA) (Fig. 12). This indicates that the observed effect is more likely to be a consequence of lacking LRRs than of aberrant protein folding. Thus, our data indicate that the LRR detected in the area of the control mutation together with the two LRRs affected in the smallest 33AA deletion are crucial for the interaction between Pramel7 with UHRF1.

UHRF1 contains multiple protein domains. Tandem-Tudor and PHD domains are involved in the recognition of the H3 tail. Most well characterized, the SRA domain binds to hemimethylated DNA regions (Avvakumov et al., 2008), (Hashimoto et al., 2008) ensuring the faithful transition of methylation marks from mother to daughter cells by recruiting DNMT1 to these particular sites (Bostick et al., 2007), (Sharif et al., 2007). The RING domain exhibits reported E3-ligase activity and the role of the C-terminal UBL domain is less clear (see Introduction chapter 3). To identify the region in UHRF1 indispensable for the interaction with Pramel7 we made use of different FLAG-tagged mutants with deletions in UBL, Tandem-Tudor and PHD domains described in the study of Liu et al. (Liu et al., 2013). It remains to be mentioned that in all mutants SRA and RING domains are absent (Fig. 13). As expected, Pramel7 was interacting most efficiently with full-length UHRF1 (Fig. 14). All other UHRF1 mutants were exhibiting weaker interactions indicating that the presence of the full-length UHRF1 protein is of great importance for a successful interaction. Consequently, this assigns a significant role to the C-terminal part of the protein comprising SRA and RING domains.

Besides Tandem-Tudor and PHD domains together mediating the interaction of UHRF1 with the H3 tail (Cheng et al., 2013), (Liu et al., 2013) the linker region connecting the two domains was reported to have a crucial function in this process (Arita et al., 2012). Furthermore, Rottach et al. reported that in UHRF1 deletion experiments the behavior of different UHRF1 mutants in chromatin association and localization was drastically changing, depending on which domains were deleted or not (Rottach et al., 2010). The authors therefore stated that observations originating from experiments sequentially testing the function of single domains are hardly applicable to the behavior of the full-length protein. Basically, all domains represent whole functional entities and, when present or deleted, might heavily influence the behavior and binding kinetics of the other domains. Thus, the exact molecular reasons for the different binding patterns of UHRF1 deletion mutants with Pramel7 remain to be elucidated.

The recognition of H3 by UHRF1 is very well documented (see Introduction chapter 3.4). Furthermore, PARP1 was identified as an interaction partner of UHRF1 (Sharif et al., 2007). Confirming these data, we were able to precipitate both H3 and PARP1 in HEK293Tcells (Fig. 10). PARP1 is very abundant at chromatin sites and was described to interact with different kinds of

histones and DNMT1 (Reale et al., 2005), (Heo et al., 2007), (Messner et al., 2010). In our experiments, using the UHRF1 deletion mutants, opposite binding patterns could be observed between H3/PARP1 and Pramel7. H3 and PARP1 among themselves both exhibited comparable binding patterns and only interacted with versions of UHRF1 containing intact Tandem-Tudor and PHD domains (UHRF1_1-408, UHRF1_95-368, UHRF1_95-408) (Fig. 14/Fig. 15). These forms of UHRF1 displayed a very low signal for Pramel7. Interestingly, the residual two deletion mutants with either incomplete Tandem-Tudor or PHD domain (UHRF1_1-298 and UHRF1_182-408) showed elevated levels of precipitated Pramel7 and very low H3/PARP1 (Fig. 14).

All UHRF1 deletion constructs were designed using the same expression plasmid (pSG5-FLAG) (Liu et al., 2013). Remarkably, very low amounts of full-length UHRF1 were detected in the input material of the respective IP when co-expressing Pramel7 (Fig. 14). As a consequence, nearly undetectable amounts of H3/PARP1 were observed in the respective precipitate. Repetition of the experiment in absence of Pramel7 revealed significantly higher amount of full-length UHRF1 in the starting material (Fig. 15). Concomitantly, a stronger UHRF1 enrichment co-precipitating more H3/PARP1 was observed after the IP. Thus, this differential outcome is conferred to the presence of Pramel7 and the accompanying degradation of full length UHRF1 as discussed below (Fig. 37). For other UHRF1 deletion mutants, no reduction was observed after co-expression of Pramel7. Moreover, binding patterns of H3/PARP1 were comparable among different mutants and thus independent on the presence of Pramel7. In addition, PARP1 seems to have a higher affinity to versions of UHRF1 containing Tandem-Tudor and PHD domains than to full-length UHRF1 (Fig. 15), indicating an effect impeding the interaction mediated by the C-terminal part of the full-length protein.

2. Additional interaction partners

We aimed at identifying additional potential binding partners of Pramel7-UHRF1 using mass spectrometry assays. In the first approach using FLAG-Pramel7 as bait we identified different types of histones, ElonginC (TCEB1) and Polyubiquitin in addition to UHRF1 in HEK293T cells. The complete list of factors was short, indicating that Pramel7 might interact with high specificity to particular proteins rather than being part of a big protein complex.

Since no potential DNA binding domain could be identified in the amino acid sequence of Pramel7 we wondered about the localization of the protein in the cell. The presence of histones, ElonginC and UHRF1 in the FLAG-Pramel7 precipitate suggested a nuclear localization. In fact, also for PRAME, a cell type-dependent cytoplasmic and/or nuclear localization was observed. Moreover, PRAME was reported to co-localize with ElonginC and to precipitate core histones. Therefore, PRAME is assumed to take over different roles in the cytoplasm and the

nucleus (Wadelin et al., 2013). This is also supported by our data from immunofluorescence experiments. Pramel7 and PRAME were localized at both cytoplasmic and nuclear sites (Fig. 29/Fig. 30). Interestingly, after separation of the soluble fraction from the chromatin in *Pramel7*-overexpressing mESCs, Western blot revealed a major bulk of Pramel7 associated to chromatin, suggesting a substantial role for Pramel7 in the nucleus directly at chromatin sites (Fig. 29).

Since UHRF1 was shown to strongly interact with histones and other chromatin modifiers, we sought for members exclusively depending on the presence of Pramel7. To gain further information we precipitated FLAG-UHRF1 in presence or absence of Pramel7. We then screened for factors present in only one of the two fractions since these hits were assumed to be dependent on the presence or absence of Pramel7, while proteins detected in both fractions were assigned to interact with UHRF1 independent of the presence of Pramel7. The only four proteins that could be detected in the presence of Pramel7 were ElonginC, HP1γ, CHD4 and SPT16. These factors are mainly involved in the establishment of chromatin and in transcription and elongation of a subset of genes (see Results chapter 1.4).

Based on the identification of ElonginC and under consideration of Costessi et al.'s study (see Introduction chapter 2.1) (Costessi et al., 2011) we propose a mechanism of Pramel7-mediated UHRF1 degradation involving ElonginC (Fig. 37). This working model is explained in more detail in the next chapter. Nevertheless, it cannot be excluded that factors as HP1γ, CHD4 and SPT16 also play a role connected to Pramel7-UHRF1. As an example, it was seen that overexpression of UHRF1 lead to misplacement of different HP1 proteins from pericentric heterochromatin, including HP1γ (Papait et al., 2008). It remains to be elucidated if a decrease in UHRF1 levels induced by the expression of Pramel7 might also have an effect on the distribution of HP1 proteins and thus on the large scale organization of pericentric heterochromatin. Indeed, our data from mESCs overexpressing *Pramel7* indicate a more active chromatin state shown by elevated levels of activating histone marks (Fig. 27). This is supported by the expression of the trophectodermal gene *Elf5* usually silenced in this cell type (Fig. 26). Summarizing, we cannot rule out a functional connection between Pramel7 and chromatin remodeling enzymes other than UHRF1.

3. Pramel7 as a substrate-recognition component of an E3-ligase complex

Our working model defines Pramel7 as the substrate recognition component specific for UHRF1 in a Cullin-RING ligase (CRL) complex. Pramel7 is assumed to interact with UHRF1 via its N-terminal LRR-rich region and with ElonginC and Cullin via C-terminal BC- and Cullin-boxes. Cullin is also associated with the E3-ligase Rbx1 (RING-box protein 1) that finally mediates the attachment of Ubiquitin residues to the substrate (UHRF1). CRLs account for approx. half of all predicted human E3-ligases and can vary in the composition of substrate recognition

components such as F-box proteins, different types of Cullin scaffold proteins and E3-ligases (Duda et al., 2012).

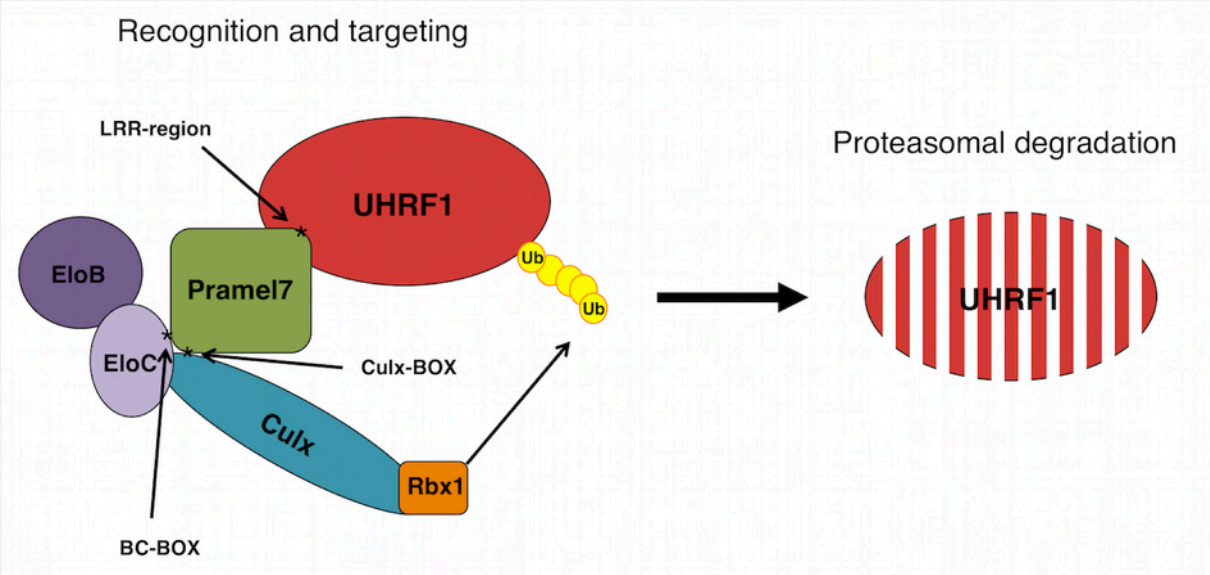

Fig. 37: Pramel7 as a substrate recognition component in a Cullin-RING ligase complex (CRL). Pramel7 is hypothesized to be the substrate recognition component specific for UHRF1. It interacts with UHRF1 (via the LRR-rich region), ElonginC (via BC-box) and one member (Culx) of the Cullin family (via Culx box). Cullin is again coupled to the E3-ligase Rbx1 (Ring-box protein 1), mediating the attachment of Ub-residues to the recognized substrate (UHRF1). Culx: Unknown member of the Cullin family. Ub: Ubiquitin. EloB/C: ElonginB/C.

Fig. 15 shows that in the presence of Pramel7 levels of full-length UHRF1 in the input fraction of the IP were drastically lower than in its absence. In different follow-up experiments we detected that Pramel7 expression in HEK293T and mESCs induced a dose-dependent, rapid and reversible downregulation of UHRF1 (Fig. 17 - Fig. 20). Chen et al. stated that UHRF1 is degraded in the steady state. A stronger degradation of UHRF1 was observed upon cellular stress such as DNA damage after UV irradiation (Chen et al., 2013). Nonetheless, we could exclude that the degradation of UHRF1 observed in our experiments is originating from the sole transfection procedure of HEK293T cells coupled with massive production of Pramel7 and potential cell stress. In contrast to Pramel7, overexpression of PRAME, Pramel6 and also different deletion mutants of Pramel7 did not lead to any alteration of UHRF1 levels (Fig. 31/Fig. 22).

All of the three LRR deletion mutants of Pramel7 were all not able to induce a degradation of UHRF1 (Fig. 22). In contrast, the control mutation could induce a small decrease in UHRF1 levels. This is in line with data from Fig. 12 where the Pramel7 control mutant was able to bind more UHRF1 than LRR deletion mutants, but could not rescue the interaction to *wt* levels. Here, we observed a similar effect in regard to UHRF1 degradation, indicating that the degradation of UHRF1 is dependent on the amount of UHRF1 bound to Pramel7.

Pramel7 was not able to degrade any of the six UHRF1 deletion mutants (Fig. 23). Since the phosphodegron at S108 identified by Chen et al. is present in all the mutant UHRF1 proteins

(Chen et al., 2013), another feature catalyzing the degradation of the protein is likely to be located in its C-terminal part containing SRA and RING domains, possibly an ubiquitin acceptor site.

Our hypothesis is based on the findings originally made for the Von Hippel-Lindau (pVHL) tumor suppressor protein. pVHL is a specific substrate recognition subunit of an E3 CRL complex (ElonginB/C, Cul2, Rbx1) targeting the protein HIF1 (Hypoxia inducible factor 1) for degradation. In many studies it was stated that lack or inappropriate expression of *pVHL* lead to increased levels of HIF1 and consequently, to numerous benign and malign tumors (Kanno et al., 1994), (Shuin et al., 1994), (Robinson and Ohh, 2014).

In general, the process of ubiquitination involves a cascade of protein reactions. The E1 ubiquitin-activating enzyme recruits and transfers a ubiquitin residue to the E2 conjugating enzyme. Finally, the E3 ubiquitin ligase interacts with E2 and coordinates the ligation of the ubiquitin to a lysine residue of the target substrate. The substrate recognition protein of the E3 complex, of which more than 1000 exist, provides specificity to the reaction. Besides this, it is not unusual that one E3 recognition subunit controls the degradation of different targets. However, the exact substrates for the major bulk of these subunits are still unknown (Zou and Mallampalli, 2014). In most cases, before interacting with an E3-ligase complex, substrates are modified via mechanisms such as phosphorylation, dephosphorylation, methylation or acetylation (Xu et al., 2009), (Ravid and Hochstrasser, 2008), (Zou and Mallampalli, 2014). Cellular localization of E3-ligase complexes can be both cytoplasmic and nuclear. For instance, one isoform of the substrate recognition subunit ßTrCP of the SCF E3-ligase complex was found localized in the nucleus whereas another was associated with the cytoplasm (Seo et al., 2009). Taken together, Pramel7 and other members of the PRAME-like family might act as substrate recognition components in the nucleus and/or the cytoplasm, depending on the presence of their target proteins. UHRF1 displays nuclear localization and, as already mentioned above, in mESCs we could identify a substantial fraction of Pramel7 protein associated with chromatin (Fig. 29). Nonetheless, it is not ultimately evident if the presence of UHRF1, specifically, is targeting Pramel7 to chromatin sites.

The $SCF^{ßTrCP}$ E3-ligase, a specific CRL complex, was identified as a mediator degrading UHRF1 under normal and in stress conditions (e.g. UV-response) via phosphorylation of UHRF1 S108 by CK1∂ (Casein kinase 1∂) (Chen et al., 2013) (see Introduction chapter 3.3). Expression of Pramel7 leads to a similar effect. Now the question is to address if Pramel7 truly acts as a substrate recognition subunit targeting UHRF1 in its own E3 CRL complex. It could also induce UHRF1 degradation indirectly such as by stimulation of ßTrCP expression or activity. However, based on our findings we favor the first possibility. We could identify ElonginC but not ßTrCP in our mass spectrometry and do not have any evidence of a connection between Pramel7 and

ßTrCP. According to our data and in contrast to ßTrCP, Pramel7 only has very few specific interaction partners. Hence, Pramel7 is likely to represent a CRL-based substrate recognition subunit in a degradation process of the specific target protein UHRF1.

4. Overexpression of Pramel7 severely reduces global DNA methylation in mESCs

As for the first time shown by Bostick et al. and Sharif et al. it is generally accepted that a decrease in UHRF1 gene expression leads to global DNA hypomethylation induced by disturbed guidance of the maintenance DNA methyltransferase DNMT1 to sites of hemimethylated DNA during the S-phase of the cell cycle (Bostick et al., 2007), (Sharif et al., 2007). Indeed, our results suggest the occurrence of a comparable effect after stable overexpression of *Pramel7* in mESCs. In two approaches, we could demonstrate that in comparison to *wt E14* mESCs the prevalence of 5mC is drastically reduced in *Pramel7*-overexpressing mESCs (Fig. 24/Fig. 25). Moreover, we observed an aberrant overexpression of the trophectodermal gene *Elf5* in *Pramel7*-overexpressing mESCs usually seen in *DNMT1/3a/3b*$^{-/-}$ mESCs (Ng et al., 2008). Abnormal activation of *Elf5* was detected in cells cultivated in steady state conditions (CM +LIF on feeders) but also in differentiated mESCs (CM -LIF, no feeders). Relative to *wt E14* control cells, differences in *Elf5* expression were drastically higher in differentiated than in pluripotent cells (Fig. 26). Taken together, these findings suggest that in mESCs through the sole overexpression of *Pramel7* a similar state as observed in *UHRF*$^{-/-}$ and in *DNMT1/3a/3b*$^{-/-}$ mESCs can be established. However, it is notable that UHRF1 levels in *Pramel7*-overexpressing cells were drastically reduced, but not fully absent (Fig. 17).

According to Leitch et al., global DNA hypomethylation is associated with naïve pluripotency. When comparing mESC lines cultivated in parallel in serum and 2i conditions a dramatic decrease in global DNA methylation was observed in cells cultured in 2i, the culture condition closely mimicking the naïve pluripotent state (Ying et al., 2008). It is thought that in 2i mESCs are shielded from differentiation and kept in a naïve state by preventing *de novo* methylation (Leitch et al., 2013). Moreover, data from 2008 suggested that in mESCs the presence of H3K4 methylation and the absence of the repressive H3K9 methylation are better predictors of unmethylated CpGs than the sequence context alone (Meissner et al., 2008). Indeed, also in *Pramel7*-overexpressing mESCs we detected a correlation between low DNA methylation and histone modifications. Most activating histone marks were found enriched whereas repressive marks were reduced (Fig. 27). However, the coordination and the hierarchy of DNA and histone modifications and the degree to which these two types of epigenetic modifications are dependent on each other remains debatable. Nevertheless, the ability of UHRF1 to read the H3 tail, to interact with the DNA and to physically associate with chromatin remodeling enzymes

such as DNMT1, G9a or HDAC makes this molecule an interesting candidate to interpret the local epigenetic environment. UHRF1 might also create feedback loops leading to concerted reinforcement of DNA and histone modulation (Jin et al., 2011).

During differentiation of mESCs, tissue-specific promoters have to be activated and genes promoting pluripotency need to be silenced. It is assumed that silencing first occurs by binding of transcriptional repressors concomitant with deacetylation of activating histone marks at the promoter region. This is followed by the establishment of repressive histone modifications such as H3K9me3 in association with deposition of HP1 (Feldman et al., 2006). Then, after subsequent *de novo* DNA methylation by DNMT3a/b, these marks are stably maintained by DNMT1. This maintaining process is orchestrated by UHRF1 (Bostick et al., 2007), (Sharif et al., 2007). Resulting from global hypomethylation, we observed that *Pramel7*-overexpressing mESCs have difficulties in undergoing terminal differentiation. After culturing these cells in differentiating conditions for 14d, expression of the pluripotency-associated genes *Oct4*, *Nanog* and *Rex1* was higher than in *wt E14* control cells. Then, the major fraction of *Pramel7*-overexpressing cells was able to rapidly regain pluripotent features demonstrated by the successful reactivation of pluripotency-associated genes. In contrast, almost all *wt* clones remained differentiated and the few re-converted *wt* clones were not able to reactivate the expression of *Rex1* and endogenous *Pramel7* (Fig. 32 - Fig. 35).

These findings are corroborated by another study of our group stating that mESCs overexpressing *Pramel7* are disturbed in differentiation. When exposed to an *in vivo* environment, *Pramel7*-overexpressing mESCs firstly were not able to generate teratoma after injection into immunodeficient mice and secondly, after morula aggregation using *Pramel7*-overexpressing mESCs, developing embryos analyzed at E5.5 showed malformations. Furthermore, when stimulated for differentiation *in vitro* with RA (retinoic acid), *Pramel7*-overexpressing mESCs were extensively undergoing cell death (Casanova et al., 2011). For the pluripotency associated gene *Oct4* Feldman et al. observed a similar phenomenon. They successfully demonstrated that *G9a*$^{-/-}$ mESCs were not able to efficiently shut down the promoter of *Oct4*. Moreover, these cells could easily be reconverted to the pluripotent state after RA-induced differentiation (Feldman et al., 2006). In conclusion, for an efficient and stable differentiation of mESCs, different components regulating epigenetic silencing on the chromatin and the DNA level are required. Reconsidering its bi-modal capacity, UHRF1 represents one of these candidates. Taken together, we hypothesize that overexpression of *Pramel7* results in an active genomic state in mESCs. When *Pramel7*-overexpressing mESCs are forced to differentiate, promoters of pluripotency genes may be silenced transiently through repressor binding and eventual establishment of repressive histone marks. However, these cells are not able to undergo efficient terminal promoter silencing ultimately characterized by robust DNA methylation (Gaspar-Maia et al., 2011). As a conse-

quence, as soon as pluripotency promoting stimuli (LIF) are re-sensed the core pluripotency network might again be induced and mESCs re-adapt pluripotent features. Therefore, we propose that as long as the mESCs express Pramel7 at a sufficient level, these cells are not able to undergo terminal differentiation.

Since *Pramel7* was initially found expressed in the pluripotent compartments of a preimplantation embryo (Cinelli et al., 2008) we would like to speculate about possible roles *in vivo*. During embryonic development of the mouse different waves of global DNA demethylation were described. After fertilization, the paternal genome is actively demethylated whereas methylation marks of the maternal genome are thought to undergo passive erasure, peaking at the ICM stage (Smith et al., 2012). How this demethylation process is orchestrated in detail is largely unknown. Relating to our data, we provide a model in which intracellular UHRF1 levels can be kept at a minimum through consecutive expression of *Pramel7*, supporting a replication-coupled, passive demethylation process.

It is not negligible that a similar mechanism could also be involved in the epigenetic reprogramming of PGCs (primordial germ cells) from E9.5-E11.5 in the mouse embryonic development. Kagiwada et al. recently showed that the erasure of DNA methylation marks during PCG reprogramming is very likely to as well take place in a replication coupled, passive manner. Also UHRF1 levels (gene expression & protein levels) during this period of embryonic development (E10.5/E11.5) were very low (Kagiwada et al., 2013). Interestingly, another study found UHRF1 to be expressed at the mRNA level in E10.5 PGCs but no UHRF1 protein was detected (Ciccarone et al., 2012). Thus, it remains to be defined to what extent Pramel7 or other proteins of the PRAME-like family are expressed in these stages of development or if they are at all implicated in the regulation of this particular epigenetic event.

PRAME is defined as a cancer-testis antigen. The expression of these genes can be detected in male and female gonads and in germ cells. Since the expression of *PRAME-like* members seems to be specifically restricted to a specific developmental period it seems that these genes may be involved modularly in different stages of gametogenesis and embryogenesis (Mistry et al., 2013). Very preliminary data from our lab displayed expression of Pramel7 in maturating mouse spermatids (data not shown). Since developmental gene promoters of sperm cells were described to be generally hypomethylated (Carrell, 2012) Pramel7 might be involved in maintaining this effect. However, very little is known about DNA methylation in spermatogenesis and more research has to be undertaken in this field.

5. Future perspectives and concluding remarks

The molecular role of *PRAME-like* genes is largely elusive. In this work, we, for the first time provide evidence of a functional role for one of its members. We demonstrate that the protein

Pramel7 is firstly interacting with and secondly rapidly mediating the degradation of UHRF1. Thirdly, as a consequence of the reduction of UHRF1 levels, global DNA methylation is drastically reduced in mESCs overexpressing *Pramel7*. This leads to a more active epigenetic state and aberrant terminal differentiation.

However, many questions still need to be answered in the future. In additional mechanistic approaches, features mediating the interaction of the two proteins could be determined in the amino acid context. Regarding Pramel7, the region containing three crucial LRRs identified in Fig. 11 and Fig. 12 has to be narrowed down by generating single amino acid mutations. In UHRF1, the C-terminal region containing SRA and RING domains should be sequentially deleted to identify possible motifs indispensable for the binding.

Since in mass spectrometry experiments only ElonginC and Polyubiquitin but no other components of a potential CRL complex were identified, it remains to be clarified if Pramel7 indeed is a recognition component specific for targeting UHRF1. This can be achieved by IP and subsequent detection of possible CRL candidates (different Cullin members, Rbx1/2). Furthermore, it has to be verified if knockdown of the above factors inhibits the degradation of UHRF1 after induction of Pramel7 expression. To obtain further understanding if the sole presence of UHRF1 attracts Pramel7 to chromatin sites, the amount of Pramel7 in chromatin and soluble fractions of *UHRF1*$^{-/-}$ mESCs should be determined. Moreover, to assess the impact of *Pramel7* expression on DNA methylation, degrees of 5mC in *UHRF1*$^{-/-}$ and *Pramel7*-overexpressing mESCs could be quantified and compared.

Caused by reduced DNA methylation, we provided evidence that *Pramel7*-overepxressing mESCs display major difficulties in the establishment of a stable terminally differentiated state. Nonetheless, *Pramel7*-overexpressing cells were able to adapt a differentiated fate as shown by differentiation into smooth muscle cells positive for SMA (Fig. 36). This implicates that these cells have the ability to activate developmental genes crucial for their specification. However, if pluripotency-associated genes as *Oct4* or *Rex1* are stably and efficiently silenced in these cells remains to be clarified.

In vivo, knockdown of *Pramel7* in preimplantation mouse embryos with subsequent determination of UHRF1 and 5mC levels would provide more evidence if Pramel7 is involved in the regulation of a replication-coupled, passive DNA methylation mechanism during the early development of the mouse embryo.

Despite all the open questions, we for the first time were able to describe a functional role for a member of the PRAME-like gene family, Pramel7. It will be interesting to see if other family members of and possibly *PRAME* itself hold similar roles. Therefore, according to our working model, every PRAME-like protein possesses the ability to induce the degradation of a specific interaction partner. As seen for UHRF1, this could heavily affect the developmental fate of a

particular cell type. In conclusion, with these findings, a new window aiming on the characterization of this manifold family of proteins has been opened.

D. Materials

1. Cell culture media and supplements

Fibro medium:	Dulbecco's Modified Eagle Medium (DMEM) (Sigma) 10% Fetal Calf Serum (PAA) 1mM Sodium Pyruvate (Sigma)
Complete medium:	Glasgow Minimal Essential Medium (GMEM) (Sigma) 10% Fetal Calf Serum (PAA) 1mM Sodium Pyruvate (Sigma) 1x Non-Essential Amino Acids (Life Technologies) 1x Penicillin-Streptomycin-L-Glutamine (Life Technologies) 0.1mM 2-Mercaptoethanol (Life Technologies)
N2B27 medium:	1:1 Neurobasal Medium:DMEM/F-12 (both Life Technologies) 1x Penicillin-Streptomycin-L-Glutamine (Life Technologies) 1x N2-Supplement (Life Technologies) 1x B27 Supplement (Life Technologies) 0.05mM 2-Mercaptoethanol (Life Technologies)
N2B27 supplements (2i):	1µM PD0325901 (Stemgent) 3µM CHIR99021 (Stemgent)
Smooth muscle differentiation:	DMEM (Sigma) 10% Fetal Calf Serum (PAA)
Cell culture supplements:	1000U/ml Leukemia Inhibitory Factor (LIF) (Millipore) 1µM MG132 proteasome inhibitor (Calbiochem) 10µg/ml cycloheximide (Sigma)
Antibiotics:	Puromycin (Sigma) G418 (Neomycin) (PAA)

Others:	0.1% Gelatin from porcine skin (Sigma)
	Trypsin EDTA (10x stock) (Sigma)
	PBS (w/o Ca and Mg) (different distributors)
	Fugene HD transfection reagent (Roche)
	Xtremegene HP transfection reagent (Roche)

2. Plasmids

2.1. Pramel7 expression constructs

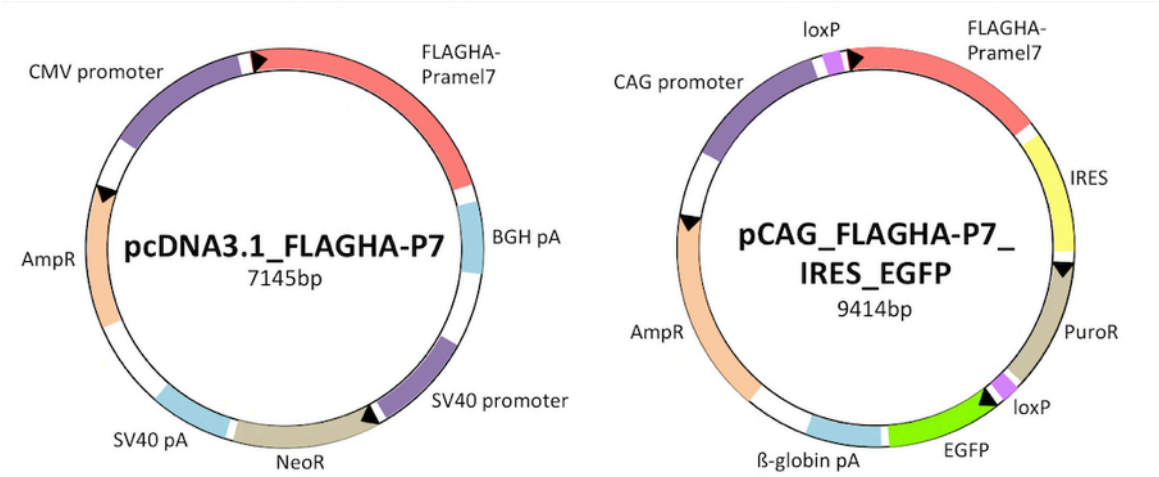

Fig. 38. Construction of constructs expressing versions of *Pramel7* (1).
A FLAGHA-tagged version was cloned under a *CMV* promoter (left, pcDNA3.1) and a *pCAG* promoter (right). *pcDNA3.1* backbone vector was provided by Raffaella Santoro, University of Zurich.

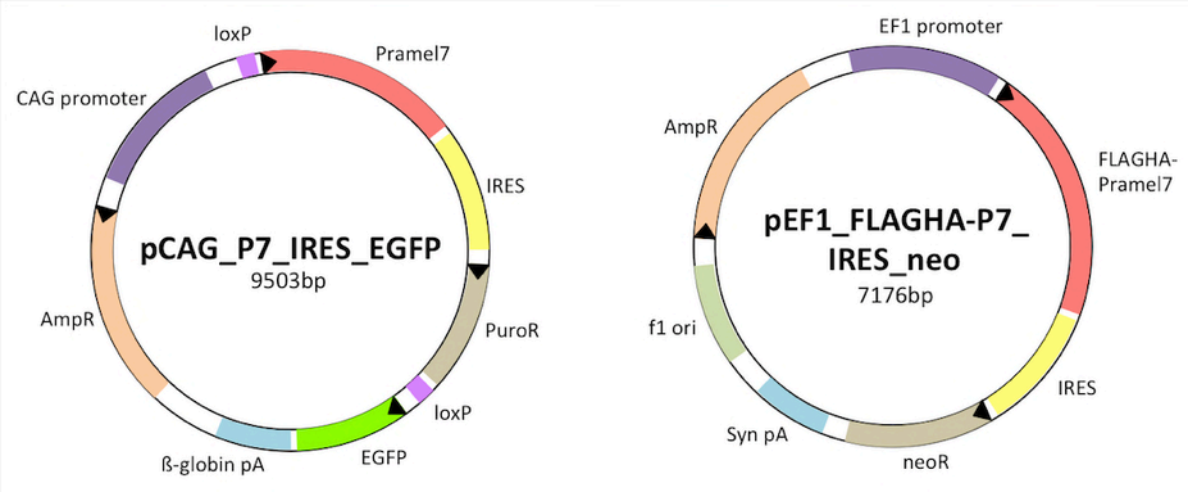

Fig. 39: Construction of constructs expressing versions of *Pramel7* (2).
Untagged *Pramel7* is expressed under a *pCAG* promoter (left) and *FLAGHA*-tagged *Pramel7* under a *pEF1* promoter (right). Dr. Elisa Casanova constructed *pCAG_P7* (left) and the empty *pEF1_IRES_neo* backbone generated by Thomas Zwaka was obtained at Addgene (www.addgene.com).

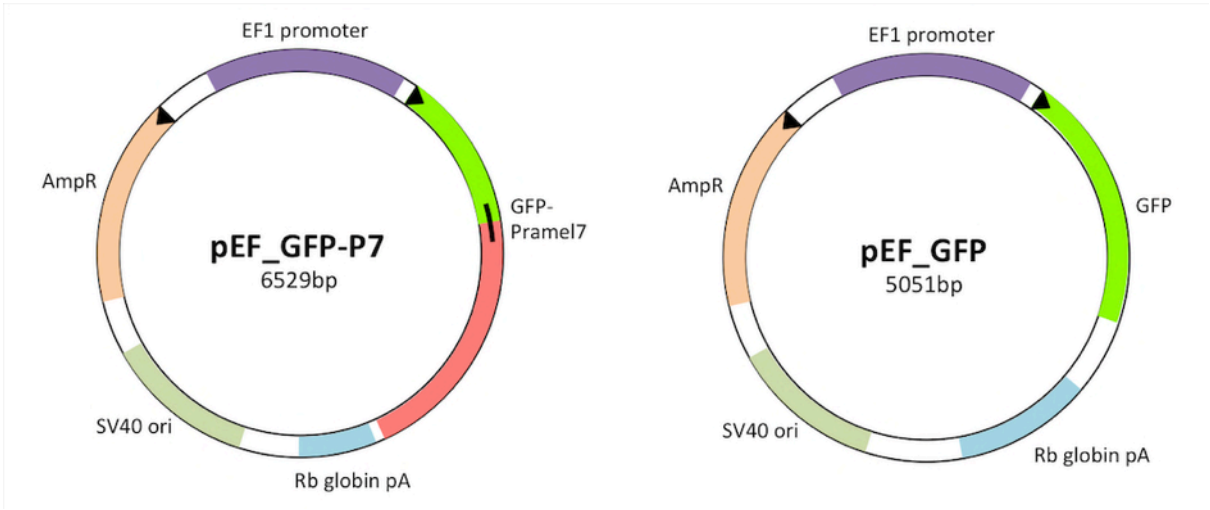

Fig. 40: Construction of constructs expressing versions of *Pramel7* (3).
A GFP-Pramel7 fusion protein is expressed under a *pEF* promoter (left). The empty *pEF_GFP* backbone (right) cloned by Dr. S. Sugano, University of Tokyo, was obtained at Addgene (www.addgene.com).

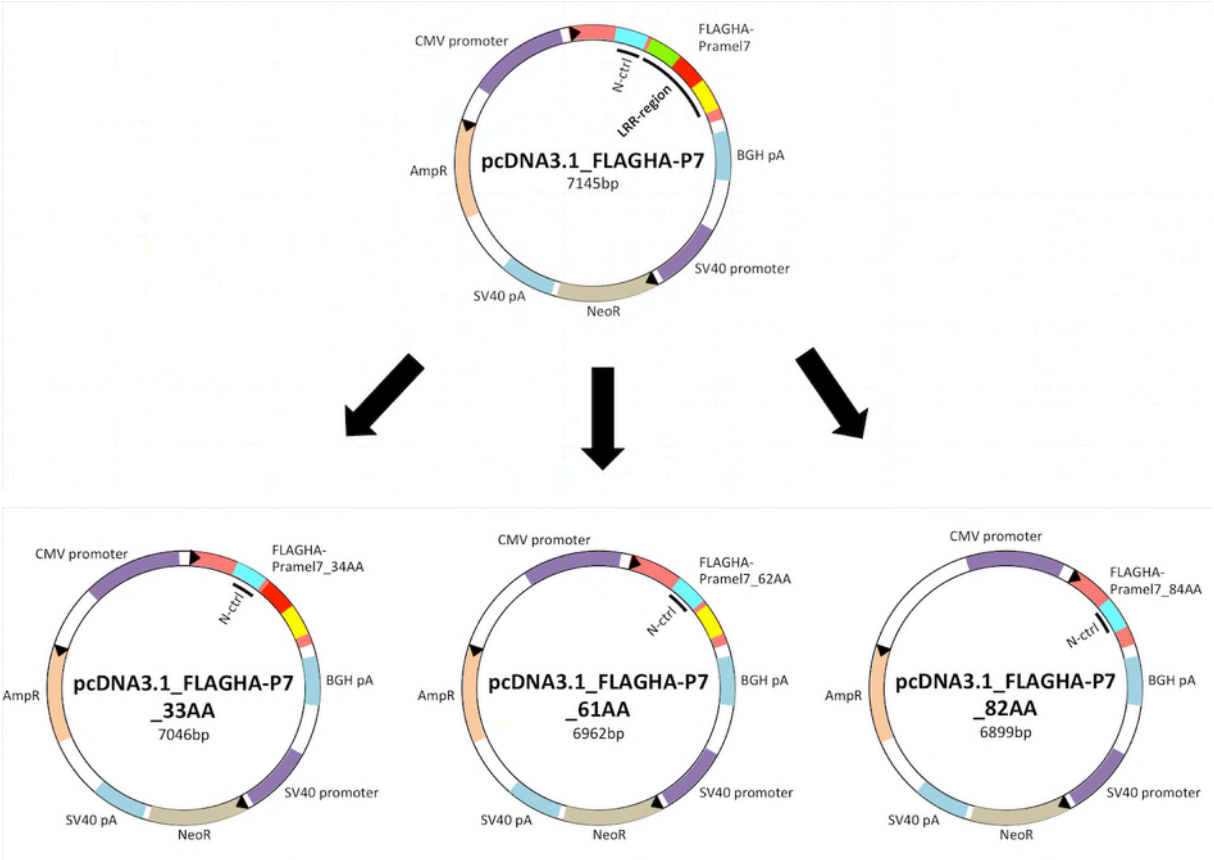

Fig. 41: Generation of Pramel7 versions mutant in the LRR region.
The *pcDNA3.1_FLAGHA-P7* expression vector was mutated in the LRR region using a PCR-based approach. 3 expression plasmids mutant in the LRR region of *Pramel7* were generated with deletions of 33AA, 41AA and 82AA, respectively (from left to right). The N-terminal control region was not affected.

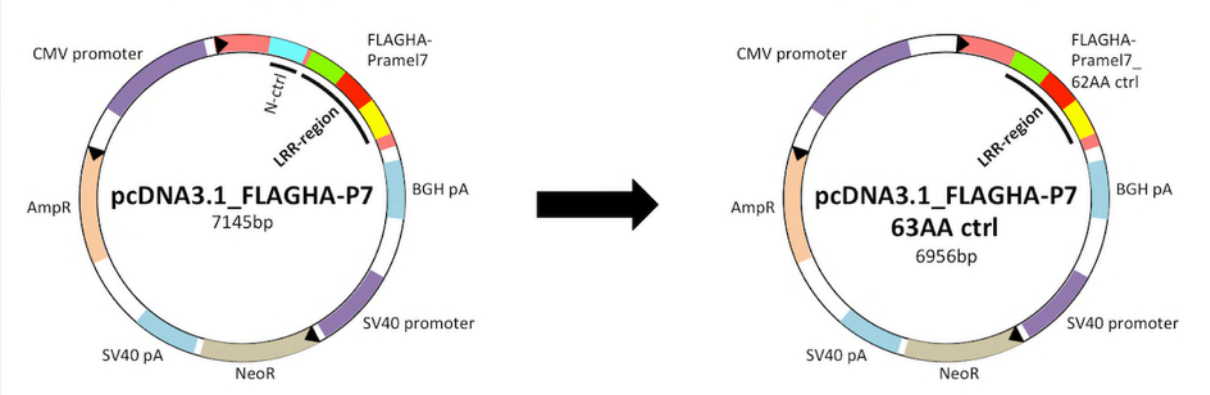

Fig. 42: Generation of a Pramel7 version with mutated N-terminal control region.
The control region is located N-terminally of the region containing predicted LRRs. Length of the deletion: 63AA.

2.2. UHRF1 expression constructs

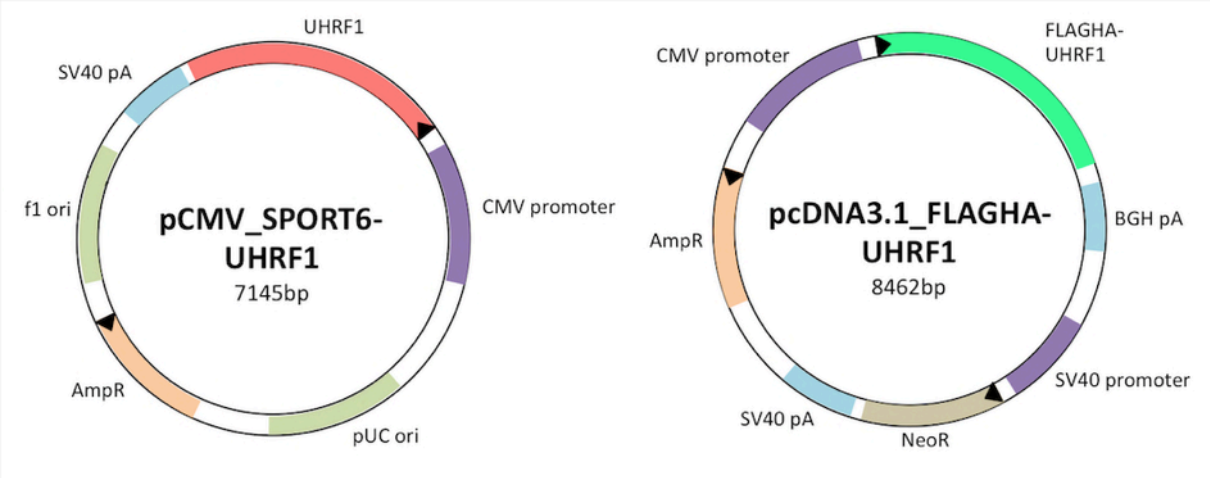

Fig. 43: Construction of constructs expressing versions of *UHRF1*.
FLAGHA was cloned in front of *UHRF1*'s N-terminus and expressed under a *pcDNA3.1* backbone (*CMV* promoter) (right). *UHRF1* CDS was cloned out of the *pCMV_SPORT6* expression vector (left) obtained from Harvard Medical School's plasmID database (plasmid.med.harvard.edu).

2.3. Other expression constructs

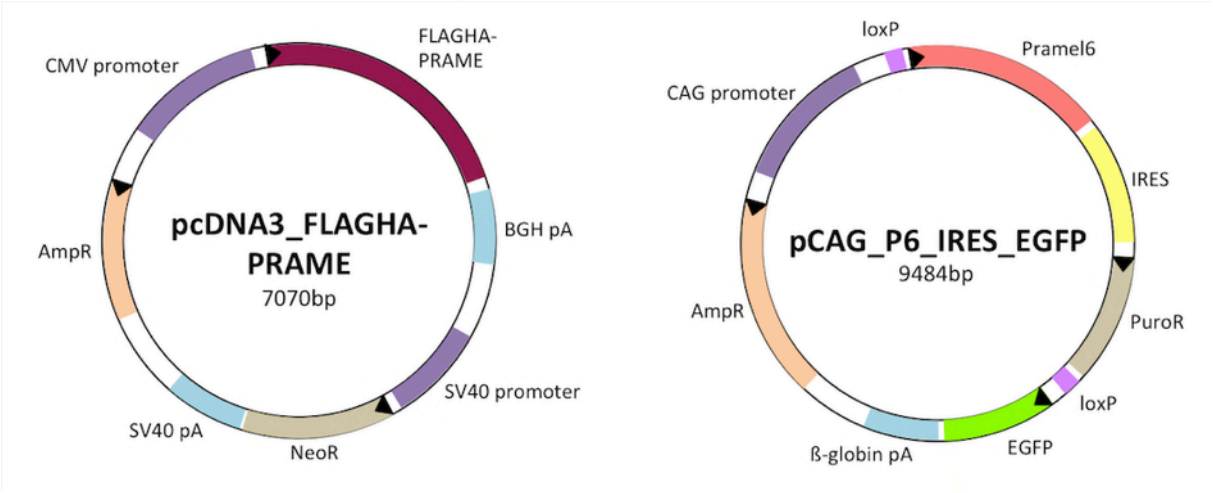

Fig. 44: Expression constructs for human *PRAME* and mouse *Pramel6*.
The CDS of *PRAME* was cloned out of a *pCMV_SPORT6* expression vector obtained from Harvard Medical School's plasmID database (plasmid.med.harvard.edu) and inserted into a *pCDNA3_FLAGHA* expression plasmid (left) from Addgene (www.addgene.com). The *pCAG_Pramel6* expression construct was cloned by Dr. Elisa Casanova (University Hospital, Zurich).

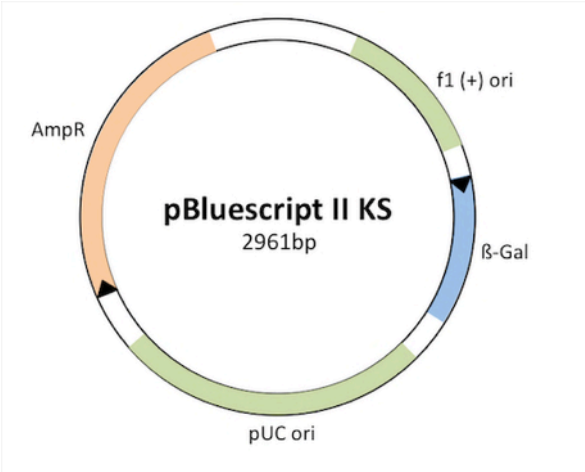

Fig. 45: *pBluescript* control plasmid.
Control transfections were carried out using a *pBluescript II KS* plasmid obtained from Silvia Marino (Barts and the London School of Medicine and Dentistry) and was originally constructed by Stratagene (Agilent).

3. Cell lines

Feeder cells:	Mitotically inactivated (Mitomycin C, Sigma) E14.5 mouse embryonic fibroblasts, cultivated in Fibro medium
E14 mESCs:	*129*-background ESC line, cultivated in complete medium +LIF
E14 CAG_FLAGHA-Pramel7 mESCs:	*E14* mESCs overexpressing *FLAGHA*-tagged *Pramel7* under *CAG* promoter, cultivated in complete medium +LIF
E14 *EF1_FLAGHA-Pramel7* mESCs: EF1	*E14* mESCs overexpressing *FLAGHA*-tagged *Pramel7* under *EF1* promoter, cultivated in complete medium +LIF
129 mESCs:	*129* background, cultivated in N2B27 +2i +LIF
129 *CAG_FLAGHA-Pramel7* mESCs:	*129* mESCs overexpressing *FLAGHA*-tagged *Pramel7* under *CAG* promoter in N2B27 +2i +LIF
HEK293T cells:	Human embryonic kidney cells (obtained from Raffaella Santoro, University of Zurich), cultivated in Fibro medium

4. Buffers and solutions

Alkaline Phosphatase (AP) buffer:	0.1M Tris-HCl 0.1M NaCl 20mM $MgCl_2$ pH 9.5
AP staining solution:	AP Buffer containing: 0.5µl/ml NBT (Nitro blue tetrazolium chloride) (Roche) 3.5µl/ml BCIP (5-bromo-4-chloro-indolyl phosphate (Roche)
BES solution:	50mM BES (Sigma) 280mM NaCl (Sigma) 1.5mM Na_2HPO_4 (Sigma) Adjust pH to exactly 7.0
RIPA buffer:	50mM Tris-HCl pH 7.4 (Sigma) 1% (v/v) NP-40 (Sigma) 0.25% (v/v) Na-Deoxycholate (Sigma) 150mM NaCl (Sigma) Add 1 tablet of complete mini proteinase inhibitor (ROCHE) /10ml
Nuclear Extraction (NE) buffer:	50mM Tris-HCl pH 7.5 (Sigma) 150mM KCl (Sigma) 5mM $MgCl_2$ (Sigma) 0.2mM EDTA (Sigma) 20% (v/v) Glycerol (Sigma) Add prior use: 0.5mM DTT (Sigma) 0.1% (v/v) NP-40 (Sigma) Add 1 tablet of complete mini proteinase inhibitor (ROCHE) /10ml

Silver staining solution A:	50% MeOH
(100ml)	10% acetic acid, fill to 100ml with ddH_20
Silver staining solution B:	5% MeOH
(100ml)	Fill to 100ml with ddH_20
Silver staining solution C:	0.2g $Na_2S_2O_3$
(1l)	Fill to 100ml with ddH_20
Silver staining solution D:	200mg $AgNO_3$
(100ml)	Fill to 100ml with ddH_20
Silver staining solution E:	3g Na_2CO_3
(100ml)	50µl HCOH (37%)
	2ml of silver staining solution C
	Fill to 100ml with ddH_20
Silver staining solution F:	10ml 0.5M EDTA
(100ml)	Fill to 100ml with ddH_20
Chromatin extraction buffer:	10mM NaCl
	30mM Hepes
	3mM $MgCl_2$
	0.5% TritonX-100
Proteinase-K buffer:	100mM NaCl
	10mM Tris-HCl pH 8.0
	0.5% SDS
gDNA elution buffer:	10nM Tris pH 8.0
	1mM EDTA pH 8.0
LB medium:	10g NaCl (Sigma)
	10g Bacteriological peptone (Sigma)
	5g Yeast Extract (Sigma)
	Fill to 1l with ddH_20 and autoclave

E. Methods

1. Cloning

Restriction digestions were performed according to manufacturers instructions (NEB, Promega). Quick Blunting Kit (NEB) was used for carrying out blunting reactions. DNA fragments were purified using QIAQuick PCR Purification and QIAQuick Gel Extraction Kits (Qiagen). Fragments were ligated with NEB T4 DNA ligase and constructs were transformed into chemically competent MAX Efficiency DH5α E.Coli (Life Technologies). Plasmid DNA from picked candidate clones was purified using QIAPrep Spin Miniprep Kit (Qiagen). After confirmation of correctly integrated clones by Sanger sequencing (Microsynth AG, Balgach, Switzerland) positive clones were multiplied in LB medium and DNA was isolated using QIAFilter Plasmid Maxi Kit (Qiagen). Agarose gel electrophoresis was performed using 5x TBE buffer (5PRIME) and agarose (Sigma) and gels were run at 120-150V.

2. Western blotting

Protein amounts were normalized using the Pierce BCA Protein Assay Kit (Thermo Scientific) and protein absorbance was measured using Nanodrop technology. Lysates were further processed with the NuPAGE SDS PAGE Gel system (Life technologies). SDS-gels were run at 160-190V and proteins were either wet-blotted overnight (40V, 4°C) or for 1.5h (120V) at room temperature (ice block-cooled) on a PVDF Immobilon-P transfer membrane (Millipore). Membranes were fixed using Western Blocking Reagent (Roche) for at least 1h and incubated with primary antibodies over night at 4°C or at room temperature for 1h (in blocking solution). Membranes were washed 3 times with 1x TBST (TBS supplemented with 1% Tween-20 (Sigma), 10’ each step) and secondary antibodies were added for 30’-1h at room temperature (in blocking solution). After four washing steps (3x TBST, 1x TBS, 10’ each) signals were enhanced using Chemiglow Peroxide Buffer and Luminol/Enhancer Solution (Protein Simple) and detection was carried out with Amersham Hyperfilm ECL high performance chemiluminescence film (GE healthcare).

Tab. 5: List of antibodies used for immunodetection by Western blotting

Antibody	Species	Supplier	Catalog No.
α-tubulin	mouse	Sigma	T8203
α-FLAG	rabbit	Sigma	F7425
α-HA	mouse	Santa Cruz	sc-7392
α-PARP1	rabbit	Cell Signaling	9532
α-Pramel7	rabbit	selfmade	
α-UHRF1	rabbit	Santa Cruz	sc-98817
α-H3	rabbit	Abcam	
α-H3K4me3	rabbit	Cell Signaling	9751
α-H3K9ac	rabbit	Cell Signaling	9649
α-H3K9me3	rabbit	Millipore	07-442
α-H3K27me3	rabbit	Cell Signaling	9756
α-H4ac	rabbit	Millipore	06-866
α-H4K5ac	rabbit	Millipore	07-327
α-mouse HRP	goat	Santa Cruz	sc-2031
α-rabbit HRP	goat	Santa Cruz	sc-2030

3. RNA extraction, reverse transcription and quantitative real-time PCR (RTQ-PCR)

First cell pellets were resuspended in RLT buffer provided with the RNEasy Mini Kit (Qiagen) containing 0.1% 2-mercaptoethanol (100%, Sigma) and RNA was extracted following manufacturer's instructions. RNA concentrations were measured with the Nanodrop technology and 500ng or 1µg of RNA were reverse transcribed using Oligo(dT)12–18 Primer (Life Technologies), 10mM dNTP Mix (Life Technologies), RNAsin Plus RNAse Inhibitor (Promega) and SuperscriptIII Reverse Transcriptase (Life Technologies). cDNA was analysed with the Rotor-Gene SYBR Green PCR Kit (FAST) (Qiagen). Primers for RTQ-PCR were obtained at Microsynth AG, Balgach, Switzerland.

Tab. 6: List of primers used for quantitative real-time PCR (RTQ-PCR)

Gene name	Sequence
β-actin_fw	5'-CAT CCA GGC TGT GCT GTC CCT GTA TGC-3'
β-actin_bw	5'-CAT CCA GGC TGT GCT GTC CCT GTA TGC-3'
hElonginC_fw	5'-ACC TAT GGT GGC TGT GAA GG-3'
hElonginC_bw	5'-AGG TGC AAT TGG GAA TTC AG-3'
FGF5_fw	5'-TCC TCA CCA GTC GCA GCT TC-3'
FGF5_bw	5'-TTC AGG GCC ACG TAC CAC TC-3'
Gata4_fw	5'-GCC TGT ATG TAA TGC CTG CG-3'
Gata4_bw	5'-CCG AGC AGG AAT TTG AAG AGG-3'
Gata6_fw	5'-GCA ATG CAT GCG GTC TCT AC-3'
Gata6_bw	5'-CTC TTG GTA GCA CCA GCT CA-3'
Nanog_fw	5'-ACA AGG GTC TGC TAC TGA GAT GC-3'
Nanog_bw	5'-GGA GAC TTC TTG CAT CTG CTG G-3'
Nestin_fw	5'-AGG CTG AGA ACT CTC GCT TGC-3'
Nestin_bw	5'-GGT GCT GGT CCT CTG GTA TCC-3'
Oct-3/4_fw	5’-GGC GTT CGC TTT GGA AAG GTG TTC -3’
Oct-3/4_bw	5’-CTC GAA CCA CAT CCT TCT CT -3’
Pax6_fw	5'-TAA CGG AGA AGA CTC GGA TGA AGC-3'
Pax6_bw	5'-CGG GCA AAC ACA TCT GGA TAA TGG-3'
Pem/Rhox5_fw	5'-CTT CCG TGG ACA AGA GGA AG-3'
Pem/Rhox5_bw	5'-TGT CAT AGC CGG CAT ATG TG-3'
hPRAME_fw	5'-TAT CGC CCA GTT CAC CTC TC-3'
hPRAME_bw	5'-TCG GGA CTT ACA TCG GTC AG-3'
Pramel7_fw	5'-GTC AGA CTT GGA GTC ATT TG-3'
Pramel7_bw	5'-CGG AGA TGT CAT TGT CAT AG-3'
Rex1/Zfp42_fw	5'-AGA AAG CAG GAT CGC CTC AC-3'
Rex1/Zfp42_bw	5'-AGG GAA CTC GCT TCC AGA AC-3'
T-Brachyury_fw	5'-ATG CCA AAG AAA GAA ACG AC-3'
T-Brachyury_bw	5'-AGA GGC TGT AGA ACA TGA TT-3'
hUHRF1_fw	5'-GCA CCA AGG AAT GTA CCA TC-3'
hUHRF1_bw	5'-GTC CAC ATC ATC CTC ATA GC-3'
mUHRF1_fw	5'-ACA GTG AAT CAG ACA AGT CGT-3'
mUHRF1_bw	5'-ATT CTT GGC GGG TTT GAC AAT GTC-3'

4. Immunofluorescent detection (wide field/confocal) and alkaline phosphatase staining

Cells were fixed by the addition of Roti-Histofix 4% formalin solution for 10-20'. For confocal analysis formalin was additionally supplemented with 1:555 100% TritonX-100 (Sigma) (18µl in 10ml). After fixation, cells were washed 3 times in PBS (10' each step). Primary antibodies were diluted in PBST (PBS containing 0.1% Tween-20) and 4% horse serum and cells were incubated over night at 4°C or at room temperature for 2-4h. After washing 3 times with PBST (10' each step) secondary antibodies were added (in PBS only) and cells were incubated for 1-4h at room temperature protected from light. Following two washing steps (PBS, 10' each) nuclei were stained with DAPI (1:2000, in PBS) (Roche) or Hoechst (1:2000, in PBS) (obtained from Lukas Sommer lab, UZH, in PBS) for 1' and washed again twice with PBS before wide field microscopic analysis. For confocal microscopy cells were cultivated directly on gelatinized conventional microscopy glass cover slips (Menzel) placed in 3.5cm dishes (Corning), mounted using mounting medium supplemented with DAPI (obtained from Massimo Lopes lab, UZH) and sealed with conventional transparent nail polish. Wide field images were taken on a Zeiss Axiovert 40 CFL and processed using AxioVision 4.6 software (Zeiss) and Adobe Photoshop CS6. Confocal pictures were shot in the Center for Microscopy and Image Analysis (ZMB) of the UZH and processed with IMARIS 7.6 software.
For alkaline phosphatase staining cells were first fixed in Roti-Histofix 4% formalin solution for 10-20' and washed 3 times 10' in PBS. After 2 washing steps in AP buffer cells were subjected to AP staining solution. Staining intensity was checked after 20' the first time and then every 10'. When staining was enough strong the reaction was stopped using 1x Tris-EDTA (20mM Tris-HCl, 5mM EDTA) and cells were washed twice in PBS.

Tab. 7: List of antibodies used for immunofluorescent staining

Antibody	Species	Supplier	Catalog No.
α-Oct-3/4	rabbit	Santa Cruz	sc-9081
α-Smooth muscle actin	mouse	Sigma	A2547
α-SSEA1	mouse	Developmental studies Hybridoma bank University of Iowa	
α-Pramel7	rabbit	Selfmade	
α-UHRF1	rabbit	Santa Cruz	sc-98817
α-5mC	mouse	Diagenode	C15200081
α-ß-Tubulin isotype III	mouse	Sigma	T8660

5. Yeast-two hybrid assay

The assay was performed in collaboration with DualsystemsBiotech in Schlieren ZH, Switzerland. Pramel7 was used as bait and a cDNA library of E14 ESCs was the pool of prey proteins. First the bait was cloned into a lexA-expression vector and tested for self-activation and successful expression. Then the cDNA library was transformed and co-expressed with the bait plasmid. Positive clones were selected and library plasmids were isolated. Finally positive clones were sequenced and BLAST analysis was performed.

The exact procedure can be obtained here:
http://www.dualsystems.com/fileadmin/user_upload/z_download/manuals/P01004_DUALhybrid.pdf

6. Derivation and testing of an antibody recognizing Pramel7

Generation of the antibody was performed in collaboration with PINEDA Antikörper Service, Berlin, Germany. To determine unique epitopes protein sequences of PRAME-family members were aligned and analysed and two suitable, unique Pramel7-epitopes were chosen for immunization. 3 rabbits were immunized with either peptide. Pre-immune sera were tested using immunohistochemical staining and final fraction of purified antibodies was verified by immunoblotting.

7. Co-immunoprecipitation, TCA precipitation and silver staining (mammalian cells)

Cell pellets were collected and washed 1x with PBS. At this step pellets could be stored at -80°C. After thawing on ice pellets were resuspended in 200-400µl of NE buffer and sonicated twice (30'' each step). Following DNAse treatment (1µl DNAse/200µl lysate) (Fermentas) lysates were incubated for 30' on ice. Meanwhile ANTI-FLAG M2 Affinity Gel beads (Sigma) were washed 3 times in PBS (centrifugation at 500g, 5', 4°C), resuspended in NE buffer and distributed in required amounts of non-safe lock 1.5ml Eppendorf tubes (20-30µl packed beads/sample). After DNAse digestion, cell lysates were again sonicated once (30'') and centrifuged at 6000rpm for 10' (4°C). Protein concentration was determined by Bradford assay, 1-2mg of protein/sample was added to the beads and tubes were filled up to 1ml with NE buffer. Following incubation over night on a rotator beads were washed 3 times with 800µl-1ml of NE buffer (5' on rotator, centrifugation 500g for 5', 4C°). After final washing and centrifugation residual NE buffer was gently removed from the beads.

7.1. Analysis by Western blotting

Beads were resuspended in appropriate amount of reducing agent and sample buffer from the NuPAGE protein analysis system (Life Technologies), heated to 80°C for 10' and finally analysed by Western blotting.

7.2. TCA precipitation for proteomic analysis

After washing, beads were eluted twice by adding 100µl M2 FLAG-peptide (stock 5mg/ml, working solution 200µg/ml) (Sigma) and rotation for 30′ (200µl eluate). 20µl of each eluate was kept for silver staining analysis. 45µl 100% trichloro-acetic acid (TCA) was added to each eluate, tubes were gently shaken by finger tipping and kept on ice for at least 30′ (also possible over night) and then centrifuged for 5′ on full speed (4°C). Supernatant was removed without affecting protein pellet and pellet was washed 4-6 times with pure acetone (-20°C) every time followed by a full-speed centrifugation step for 5′ (4°C). After last washing pellet was shortly dried at 95°C and then stored at 4°C. Proteomic analysis was carried out by the Protein Analysis group of the Functional Genomics Centre (FGCZ) of the ETH/UZH.

7.3. Silver staining

Inputs and eluates were loaded on an SDS gel and gel was run on 140V for 2h. After fixation for 30′ in solution A (gently shaking) the gel was washed in solution B for 15′. Then the gel was washed 3 times in ddH_2O for 5′ and sensitized for 2′ in solution C by repeatedly adding and spilling solution C using up all 500ml during 2′, always shaking by hand. Following 3 washing steps with ddH_2O for 30′′ the gel was stained for 25′ in solution D and then washed 3 times for 1′ in ddH_2O. The staining was developed in solution E for 5-10′, always checking staining intensity, and the reaction was stopped by incubation in solution F for 10′ minimum. Finally the gel was washed in ddH_2O and stored at 4°C.

8. Cell culture experiments

8.1. $CaCl_2$-transfection of plasmid DNA in HEK293T

Plasmid DNA was mixed with 2.5M $CaCl_2$ and H_2O was added to reach the reaction volume (Tab. 8). While vortexing BES solution was added drop wise within 10'' on a vortex, tube was removed from vortex for 10'' and re-vortexed for another 10''. Then the solution was equally distributed on the adherent cells. To reach the indicated amounts of DNA, the transfection mix was equalized with *pBluescript* DNA. As a transfection control plasmids expressing EGFP or mRFP were used. The next morning culture medium was changed.

Tab. 8: Amounts and volumes used for $CaCl_2$ transfection

Plate size	Cell number	DNA (µg)	2.5M CaCl2 (µl)	Total reaction volume (µl)	2x BES (µl)
15cm	$2.5x10^6$	40	100	1000	1000
10cm	10^6	20	50	500	500
6cm	$0.5x10^6$	10	20	200	200
6well	$1.7x10^6$	2.5	7	72	72
12well	10^5	1.2-2.4	4	40	40
24well	$0.5x10^5$	0.5	2	20	20

8.2. Transfection of plasmid DNA in HEK293T cells using transfection reagent

After DNA, DMEM and Xtremegene HP transfection reagent had reached room temperature desired amount of DNA was added to a corresponding amount of DMEM and everything was mixed well. Required amount of transfection reagent (for exact amounts see supplier's manual) was added drop wise to the DNA/DMEM mix, gently mixed by finger tipping and incubated for 15' at room temperature. After incubation, the solution was equally distributed on the adherent cells and gently mixed with the culture medium when placing the dishes back into the incubator. After 48h the medium was changed.

8.3. Separation of mESCs from feeders, electroporation of plasmid DNA, selection and expansion of ESCs

For stable integration of plasmid DNA mESCs were first separated from feeder cells by 4' trypsinisation (1x trypsin), 4' centrifugation (1000rpm) and incubation on a non-gelatinized culture dish. Feeder cells were attached after 20' and the supernatant containing the mESC-fraction was collected and centrifuged (4', 1000rpm). After washing the pellet 1x with PBS and re-centrifugation (4', 1000rpm) plasmid DNA was added to the pellet and pellets were incubated for 4'. Pellet with DNA

was resuspended in 800µl of PBS and loaded on a 0.4cm gap Gene Pulser/Micro Pulser electroporation cuvette for mammalian cells (Bio Rad). Cells were electroporated at 500µF capacitance and 240V using a Bio Rad Gene Pulser II. Electroporated cells were resuspended in an appropriate amount of culture medium and distributed on culture dishes. Antibiotic selection was started 24-48h after electroporation and selection was carried out for 4 days (puromycin) or 8-10 days (neomycin). After selection medium was changed to standard conditions and resistant colonies were grown to a pickable size. For picking a 96-well plate (BD Falcon) with 60µl PBS/well/colony was prepared. Colonies were picked (before picking cells were washed 1x with PBS and then picked in PBS or pure DMEM) into 60µl of PBS and 60µl 2x trypsin was added. Trypsinisation was stopped after 4-6' by the addition of 120µl culture medium containing serum, cells were resuspended well and added to a previously prepared 24-well plate (Thermo Scientific) containing feeders. Resulting clones were expanded, analysed and frozen.

8.4. Time course experiment UHRF1 degradation

300'000 to 500'000 HEK293T cells were seeded onto 3.5cm culture dishes (Corning). The next day the medium was changed. After 1h of recovery cells were transfected with *CAG-Pramel7* plasmid DNA or *pBluescript*, respectively, using Xtremegene HP (see 8.2). At desired time points (8h, 12h, 24h, 36h, 48h, 72h, 96h) after transfection cells were scraped directly in the culture medium and centrifuged for 4' (1000rpm). The pellet was washed 1x with PBS, re-centrifuged and finally resuspended in 100-300µl of RIPA buffer, depending on the number of cells. Protein concentrations were determined and expression levels of Pramel7 and UHRF1 were determined by Western blotting (see 7.1).

8.5. Inhibition of UHRF1-degradation by MG132

UHRF1 degradation experiment was carried out as described above. 24h after transfection of *Pramel7/pBluescript* the proteasome inhibitor MG132 was added to the culture medium (1µM final concentration). Cells were incubated with MG132 for desired time periods (4h, 8h, 12h, 24h, 30h) and cells were harvested, protein amounts normalized and expression was determined by Western blotting (see 7.1).

8.6. MG132 functionality test

To test the functionality of MG132 untransfected HEK293T cells were incubated with 50µg/µl cycloheximide for indicated time (4h, 8h, 12h, 24h) in presence or absence of MG132, harvested and analysed as described above (see 7.1).

8.7. Differentiation and reversion of *wildtype E14* and *CAG_FLAGHA-Pramel7*-overexpressing mESCs

Wt E14 and *Pramel7*-overexpressing mESCs were separated from feeders (see 8.3) and differentiated on gelatinized 6cm culture dishes (Corning) in complete medium without LIF. Cells were split after 6 days and 10 days. After 14 days cells were trypsinised and distributed at a dilution of 10cells/well on two 96-well plates containing feeders (for each cell type). Replicates of 14 days-differentiated cells were harvested and analysed for the expression of pluripotency factors by RTQ-PCR and protein levels of Pramel7 and UHRF1 were verified by Western blotting. In addition methylation of genomic DNA was assessed (see 9). Cells in 96-well plates were cultivated in complete medium containing LIF for 1 week and analysed for colony formation. 10 clones per cell type were selected on morphological criteria and split on 24-well plates. Residual wells of 96-well plates were fixed in 4% formalin and analysed for the expression of alkaline phosphatase and positive colony formation was assessed counting wells containing AP-positive colonies. Different clones were expanded for 3 to 4 passages and expression of pluripotency markers was tested using RTQ-PCR and immunofluorescent staining.

8.8. Smooth muscle differentiation

Wt E14 and *Pramel7*-overexpressing mESCs were separated from feeders and plated on gelatinized 6well plates (Thermo Scientific). 50'000 Cells were cultivated in smooth muscle differentiation medium for 9 days, fixed with 4% formalin and analysed by staining against smooth muscle actin (SMA).

9. Isolation of genomic DNA and methylation-sensitive restriction digestion

9.1. Isolation of genomic DNA

After trypsinisation and centrifugation (4', 1000rpm) and 1x washing (PBS) cell pellets were carefully resuspended in 100-400µl of proteinase-K buffer and 4µl proteinase-K (10mg/ml) was added. The mixture was incubated over night at 50°C on a shaker. The next day, following the addition of 2µl RNAse A (Fermentas) and incubation for 30' at 37°C, 25:24:1 Phenol:Chloroform:Isoamyl Alcohol (Sigma) was added and lysates were shaken (avoid vortexing) and centrifuged for 10' at 7500rpm. Meanwhile new tubes with 0.5 volumes of 7.5M NH_4Ac were prepared. After centrifugation upper and interphases were transferred into NH_4Ac-containing tubes, two volumes of 100% EtOH were added and samples were centrifuged at 4200rpm for 2'. Supernatants were carefully discarded without touching the pellet and pellets were dried on 40°C for 1h maximum. Pellets were resuspended in gDNA elution buffer, incubated for 15' and shaken at 65°C to dissolve and then, if needed, further dissolved in required amount of gDNA elution buffer.

9.2. Restriction digestion for methylation assay

4µg of gDNA were digested over night with 3µl HpaII or McrBC in 20µl total reaction volume containing 0.5ng of *pBluescript* plasmid DNA for testing the efficiency of the HpaII digest. The next day the reaction was heat-inactivated for 15′ and 2µg (10µl) of DNA were loaded on a 1% agarose gel. The gel was run for 1h at 180V and degrees of digestion were analysed.

2µl of the mixture were diluted 1:5 with H2O and digestion efficiencies were additionally quantified by amplification of *pBluescript* sequences containing HpaII (+2049 to +2606, HpaII site +2580). Data was normalized to the total amount of *pBluescript* DNA calculated by amplification of sequences lacking HpaII (+2049 to +2573).

10. PI-staining of DNA for flow cytometry

Cells were trypsinised and centrifuged for 4′ at 1000rpm. Pellets were washed once with 4°C PBS and re-centrifuged. PBS was then discarded and pellet was resuspended by finger tipping the tube. While gently vortexing, 1ml of ice cold 70% EtOH was added to the cells drop per drop. Cells were incubated on ice for at least 30′ (can also be stored at 4°C for 2-3 weeks at this step). Following 5′ of centrifugation (400g) cells were washed with 1ml of PBS and spun down again (400g, 5′). Supernatant was discarded and 500µl of RNAse A (100µg/ml) and 5µl of PI (2.5mg/ml) were added. Finally cells were incubated for 30′ at least and then analyzed by flow cytometry.

F. Bibliography

Achour, M., Jacq, X., Rondé, P., Alhosin, M., Charlot, C., Chataigneau, T., Jeanblanc, M., Macaluso, M., Giordano, A., Hughes, A.D., *et al.* (2008). The interaction of the SRA domain of ICBP90 with a novel domain of DNMT1 is involved in the regulation of VEGF gene expression. In Oncogene, pp. 2187-2197.
Adams-Cioaba, M.A., and Min, J. (2009). Structure and function of histone methylation binding proteins. In Biochem Cell Biol, pp. 93-105.

Adenot, P.G., Mercier, Y., Renard, J.P., and Thompson, E.M. (1997). Differential H4 acetylation of paternal and maternal chromatin precedes DNA replication and differential transcriptional activity in pronuclei of 1-cell mouse embryos. In Development, pp. 4615-4625.

Arita, K., Ariyoshi, M., Tochio, H., Nakamura, Y., and Shirakawa, M. (2008). Recognition of hemi-methylated DNA by the SRA protein UHRF1 by a base-flipping mechanism. In Nature, pp. 818-821.

Arita, K., Isogai, S., Oda, T., Unoki, M., Sugita, K., Sekiyama, N., Kuwata, K., Hamamoto, R., Tochio, H., Sato, M., *et al.* (2012). Recognition of modification status on a histone H3 tail by linked histone reader modules of the epigenetic regulator UHRF1. In Proc Natl Acad Sci USA.

Avvakumov, G.V., Walker, J.R., Xue, S., Li, Y., Duan, S., Bronner, C., Arrowsmith, C.H., and Dhe-Paganon, S. (2008). Structural basis for recognition of hemi-methylated DNA by the SRA domain of human UHRF1. In Nature, pp. 822-825.

Azuara, V., Perry, P., Sauer, S., Spivakov, M., Jørgensen, H.F., John, R.M., Gouti, M., Casanova, M., Warnes, G., Merkenschlager, M., *et al.* (2006). Chromatin signatures of pluripotent cell lines. In Nat Cell Biol, pp. 532-538.

Badeaux, A.I., and Shi, Y. (2013). Emerging roles for chromatin as a signal integration and storage platform. In Nat Rev Mol Cell Biol, pp. 211-224.

Bannister, A.J., and Kouzarides, T. (2011). Regulation of chromatin by histone modifications. In Cell Res, pp. 381-395.

Barski, A., Cuddapah, S., Cui, K., Roh, T.-Y., Schones, D.E., Wang, Z., Wei, G., Chepelev, I., and Zhao, K. (2007). High-resolution profiling of histone methylations in the human genome. In Cell, pp. 823-837.

Bartke, T., Vermeulen, M., Xhemalce, B., Robson, S.C., Mann, M., and Kouzarides, T. (2010). Nucleosome-interacting proteins regulated by DNA and histone methylation. In Cell, pp. 470-484.

Bashtrykov, P., Jankevicius, G., Jurkowska, R.Z., Ragozin, S., and Jeltsch, A. (2013). The Uhrf1 protein stimulates the activity and specificity of the maintenance DNA methyltransferase Dnmt1 by an allosteric mechanism. In J Biol Chem.

Bella, J., Hindle, K.L., McEwan, P.A., and Lovell, S.C. (2008). The leucine-rich repeat structure. In Cell Mol Life Sci, pp. 2307-2333.

Benevolenskaya, E.V. (2007). Histone H3K4 demethylases are essential in development and differentiation. In Biochem Cell Biol, pp. 435-443.

Bernstein, B.E., Mikkelsen, T.S., Xie, X., Kamal, M., Huebert, D.J., Cuff, J., Fry, B., Meissner, A., Wernig, M., Plath, K., *et al.* (2006). A bivalent chromatin structure marks key developmental genes in embryonic stem cells. In Cell, pp. 315-326.

Birtle, Z., Goodstadt, L., and Ponting, C. (2005). Duplication and positive selection among hominin-specific PRAME genes. In BMC Genomics, pp. 120.

Bonapace, I.M., Latella, L., Papait, R., Nicassio, F., Sacco, A., Muto, M., Crescenzi, M., and Di Fiore, P.P. (2002). Np95 is regulated by E1A during mitotic reactivation of terminally differentiated cells and is essential for S phase entry. In J Cell Biol, pp. 909-914.

Bortvin, A., Eggan, K., Skaletsky, H., Akutsu, H., Berry, D.L., Yanagimachi, R., Page, D.C., and Jaenisch, R. (2003). Incomplete reactivation of Oct4-related genes in mouse embryos cloned from somatic nuclei. In Development, pp. 1673-1680.

Bostick, M., Kim, J.K., Estève, P.-O., Clark, A., Pradhan, S., and Jacobsen, S.E. (2007). UHRF1 plays a role in maintaining DNA methylation in mammalian cells. In Science, pp. 1760-1764.

Boyer, L.A., Plath, K., Zeitlinger, J., Brambrink, T., Medeiros, L.A., Lee, T.I., Levine, S.S., Wernig, M., Tajonar, A., Ray, M.K., *et al.* (2006). Polycomb complexes repress developmental regulators in murine embryonic stem cells. In Nature, pp. 349-353.

Brivanlou, A.H., Gage, F.H., Jaenisch, R., Jessell, T., Melton, D., and Rossant, J. (2003). Stem cells. Setting standards for human embryonic stem cells. In Science, pp. 913-916.

Bronner, C., Achour, M., Arima, Y., Chataigneau, T., Saya, H., and Schini-Kerth, V.B. (2007). The UHRF family: oncogenes that are drugable targets for cancer therapy in the near future? In Pharmacol Ther, pp. 419-434.

Cantone, I., and Fisher, A.G. (2013). Epigenetic programming and reprogramming during development. In Nat Struct Mol Biol, pp. 282-289.

Carrell, D.T. (2012). Epigenetics of the male gamete. In Fertil Steril, pp. 267-274.

Casanova, E.A., Shakhova, O., Patel, S.S., Asner, I.N., Pelczar, P., Weber, F.A., Graf, U., Sommer, L., Bürki, K., and Cinelli, P. (2011). Pramel7 mediates LIF/STAT3-dependent self-renewal in embryonic stem cells. In Stem Cells, pp. 474-485.

Chamberlain, S.J., Yee, D., and Magnuson, T. (2008). Polycomb repressive complex 2 is dispensable for maintenance of embryonic stem cell pluripotency. In Stem Cells, pp. 1496-1505.

Chambers, I., Silva, J., Colby, D., Nichols, J., Nijmeijer, B., Robertson, M., Vrana, J., Jones, K., Grotewold, L., and Smith, A. (2007). Nanog safeguards pluripotency and mediates germline development. In Nature, pp. 1230-1234.

Chan, E.M., Ratanasirintrawoot, S., Park, I.-H., Manos, P.D., Loh, Y.-H., Huo, H., Miller, J.D., Hartung, O., Rho, J., Ince, T.A., *et al.* (2009). Live cell imaging distinguishes bona fide human iPS cells from partially reprogrammed cells. In Nat Biotechnol, pp. 1033-1037.

Chen, C.-m., Krohn, J., Bhattacharya, S., and Davies, B. (2011). A comparison of exogenous promoter activity at the ROSA26 locus using a ΦiC31 integrase mediated cassette exchange approach in mouse ES cells. In PLoS ONE, pp. e23376.

Chen, H., Ma, H., Inuzuka, H., Diao, J., Lan, F., Shi, Y.G., Wei, W., and Shi, Y. (2013). DNA damage regulates UHRF1 stability via the SCF(β-TrCP) E3 ligase. In Mol Cell Biol, pp. 1139-1148.

Chen, H.Y., Sun, J.M., Zhang, Y., Davie, J.R., and Meistrich, M.L. (1998). Ubiquitination of histone H3 in elongating spermatids of rat testes. In J Biol Chem, pp. 13165-13169.

Cheng, J., Yang, Y., Fang, J., Xiao, J., Zhu, T., Chen, F., Wang, P., Li, Z., Yang, H., and Xu, Y. (2013). Structural insight into coordinated recognition of trimethylated histone H3 lysine 9 (H3K9me3) by the plant homeodomain (PHD) and tandem tudor domain (TTD) of UHRF1 (ubiquitin-like, containing PHD and RING finger domains, 1) protein. In J Biol Chem, pp. 1329-1339.

Ciccarone, F., Klinger, F.G., Catizone, A., Calabrese, R., Zampieri, M., Bacalini, M.G., De Felici, M., and Caiafa, P. (2012). Poly(ADP-ribosyl)ation acts in the DNA demethylation of mouse primordial germ cells also with DNA damage-independent roles. In PLoS ONE, pp. e46927.

Cinelli, P., Casanova, E.A., Uhlig, S., Lochmatter, P., Matsuda, T., Yokota, T., Rülicke, T., Ledermann, B., and Bürki, K. (2008). Expression profiling in transgenic FVB/N embryonic stem cells overexpressing STAT3. In BMC Dev Biol, pp. 57.

Citterio, E., Papait, R., Nicassio, F., Vecchi, M., Gomiero, P., Mantovani, R., Di Fiore, P.P., and Bonapace, I.M. (2004). Np95 is a histone-binding protein endowed with ubiquitin ligase activity. In Mol Cell Biol, pp. 2526-2535.

Cloos, P.A.C., Christensen, J., Agger, K., Maiolica, A., Rappsilber, J., Antal, T., Hansen, K.H., and Helin, K. (2006). The putative oncogene GASC1 demethylates tri- and dimethylated lysine 9 on histone H3. In Nature, pp. 307-311.

Costello, I., Biondi, C.A., Taylor, J.M., Bikoff, E.K., and Robertson, E.J. (2009). Smad4-dependent pathways control basement membrane deposition and endodermal cell migration at early stages of mouse development. In BMC Dev Biol, pp. 54.

Costessi, A., Mahrour, N., Tijchon, E., Stunnenberg, R., Stoel, M.A., Jansen, P.W., Sela, D., Martin-Brown, S., Washburn, M.P., Florens, L., *et al.* (2011). The tumour antigen PRAME is a subunit of a Cul2 ubiquitin ligase and associates with active NFY promoters. In EMBO J.

Creyghton, M.P., Cheng, A.W., Welstead, G.G., Kooistra, T., Carey, B.W., Steine, E.J., Hanna, J., Lodato, M.A., Frampton, G.M., Sharp, P.A., *et al.* (2010). Histone H3K27ac separates active from poised enhancers and predicts developmental state. In Proc Natl Acad Sci USA, pp. 21931-21936.

Czermin, B., Melfi, R., McCabe, D., Seitz, V., Imhof, A., and Pirrotta, V. (2002). Drosophila enhancer of Zeste/ESC complexes have a histone H3 methyltransferase activity that marks chromosomal Polycomb sites. In Cell, pp. 185-196.

Dirscherl, S.S., and Krebs, J.E. (2004). Functional diversity of ISWI complexes. In Biochem Cell Biol, pp. 482-489.

Dodge, J.E., Kang, Y.-K., Beppu, H., Lei, H., and Li, E. (2004). Histone H3-K9 methyltransferase ESET is essential for early development. In Mol Cell Biol, pp. 2478-2486.

Du, Z., Song, J., Wang, Y., Zhao, Y., Guda, K., Yang, S., Kao, H.-Y., Xu, Y., Willis, J., Markowitz, S.D.*, et al.* (2010). DNMT1 stability is regulated by proteins coordinating deubiquitination and acetylation-driven ubiquitination. In Sci Signal, pp. ra80.

Duda, D.M., Olszewski, J.L., Tron, A.E., Hammel, M., Lambert, L.J., Waddell, M.B., Mittag, T., DeCaprio, J.A., and Schulman, B.A. (2012). Structure of a glomulin-RBX1-CUL1 complex: inhibition of a RING E3 ligase through masking of its E2-binding surface. In Mol Cell, pp. 371-382.

Dul, B.E., and Walworth, N.C. (2007). The plant homeodomain fingers of fission yeast Msc1 exhibit E3 ubiquitin ligase activity. In J Biol Chem, pp. 18397-18406.

Eberharter, A., Vetter, I., Ferreira, R., and Becker, P.B. (2004). ACF1 improves the effectiveness of nucleosome mobilization by ISWI through PHD-histone contacts. In EMBO J, pp. 4029-4039.

Epping, M.T., Wang, L., Edel, M.J., Carlée, L., Hernandez, M., and Bernards, R. (2005). The human tumor antigen PRAME is a dominant repressor of retinoic acid receptor signaling. In Cell, pp. 835-847.

Etchegaray, J.-P., Machida, K.K., Noton, E., Constance, C.M., Dallmann, R., Di Napoli, M.N., DeBruyne, J.P., Lambert, C.M., Yu, E.A., Reppert, S.M.*, et al.* (2009). Casein kinase 1 delta regulates the pace of the mammalian circadian clock. In Mol Cell Biol, pp. 3853-3866.

Evans, M.J., and Kaufman, M.H. (1981). Establishment in culture of pluripotential cells from mouse embryos. In Nature, pp. 154-156.

Fanti, L., Berloco, M., Piacentini, L., and Pimpinelli, S. (2003). Chromosomal distribution of heterochromatin protein 1 (HP1) in Drosophila: a cytological map of euchromatic HP1 binding sites. In Genetica, pp. 135-147.

Feldman, N., Gerson, A., Fang, J., Li, E., Zhang, Y., Shinkai, Y., Cedar, H., and Bergman, Y. (2006). G9a-mediated irreversible epigenetic inactivation of Oct-3/4 during early embryogenesis. In Nat Cell Biol, pp. 188-194.

Felle, M., Joppien, S., Németh, A., Diermeier, S., Thalhammer, V., Dobner, T., Kremmer, E., Kappler, R., and Längst, G. (2011). The USP7/Dnmt1 complex stimulates the DNA methylation activity of Dnmt1 and regulates the stability of UHRF1. In Nucleic Acids Res, pp. 8355-8365.

Fodor, B.D., Kubicek, S., Yonezawa, M., O'Sullivan, R.J., Sengupta, R., Perez-Burgos, L., Opravil, S., Mechtler, K., Schotta, G., and Jenuwein, T. (2006). Jmjd2b antagonizes H3K9 trimethylation at pericentric heterochromatin in mammalian cells. In Genes Dev, pp. 1557-1562.

Freemont, P.S. (2000). RING for destruction? In Curr Biol, pp. R84-87.

Fujimori, A., Matsuda, Y., Takemoto, Y., Hashimoto, Y., Kubo, E., Araki, R., Fukumura, R., Mita, K., Tatsumi, K., and Muto, M. (1998). Cloning and mapping of Np95 gene which encodes a novel nuclear protein associated with cell proliferation. In Mamm Genome, pp. 1032-1035.

Gao, Z., Zhang, J., Bonasio, R., Strino, F., Sawai, A., Parisi, F., Kluger, Y., and Reinberg, D. (2012). PCGF homologs, CBX proteins, and RYBP define functionally distinct PRC1 family complexes. In Mol Cell, pp. 344-356.

Garrett, K.P., Tan, S., Bradsher, J.N., Lane, W.S., Conaway, J.W., and Conaway, R.C. (1994). Molecular cloning of an essential subunit of RNA polymerase II elongation factor SIII. In Proc Natl Acad Sci USA, pp. 5237-5241.

Gaspar-Maia, A., Alajem, A., Meshorer, E., and Ramalho-Santos, M. (2011). Open chromatin in pluripotency and reprogramming. In Nat Rev Mol Cell Biol, pp. 36-47.

Grewal, S.I.S., and Moazed, D. (2003). Heterochromatin and epigenetic control of gene expression. In Science, pp. 798-802.

Haas, A.L., Warms, J.V., Hershko, A., and Rose, I.A. (1982). Ubiquitin-activating enzyme. Mechanism and role in protein-ubiquitin conjugation. In J Biol Chem, pp. 2543-2548.

Hamatani, T., Carter, M.G., Sharov, A.A., and Ko, M.S.H. (2004). Dynamics of global gene expression changes during mouse preimplantation development. In Dev Cell, pp. 117-131.

Hamdi, A., and Colas, P. (2012). Yeast two-hybrid methods and their applications in drug discovery. In Trends Pharmacol Sci, pp. 109-118.

Haqq, C., Nosrati, M., Sudilovsky, D., Crothers, J., Khodabakhsh, D., Pulliam, B.L., Federman, S., Miller, J.R., Allen, R.E., Singer, M.I.*, et al.* (2005). The gene expression signatures of melanoma progression. In Proc Natl Acad Sci USA, pp. 6092-6097.

Hashimoto, H., Horton, J.R., Zhang, X., Bostick, M., Jacobsen, S.E., and Cheng, X. (2008). The SRA domain of UHRF1 flips 5-methylcytosine out of the DNA helix. In Nature, pp. 826-829.

Hatano, S.-Y., Tada, M., Kimura, H., Yamaguchi, S., Kono, T., Nakano, T., Suemori, H., Nakatsuji, N., and Tada, T. (2005). Pluripotential competence of cells associated with Nanog activity. In Mech Dev, pp. 67-79.

Hathaway, N.A., Bell, O., Hodges, C., Miller, E.L., Neel, D.S., and Crabtree, G.R. (2012). Dynamics and memory of heterochromatin in living cells. In Cell, pp. 1447-1460.

Hattori, N., Imao, Y., Nishino, K., Hattori, N., Ohgane, J., Yagi, S., Tanaka, S., and Shiota, K. (2007). Epigenetic regulation of Nanog gene in embryonic stem and trophoblast stem cells. In Genes Cells, pp. 387-396.

Hattori, N., Nishino, K., Ko, Y.-G., Hattori, N., Ohgane, J., Tanaka, S., and Shiota, K. (2004). Epigenetic control of mouse Oct-4 gene expression in embryonic stem cells and trophoblast stem cells. In J Biol Chem, pp. 17063-17069.

He, Y.-F., Li, B.-Z., Li, Z., Liu, P., Wang, Y., Tang, Q., Ding, J., Jia, Y., Chen, Z., Li, L.*, et al.* (2011). Tet-mediated formation of 5-carboxylcytosine and its excision by TDG in mammalian DNA. In Science, pp. 1303-1307.

Heo, K., Kim, B., Kim, K., Choi, J., Kim, H., Zhan, Y., Ranish, J.A., and An, W. (2007). Isolation and characterization of proteins associated with histone H3 tails in vivo. In J Biol Chem, pp. 15476-15483.

Hirasawa, R., Chiba, H., Kaneda, M., Tajima, S., Li, E., Jaenisch, R., and Sasaki, H. (2008). Maternal and zygotic Dnmt1 are necessary and sufficient for the maintenance of DNA methylation imprints during preimplantation development. In Genes Dev, pp. 1607-1616.

Hoekstra, M.F., Liskay, R.M., Ou, A.C., DeMaggio, A.J., Burbee, D.G., and Heffron, F. (1991). HRR25, a putative protein kinase from budding yeast: association with repair of damaged DNA. In Science, pp. 1031-1034.

Hopfner, R., Mousli, M., Jeltsch, J.M., Voulgaris, A., Lutz, Y., Marin, C., Bellocq, J.P., Oudet, P., and Bronner, C. (2000). ICBP90, a novel human CCAAT binding protein, involved in the regulation of topoisomerase IIalpha expression. In Cancer Res, pp. 121-128.

Hosler, B.A., LaRosa, G.J., Grippo, J.F., and Gudas, L.J. (1989). Expression of REX-1, a gene containing zinc finger motifs, is rapidly reduced by retinoic acid in F9 teratocarcinoma cells. In Mol Cell Biol, pp. 5623-5629.

Huang, J.-Y., Chen, W.-H., Chang, Y.-L., Wang, H.-T., Chuang, W.-t., and Lee, S.-C. (2006). Modulation of nucleosome-binding activity of FACT by poly(ADP-ribosyl)ation. In Nucleic Acids Res, pp. 2398-2407.

Ikeda, H., Lethé, B., Lehmann, F., van Baren, N., Baurain, J.F., de Smet, C., Chambost, H., Vitale, M., Moretta, A., Boon, T.*, et al.* (1997). Characterization of an antigen that is recognized on a melanoma showing partial HLA loss by CTL expressing an NK inhibitory receptor. In Immunity, pp. 199-208.

Inoue, A., and Zhang, Y. (2011). Replication-dependent loss of 5-hydroxymethylcytosine in mouse preimplantation embryos. In Science, pp. 194.

Iqbal, K., Jin, S.-G., Pfeifer, G.P., and Szabó, P.E. (2011). Reprogramming of the paternal genome upon fertilization involves genome-wide oxidation of 5-methylcytosine. In Proc Natl Acad Sci USA, pp. 3642-3647.

Ito, S., Shen, L., Dai, Q., Wu, S.C., Collins, L.B., Swenberg, J.A., He, C., and Zhang, Y. (2011). Tet proteins can convert 5-methylcytosine to 5-formylcytosine and 5-carboxylcytosine. In Science, pp. 1300-1303.

Jackson, M., Krassowska, A., Gilbert, N., Chevassut, T., Forrester, L., Ansell, J., and Ramsahoye, B. (2004). Severe global DNA hypomethylation blocks differentiation and induces histone hyperacetylation in embryonic stem cells. In Mol Cell Biol, pp. 8862-8871.

Jair, K.-W., Bachman, K.E., Suzuki, H., Ting, A.H., Rhee, I., Yen, R.-W.C., Baylin, S.B., and Schuebel, K.E. (2006). De novo CpG island methylation in human cancer cells. In Cancer Res, pp. 682-692.

Jenkins, Y., Markovtsov, V., Lang, W., Sharma, P., Pearsall, D., Warner, J., Franci, C., Huang, B., Huang, J., Yam, G.C.*, et al.* (2005). Critical role of the ubiquitin ligase activity of UHRF1, a nuclear RING finger protein, in tumor cell growth. In Mol Biol Cell, pp. 5621-5629.

Jiang, Y., Jahagirdar, B.N., Reinhardt, R.L., Schwartz, R.E., Keene, C.D., Ortiz-Gonzalez, X.R., Reyes, M., Lenvik, T., Lund, T., Blackstad, M.*, et al.* (2002). Pluripotency of mesenchymal stem cells derived from adult marrow. In Nature, pp. 41-49.

Jin, B., Li, Y., and Robertson, K.D. (2011). DNA methylation: superior or subordinate in the epigenetic hierarchy? In Genes Cancer, pp. 607-617.

Kagiwada, S., Kurimoto, K., Hirota, T., Yamaji, M., and Saitou, M. (2013). Replication-coupled passive DNA demethylation for the erasure of genome imprints in mice. In EMBO J, pp. 340-353.

Kajava, A.V. (1998). Structural diversity of leucine-rich repeat proteins. In J Mol Biol, pp. 519-527.

Kanno, H., Kondo, K., Ito, S., Yamamoto, I., Fujii, S., Torigoe, S., Sakai, N., Hosaka, M., Shuin, T., and Yao, M. (1994). Somatic mutations of the von Hippel-Lindau tumor suppressor gene in sporadic central nervous system hemangioblastomas. In Cancer Res, pp. 4845-4847.

Karlmark, K.R., Freilinger, A., Marton, E., Rosner, M., Lubec, G., and Hengstschläger, M. (2005). Activation of ectopic Oct-4 and Rex-1 promoters in human amniotic fluid cells. In Int J Mol Med, pp. 987-992.

Kelley, L.A., and Sternberg, M.J.E. (2009). Protein structure prediction on the Web: a case study using the Phyre server. In Nat Protoc, pp. 363-371.

Kerscher, O., Felberbaum, R., and Hochstrasser, M. (2006). Modification of proteins by ubiquitin and ubiquitin-like proteins. In Annu Rev Cell Dev Biol, pp. 159-180.

Kewitz, S., and Staege, M.S. (2013). Knock-Down of PRAME Increases Retinoic Acid Signaling and Cytotoxic Drug Sensitivity of Hodgkin Lymphoma Cells. In PLoS ONE, pp. e55897.

Kim, J.K., Estève, P.-O., Jacobsen, S.E., and Pradhan, S. (2009). UHRF1 binds G9a and participates in p21 transcriptional regulation in mammalian cells. In Nucleic Acids Res, pp. 493-505.

Kim, K., Doi, A., Wen, B., Ng, K., Zhao, R., Cahan, P., Kim, J., Aryee, M.J., Ji, H., Ehrlich, L.I.R.*, et al.* (2010). Epigenetic memory in induced pluripotent stem cells. In Nature, pp. 285-290.

Klose, R.J., Yamane, K., Bae, Y., Zhang, D., Erdjument-Bromage, H., Tempst, P., Wong, J., and Zhang, Y. (2006). The transcriptional repressor JHDM3A demethylates trimethyl histone H3 lysine 9 and lysine 36. In Nature, pp. 312-316.

Kobe, B., and Deisenhofer, J. (1994). The leucine-rich repeat: a versatile binding motif. In Trends Biochem Sci, pp. 415-421.

Koch, C.M., Andrews, R.M., Flicek, P., Dillon, S.C., Karaöz, U., Clelland, G.K., Wilcox, S., Beare, D.M., Fowler, J.C., Couttet, P.*, et al.* (2007). The landscape of histone modifications across 1% of the human genome in five human cell lines. In Genome Res, pp. 691-707.

Ku, M., Koche, R.P., Rheinbay, E., Mendenhall, E.M., Endoh, M., Mikkelsen, T.S., Presser, A., Nusbaum, C., Xie, X., Chi, A.S.*, et al.* (2008). Genomewide analysis of PRC1 and PRC2 occupancy identifies two classes of bivalent domains. In PLoS Genet, pp. e1000242.

Kuroda, T., Tada, M., Kubota, H., Kimura, H., Hatano, S.-Y., Suemori, H., Nakatsuji, N., and Tada, T. (2005). Octamer and Sox elements are required for transcriptional cis regulation of Nanog gene expression. In Mol Cell Biol, pp. 2475-2485.

Kwon, S.H., Florens, L., Swanson, S.K., Washburn, M.P., Abmayr, S.M., and Workman, J.L. (2010). Heterochromatin protein 1 (HP1) connects the FACT histone chaperone complex to the phosphorylated CTD of RNA polymerase II. In Genes Dev, pp. 2133-2145.

Lee, J., Thompson, J.R., Botuyan, M.V., and Mer, G. (2008). Distinct binding modes specify the recognition of methylated histones H3K4 and H4K20 by JMJD2A-tudor. In Nat Struct Mol Biol, pp. 109-111.

Leitch, H.G., McEwen, K.R., Turp, A., Encheva, V., Carroll, T., Grabole, N., Mansfield, W., Nashun, B., Knezovich, J.G., Smith, A.*, et al.* (2013). Naive pluripotency is associated with global DNA hypomethylation. In Nat Struct Mol Biol, pp. 311-316.

Liu, X., Gao, Q., Li, P., Zhao, Q., Zhang, J., Li, J., Koseki, H., and Wong, J. (2013). UHRF1 targets DNMT1 for DNA methylation through cooperative binding of hemi-methylated DNA and methylated H3K9. In Nat Commun, pp. 1563.

Luger, K., Mäder, A.W., Richmond, R.K., Sargent, D.F., and Richmond, T.J. (1997). Crystal structure of the nucleosome core particle at 2.8 A resolution. In Nature, pp. 251-260.

Ma, P., and Schultz, R.M. (2008). Histone deacetylase 1 (HDAC1) regulates histone acetylation, development, and gene expression in preimplantation mouse embryos. In Dev Biol, pp. 110-120.

Margueron, R., and Reinberg, D. (2011). The Polycomb complex PRC2 and its mark in life. In Nature, pp. 343-349.

Martin, D.G.E., Baetz, K., Shi, X., Walter, K.L., MacDonald, V.E., Wlodarski, M.J., Gozani, O., Hieter, P., and Howe, L. (2006). The Yng1p plant homeodomain finger is a methyl-histone binding module that recognizes lysine 4-methylated histone H3. In Mol Cell Biol, pp. 7871-7879.

Martin, G.R. (1981). Isolation of a pluripotent cell line from early mouse embryos cultured in medium conditioned by teratocarcinoma stem cells. In Proc Natl Acad Sci USA, pp. 7634-7638.

May, A., Kirchner, R., Müller, H., Hartmann, P., El Hajj, N., Tresch, A., Zechner, U., Mann, W., and Haaf, T. (2009). Multiplex rt-PCR expression analysis of developmentally important genes in individual mouse preimplantation embryos and blastomeres. In Biol Reprod, pp. 194-202.

Mayer, W., Niveleau, A., Walter, J., Fundele, R., and Haaf, T. (2000). Demethylation of the zygotic paternal genome. In Nature, pp. 501-502.

Meilinger, D., Fellinger, K., Bultmann, S., Rothbauer, U., Bonapace, I.M., Klinkert, W.E.F., Spada, F., and Leonhardt, H. (2009). Np95 interacts with de novo DNA methyltransferases, Dnmt3a and Dnmt3b, and mediates epigenetic silencing of the viral CMV promoter in embryonic stem cells. In EMBO Rep, pp. 1259-1264.

Meissner, A., Mikkelsen, T.S., Gu, H., Wernig, M., Hanna, J., Sivachenko, A., Zhang, X., Bernstein, B.E., Nusbaum, C., Jaffe, D.B.*, et al.* (2008). Genome-scale DNA methylation maps of pluripotent and differentiated cells. In Nature, pp. 766-770.

Messner, S., Altmeyer, M., Zhao, H., Pozivil, A., Roschitzki, B., Gehrig, P., Rutishauser, D., Huang, D., Caflisch, A., and Hottiger, M.O. (2010). PARP1 ADP-ribosylates lysine residues of the core histone tails. In Nucleic Acids Res, pp. 6350-6362.

Mikkelsen, T.S., Ku, M., Jaffe, D.B., Issac, B., Lieberman, E., Giannoukos, G., Alvarez, P., Brockman, W., Kim, T.-K., Koche, R.P.*, et al.* (2007). Genome-wide maps of chromatin state in pluripotent and lineage-committed cells. In Nature, pp. 553-560.

Mistry, B.V., Zhao, Y., Chang, T.-C., Yasue, H., Chiba, M., Oatley, J., Diaz, F., and Liu, W.-S. (2013). Differential Expression of PRAMEL1, a Cancer/Testis Antigen, during Spermatogenesis in the Mouse. In PLoS ONE, pp. e60611.

Mitsui, K., Tokuzawa, Y., Itoh, H., Segawa, K., Murakami, M., Takahashi, K., Maruyama, M., Maeda, M., and Yamanaka, S. (2003). The homeoprotein Nanog is required for maintenance of pluripotency in mouse epiblast and ES cells. In Cell, pp. 631-642.

Musselman, C.A., and Kutateladze, T.G. (2011). Handpicking epigenetic marks with PHD fingers. In Nucleic Acids Res, pp. 9061-9071.

Nady, N., Lemak, A., Walker, J.R., Avvakumov, G.V., Kareta, M.S., Achour, M., Xue, S., Duan, S., Allali-Hassani, A., Zuo, X., *et al.* (2011). Recognition of multivalent histone states associated with heterochromatin by UHRF1. In J Biol Chem.

Nakamura, T., Liu, Y.-J., Nakashima, H., Umehara, H., Inoue, K., Matoba, S., Tachibana, M., Ogura, A., Shinkai, Y., and Nakano, T. (2012). PGC7 binds histone H3K9me2 to protect against conversion of 5mC to 5hmC in early embryos. In Nature, pp. 415-419.

Ng, R.K., Dean, W., Dawson, C., Lucifero, D., Madeja, Z., Reik, W., and Hemberger, M. (2008). Epigenetic restriction of embryonic cell lineage fate by methylation of Elf5. In Nat Cell Biol, pp. 1280-1290.

Ngounou Wetie, A.G., Sokolowska, I., Woods, A.G., Roy, U., Deinhardt, K., and Darie, C.C. (2014). Protein-protein interactions: switch from classical methods to proteomics and bioinformatics-based approaches. In Cell Mol Life Sci, pp. 205-228.

Nichols, J., Zevnik, B., Anastassiadis, K., Niwa, H., Klewe-Nebenius, D., Chambers, I., Schöler, H., and Smith, A. (1998). Formation of pluripotent stem cells in the mammalian embryo depends on the POU transcription factor Oct4. In Cell, pp. 379-391.

Nishioka, N., Yamamoto, S., Kiyonari, H., Sato, H., Sawada, A., Ota, M., Nakao, K., and Sasaki, H. (2008). Tead4 is required for specification of trophectoderm in pre-implantation mouse embryos. In Mech Dev, pp. 270-283.

Nishiyama, A., Xin, L., Sharov, A.A., Thomas, M., Mowrer, G., Meyers, E., Piao, Y., Mehta, S., Yee, S., Nakatake, Y., *et al.* (2009). Uncovering early response of gene regulatory networks in ESCs by systematic induction of transcription factors. In Cell Stem Cell, pp. 420-433.

Nishiyama, A., Yamaguchi, L., Sharif, J., Johmura, Y., Kawamura, T., Nakanishi, K., Shimamura, S., Arita, K., Kodama, T., Ishikawa, F., *et al.* (2013). Uhrf1-dependent H3K23 ubiquitylation couples maintenance DNA methylation and replication. In Nature.

Niwa, H., Burdon, T., Chambers, I., and Smith, A. (1998). Self-renewal of pluripotent embryonic stem cells is mediated via activation of STAT3. In Genes Dev, pp. 2048-2060.

Niwa, H., Miyazaki, J., and Smith, A.G. (2000). Quantitative expression of Oct-3/4 defines differentiation, dedifferentiation or self-renewal of ES cells. In Nat Genet, pp. 372-376.

Nothias, J.Y., Majumder, S., Kaneko, K.J., and DePamphilis, M.L. (1995). Regulation of gene expression at the beginning of mammalian development. In J Biol Chem, pp. 22077-22080.

O'Carroll, D., Scherthan, H., Peters, A.H., Opravil, S., Haynes, A.R., Laible, G., Rea, S., Schmid, M., Lebersorger, A., Jerratsch, M., *et al.* (2000). Isolation and characterization of Suv39h2, a second histone H3 methyltransferase gene that displays testis-specific expression. In Mol Cell Biol, pp. 9423-9433.

Oberthuer, A., Hero, B., Spitz, R., Berthold, F., and Fischer, M. (2004). The tumor-associated antigen PRAME is universally expressed in high-stage neuroblastoma and associated with poor outcome. In Clin Cancer Res, pp. 4307-4313.

Ogawa, H., Ishiguro, K.-I., Gaubatz, S., Livingston, D.M., and Nakatani, Y. (2002). A complex with chromatin modifiers that occupies E2F- and Myc-responsive genes in G0 cells. In Science, pp. 1132-1136.

Okano, M., Bell, D.W., Haber, D.A., and Li, E. (1999). DNA methyltransferases Dnmt3a and Dnmt3b are essential for de novo methylation and mammalian development. In Cell, pp. 247-257.

Orkin, S.H., and Hochedlinger, K. (2011). Chromatin connections to pluripotency and cellular reprogramming. In Cell, pp. 835-850.

Orphanides, G., LeRoy, G., Chang, C.H., Luse, D.S., and Reinberg, D. (1998). FACT, a factor that facilitates transcript elongation through nucleosomes. In Cell, pp. 105-116.

Overington, J.P., Al-Lazikani, B., and Hopkins, A.L. (2006). How many drug targets are there? In Nat Rev Drug Discov, pp. 993-996.

Palacios, A., Muñoz, I.G., Pantoja-Uceda, D., Marcaida, M.J., Torres, D., Martín-García, J.M., Luque, I., Montoya, G., and Blanco, F.J. (2008). Molecular basis of histone H3K4me3 recognition by ING4. In J Biol Chem, pp. 15956-15964.

Pan, G., Tian, S., Nie, J., Yang, C., Ruotti, V., Wei, H., Jonsdottir, G.A., Stewart, R., and Thomson, J.A. (2007). Whole-genome analysis of histone H3 lysine 4 and lysine 27 methylation in human embryonic stem cells. In Cell Stem Cell, pp. 299-312.

Papait, R., Pistore, C., Grazini, U., Babbio, F., Cogliati, S., Pecoraro, D., Brino, L., Morand, A.-L., Dechampesme, A.-M., Spada, F., *et al.* (2008). The PHD domain of Np95 (mUHRF1) is involved in large-scale reorganization of pericentromeric heterochromatin. In Mol Biol Cell, pp. 3554-3563.

Pasini, D., Bracken, A.P., Hansen, J.B., Capillo, M., and Helin, K. (2007). The polycomb group protein Suz12 is required for embryonic stem cell differentiation. In Mol Cell Biol, pp. 3769-3779.

Pastor, W.A., Aravind, L., and Rao, A. (2013). TETonic shift: biological roles of TET proteins in DNA demethylation and transcription. In Nat Rev Mol Cell Biol, pp. 341-356.

Peters, J.M., McKay, R.M., McKay, J.P., and Graff, J.M. (1999). Casein kinase I transduces Wnt signals. In Nature, pp. 345-350.

Pickart, C.M. (2001). Mechanisms underlying ubiquitination. In Annu Rev Biochem, pp. 503-533.

Pinnola, A., Naumova, N., Shah, M., and Tulin, A.V. (2007). Nucleosomal core histones mediate dynamic regulation of poly(ADP-ribose) polymerase 1 protein binding to chromatin and induction of its enzymatic activity. In J Biol Chem, pp. 32511-32519.

Radzisheuskaya, A., Le Bin Chia, G., Dos Santos, R.L., Theunissen, T.W., Castro, L.F.C., Nichols, J., and Silva, J.C.R. (2013). A defined Oct4 level governs cell state transitions of pluripotency entry and differentiation into all embryonic lineages. In Nat Cell Biol.

Ragvin, A., Valvatne, H., Erdal, S., Arskog, V., Tufteland, K.R., Breen, K., ØYan, A.M., Eberharter, A., Gibson, T.J., Becker, P.B.*, et al.* (2004). Nucleosome binding by the bromodomain and PHD finger of the transcriptional cofactor p300. In J Mol Biol, pp. 773-788.

Ralston, A., and Rossant, J. (2005). Genetic regulation of stem cell origins in the mouse embryo. In Clin Genet, pp. 106-112.

Ramakrishnan, V., Finch, J.T., Graziano, V., Lee, P.L., and Sweet, R.M. (1993). Crystal structure of globular domain of histone H5 and its implications for nucleosome binding. In Nature, pp. 219-223.

Ramsahoye, B.H., Biniszkiewicz, D., Lyko, F., Clark, V., Bird, A.P., and Jaenisch, R. (2000). Non-CpG methylation is prevalent in embryonic stem cells and may be mediated by DNA methyltransferase 3a. In Proc Natl Acad Sci USA, pp. 5237-5242.

Ravid, T., and Hochstrasser, M. (2008). Diversity of degradation signals in the ubiquitin-proteasome system. In Nat Rev Mol Cell Biol, pp. 679-690.

Rea, S., Eisenhaber, F., O'Carroll, D., Strahl, B.D., Sun, Z.W., Schmid, M., Opravil, S., Mechtler, K., Ponting, C.P., Allis, C.D.*, et al.* (2000). Regulation of chromatin structure by site-specific histone H3 methyltransferases. In Nature, pp. 593-599.

Reale, A., Matteis, G.D., Galleazzi, G., Zampieri, M., and Caiafa, P. (2005). Modulation of DNMT1 activity by ADP-ribose polymers. In Oncogene, pp. 13-19.

Robinson, C.M., and Ohh, M. (2014). The multifaceted von Hippel-Lindau tumour suppressor protein. In FEBS Lett.

Rogers, M.B., Hosler, B.A., and Gudas, L.J. (1991). Specific expression of a retinoic acid-regulated, zinc-finger gene, Rex-1, in preimplantation embryos, trophoblast and spermatocytes. In Development, pp. 815-824.

Rosenfeld, J.A., Wang, Z., Schones, D.E., Zhao, K., DeSalle, R., and Zhang, M.Q. (2009). Determination of enriched histone modifications in non-genic portions of the human genome. In BMC Genomics, pp. 143.

Rottach, A., Frauer, C., Pichler, G., Bonapace, I.M., Spada, F., and Leonhardt, H. (2010). The multi-domain protein Np95 connects DNA methylation and histone modification. In Nucleic Acids Res, pp. 1796-1804.

Rougier, N., Bourc'his, D., Gomes, D.M., Niveleau, A., Plachot, M., Pàldi, A., and Viegas-Péquignot, E. (1998). Chromosome methylation patterns during mammalian preimplantation development. In Genes Dev, pp. 2108-2113.

Russo, V.E.A. (1996). Epigenetic mechanisms of gene regulation (Cold Spring Harbor Laboratory Pr), pp. 692.

Santos, F., Hendrich, B., Reik, W., and Dean, W. (2002). Dynamic reprogramming of DNA methylation in the early mouse embryo. In Dev Biol, pp. 172-182.

Sasaki, H. (2010). Mechanisms of trophectoderm fate specification in preimplantation mouse development. In Dev Growth Differ, pp. 263-273.

Schrader, E.K., Harstad, K.G., and Matouschek, A. (2009). Targeting proteins for degradation. In Nat Methods, pp. 815-822.

Schuettengruber, B., Chourrout, D., Vervoort, M., Leblanc, B., and Cavalli, G. (2007). Genome regulation by polycomb and trithorax proteins. In Cell, pp. 735-745.

Schultz, D.C., Ayyanathan, K., Negorev, D., Maul, G.G., and Rauscher, F.J. (2002). SETDB1: a novel KAP-1-associated histone H3, lysine 9-specific methyltransferase that contributes to HP1-mediated silencing of euchromatic genes by KRAB zinc-finger proteins. In Genes Dev, pp. 919-932.

Seo, E., Kim, H., Kim, R., Yun, S., Kim, M., Han, J.-K., Costantini, F., and Jho, E.-H. (2009). Multiple isoforms of beta-TrCP display differential activities in the regulation of Wnt signaling. In Cell Signal, pp. 43-51.

Sharif, J., Muto, M., Takebayashi, S.-i., Suetake, I., Iwamatsu, A., Endo, T.A., Shinga, J., Mizutani-Koseki, Y., Toyoda, T., Okamura, K.*, et al.* (2007). The SRA protein Np95 mediates epigenetic inheritance by recruiting Dnmt1 to methylated DNA. In Nature, pp. 908-912.

Sharov, A.A., Nishiyama, A., Piao, Y., Correa-Cerro, L.S., Amano, T., Thomas, M., Mehta, S., and Ko, M.S.H. (2011). Responsiveness of genes to manipulation of transcription factors in ES cells is associated with histone modifications and tissue specificity. In BMC Genomics, pp. 102.

Shen, X., Liu, Y., Hsu, Y.-J., Fujiwara, Y., Kim, J., Mao, X., Yuan, G.-C., and Orkin, S.H. (2008). EZH1 mediates methylation on histone H3 lysine 27 and complements EZH2 in maintaining stem cell identity and executing pluripotency. In Mol Cell, pp. 491-502.

Shi, L., and Wu, J. (2009). Epigenetic regulation in mammalian preimplantation embryo development. In Reprod Biol Endocrinol, pp. 59.

Shi, X., Hong, T., Walter, K.L., Ewalt, M., Michishita, E., Hung, T., Carney, D., Peña, P., Lan, F., Kaadige, M.R.*, et al.* (2006). ING2 PHD domain links histone H3 lysine 4 methylation to active gene repression. In Nature, pp. 96-99.

Shilatifard, A. (2012). The COMPASS family of histone H3K4 methylases: mechanisms of regulation in development and disease pathogenesis. In Annu Rev Biochem, pp. 65-95.

Shuin, T., Kondo, K., Torigoe, S., Kishida, T., Kubota, Y., Hosaka, M., Nagashima, Y., Kitamura, H., Latif, F., and Zbar, B. (1994). Frequent somatic mutations and loss of heterozygosity of the von Hippel-Lindau tumor suppressor gene in primary human renal cell carcinomas. In Cancer Res, pp. 2852-2855.

Simon, J.A., and Kingston, R.E. (2009). Mechanisms of polycomb gene silencing: knowns and unknowns. In Nat Rev Mol Cell Biol, pp. 697-708.

Simon, J.A., and Kingston, R.E. (2013). Occupying chromatin: Polycomb mechanisms for getting to genomic targets, stopping transcriptional traffic, and staying put. In Mol Cell, pp. 808-824.

Smith, A.G. (2001). Embryo-derived stem cells: of mice and men. In Annu Rev Cell Dev Biol, pp. 435-462.

Smith, Z.D., Chan, M.M., Mikkelsen, T.S., Gu, H., Gnirke, A., Regev, A., and Meissner, A. (2012). A unique regulatory phase of DNA methylation in the early mammalian embryo. In Nature, pp. 339-344.

Smith, Z.D., and Meissner, A. (2013). DNA methylation: roles in mammalian development. In Nat Rev Genet, pp. 204-220.

Sprinzak, E., Sattath, S., and Margalit, H. (2003). How reliable are experimental protein-protein interaction data? In J Mol Biol, pp. 919-923.

Steger, D.J., Lefterova, M.I., Ying, L., Stonestrom, A.J., Schupp, M., Zhuo, D., Vakoc, A.L., Kim, J.-E., Chen, J., Lazar, M.A., *et al.* (2008). DOT1L/KMT4 recruitment and H3K79 methylation are ubiquitously coupled with gene transcription in mammalian cells. In Mol Cell Biol, pp. 2825-2839.

Sun, Y. (2003). Targeting E3 ubiquitin ligases for cancer therapy. In Cancer Biol Ther, pp. 623-629.

Tachibana, M., Sugimoto, K., Nozaki, M., Ueda, J., Ohta, T., Ohki, M., Fukuda, M., Takeda, N., Niida, H., Kato, H., *et al.* (2002). G9a histone methyltransferase plays a dominant role in euchromatic histone H3 lysine 9 methylation and is essential for early embryogenesis. In Genes Dev, pp. 1779-1791.

Tahiliani, M., Koh, K.P., Shen, Y., Pastor, W.A., Bandukwala, H., Brudno, Y., Agarwal, S., Iyer, L.M., Liu, D.R., Aravind, L., *et al.* (2009). Conversion of 5-methylcytosine to 5-hydroxymethylcytosine in mammalian DNA by MLL partner TET1. In Science, pp. 930-935.

Takahashi, K., and Yamanaka, S. (2006). Induction of pluripotent stem cells from mouse embryonic and adult fibroblast cultures by defined factors. In Cell, pp. 663-676.

Takeda, J., Seino, S., and Bell, G.I. (1992). Human Oct3 gene family: cDNA sequences, alternative splicing, gene organization, chromosomal location, and expression at low levels in adult tissues. In Nucleic Acids Res, pp. 4613-4620.

Tanaka, N., Wang, Y.-H., Shiseki, M., Takanashi, M., and Motoji, T. (2011). Inhibition of PRAME expression causes cell cycle arrest and apoptosis in leukemic cells. In Leuk Res, pp. 1219-1225.

Thomas, P., and Smart, T.G. (2005). HEK293 cell line: a vehicle for the expression of recombinant proteins. In J Pharmacol Toxicol Methods, pp. 187-200.

Toyooka, Y., Shimosato, D., Murakami, K., Takahashi, K., and Niwa, H. (2008). Identification and characterization of subpopulations in undifferentiated ES cell culture. In Development, pp. 909-918.

Tsukada, Y.-i., Fang, J., Erdjument-Bromage, H., Warren, M.E., Borchers, C.H., Tempst, P., and Zhang, Y. (2006). Histone demethylation by a family of JmjC domain-containing proteins. In Nature, pp. 811-816.

Tsumura, A., Hayakawa, T., Kumaki, Y., Takebayashi, S.-i., Sakaue, M., Matsuoka, C., Shimotohno, K., Ishikawa, F., Li, E., Ueda, H.R., *et al.* (2006). Maintenance of self-renewal ability of mouse embryonic stem cells in the absence of DNA methyltransferases Dnmt1, Dnmt3a and Dnmt3b. In Genes Cells, pp. 805-814.

Tuteja, R., and Tuteja, N. (2000). Ku autoantigen: a multifunctional DNA-binding protein. In Crit Rev Biochem Mol Biol, pp. 1-33.

Vakoc, C.R., Mandat, S.A., Olenchock, B.A., and Blobel, G.A. (2005). Histone H3 lysine 9 methylation and HP1gamma are associated with transcription elongation through mammalian chromatin. In Mol Cell, pp. 381-391.

van 't Veer, L.J., Dai, H., van de Vijver, M.J., He, Y.D., Hart, A.A.M., Mao, M., Peterse, H.L., van der Kooy, K., Marton, M.J., Witteveen, A.T., *et al.* (2002). Gene expression profiling predicts clinical outcome of breast cancer. In Nature, pp. 530-536.

Vaskova, E.A., Stekleneva, A.E., Medvedev, S.P., and Zakian, S.M. (2013). "Epigenetic memory" phenomenon in induced pluripotent stem cells. In Acta Naturae, pp. 15-21.

Vermeulen, M., Mulder, K.W., Denissov, S., Pijnappel, W.W.M.P., van Schaik, F.M.A., Varier, R.A., Baltissen, M.P.A., Stunnenberg, H.G., Mann, M., and Timmers, H.T.M. (2007). Selective anchoring of TFIID to nucleosomes by trimethylation of histone H3 lysine 4. In Cell, pp. 58-69.

Voigt, P., Tee, W.-W., and Reinberg, D. (2013). A double take on bivalent promoters. In Genes Dev, pp. 1318-1338.

Wadelin, F.R., Fulton, J., Collins, H.M., Tertipis, N., Bottley, A., Spriggs, K.A., Falcone, F.H., and Heery, D.M. (2013). PRAME Is a Golgi-Targeted Protein That Associates with the Elongin BC Complex and Is Upregulated by Interferon-Gamma and Bacterial PAMPs. In PLoS ONE, pp. e58052.

Wang, H., and Dey, S.K. (2006). Roadmap to embryo implantation: clues from mouse models. In Nat Rev Genet, pp. 185-199.

Wang, P.J., McCarrey, J.R., Yang, F., and Page, D.C. (2001). An abundance of X-linked genes expressed in spermatogonia. In Nat Genet, pp. 422-426.

Wernig, M., Meissner, A., Foreman, R., Brambrink, T., Ku, M., Hochedlinger, K., Bernstein, B.E., and Jaenisch, R. (2007). In vitro reprogramming of fibroblasts into a pluripotent ES-cell-like state. In Nature, pp. 318-324.

Xu, C., Kim, N.-G., and Gumbiner, B.M. (2009). Regulation of protein stability by GSK3 mediated phosphorylation. In Cell Cycle, pp. 4032-4039.

Yang, L., Xia, L., Wu, D.Y., Wang, H., Chansky, H.A., Schubach, W.H., Hickstein, D.D., and Zhang, Y. (2002). Molecular cloning of ESET, a novel histone H3-specific methyltransferase that interacts with ERG transcription factor. In Oncogene, pp. 148-152.

Ying, Q.L., Nichols, J., Chambers, I., and Smith, A. (2003). BMP induction of Id proteins suppresses differentiation and sustains embryonic stem cell self-renewal in collaboration with STAT3. In Cell, pp. 281-292.

Ying, Q.L., Wray, J., Nichols, J., Batlle-Morera, L., Doble, B., Woodgett, J., Cohen, P., and Smith, A. (2008). The ground state of embryonic stem cell self-renewal. In Nature, pp. 519-523.

You, J.S., Kelly, T.K., De Carvalho, D.D., Taberlay, P.C., Liang, G., and Jones, P.A. (2011). OCT4 establishes and maintains nucleosome-depleted regions that provide additional layers of epigenetic regulation of its target genes. In Proc Natl Acad Sci USA, pp. 14497-14502.

Zhang, J., Tam, W.-L., Tong, G.Q., Wu, Q., Chan, H.-Y., Soh, B.-S., Lou, Y., Yang, J., Ma, Y., Chai, L.*, et al.* (2006). Sall4 modulates embryonic stem cell pluripotency and early embryonic development by the transcriptional regulation of Pou5f1. In Nat Cell Biol, pp. 1114-1123.

Zhao, X.-D., Han, X., Chew, J.-L., Liu, J., Chiu, K.-P., Choo, A., Orlov, Y.L., Sung, W.-K., Shahab, A., Kuznetsov, V.A.*, et al.* (2007). Whole-genome mapping of histone H3 Lys4 and 27 trimethylations reveals distinct genomic compartments in human embryonic stem cells. In Cell Stem Cell, pp. 286-298.
Zhou, V.W., Goren, A., and Bernstein, B.E. (2011). Charting histone modifications and the functional organization of mammalian genomes. In Nat Rev Genet, pp. 7-18.

Ziller, M.J., Müller, F., Liao, J., Zhang, Y., Gu, H., Bock, C., Boyle, P., Epstein, C.B., Bernstein, B.E., Lengauer, T.*, et al.* (2011). Genomic distribution and inter-sample variation of non-CpG methylation across human cell types. In PLoS Genet, pp. e1002389.

Zou, C., and Mallampalli, R.K. (2014). Regulation of histone modifying enzymes by the ubiquitin-proteasome system. In Biochim Biophys Acta, pp. 694-702.

Curriculum Vitae

Surname: GRAF
First name: Urs
Date of Birth: 18. 07. 1985
Nationality: Swiss
Place of origin: Rebstein SG

EDUCATION:

02/ 2010 – 06/ 2014	**PhD in Stem Cell Biology, University of Zurich, Switzerland** Institute of Laboratory Animal Science, University of Zurich Klinik für Unfallchirurgie, University Hospital, Zurich Member of the Molecular Life Sciences PhD program of University and ETH Zurich PhD Thesis supervisor: PD Dr. Paolo Cinelli PhD Thesis title: *An Epigenetic Role for Pramel7 in Pluripotent Stem Cells*
09/ 2008 – 11/ 2009	**MSc in Human Biology, University of Zurich, Switzerland** Master thesis title: *The Role of the Pluripotency-related Genes Nanog and STAT3 in the Generation of Induced Pluripotent Stem Cells* Supervisors: Prof. Kurt Bürki, PD Dr. Paolo Cinelli
10/ 2005 – 06/ 2008	**BSc in Biology, University of Zurich, Switzerland**
11/ 2004 – 08/ 2005	**Rekrutenschule, Anwärterschule und Abverdienen Wm, Schweizer Armee**
08/ 2000 – 06/ 2004	**Kantonsschule Heerbrugg SG, Matura mit Schwerpunkt Latein**

GRANTS

2010 – 2012	**Forschungskredit der Universität Zürich**
2012 – 2013	**Olga Mayenfisch Stiftung für medizinische Forschung in der Schweiz**

PUBLICATIONS:

Casanova E.A., Shakhova O., Patel S.S., Asner I.N., Pelczar P., Weber F.A., Graf U., Sommer L., Bürki K., Cinelli P. (2011). Pramel7 Mediates LIF/STAT3-dependent Self-renewal in Embryonic Stem Cells. Stem Cells 29(3), 474-85.

Graf U., Casanova E.A., Cinelli P. (2011). The Role of the Leukemia Inhibitory Factor (LIF)-Pathway in Derivation and Maintenance of Murine Pluripotent Stem Cells. Genes 2(1), 280-297.

Weber F.A., Graf U., Okoniewski M.J., Meshorer E., Cinelli P. (2014). Fgf4 Controls Mesenchymal to Epithelial Transition During the Early Phases of Reprogramming. Stem Cells Dev. *Submitted.*